Metal/Polymer Interactions in Polyimide Adhesives

by

Matthew M. Ellison

Dissertation submitted to the faculty of the

Virginia Polytechnic Institute and State University

in partial fulfillment of the requirements for the degree of

DOCTOR OF PHILOSOPHY

IN

CHEMISTRY

APPROVED:

Dr. L. T. Taylor, Chairman

Dr. M. R. Anderson

Dr. J. G. Dillard

Dr. B. E. Hanson

Dr. J. P. Wightman

April 1995

Blacksburg, Virginia

Key Words: Adhesion, Sulfur Oxidation, Steel, Aluminum, Magnetism

METAL/POLYMER INTERACTIONS IN POLYIMIDE ADHESIVES

by

Matthew M. Ellison

Dr. Larry T. Taylor, Chairman

Chemistry

(ABSTRACT)

Due to their superior thermal and chemical stability, polyimides are often used as adhesives in hazardous environments. This study examines the effect of thioether sulfur in the polyimide backbone on bond strength. X-ray photoelecton spectroscopy (XPS) and reflectance infrared spectroscopy indicated that certain metals catalyze the oxidation of the thioether sulfur. It was believed that this oxidation could lead to direct metal-oxygen-sulfur bonds across the polymer/metal interface which would serve to enhance interfacial strength. Bonds were made using substrates that were believed to catalyze the oxidation strongly (steel) and minimally (aluminum). In addition, non-sulfur containing polyimides with similar Tg were also studied for comparison. The polymer/metal interface was studied using both the T-peel and wedge tests. In some

cases, oxidized sulfur was detected on the failed surfaces via XPS. No apparent effect was observed in the T-peel test, where the T-peel strengths of non-sulfur and sulfur containing polyimides were similar. In the wedge test, however, the sulfur containing BDSDA/ODA bonded to steel had an initial crack length of 34 mm. Even after eleven days the crack length was only 47 mm, which was the initial crack length for the next best polyimide. Thus, metal-catalyzed oxidation of sulfur did take place, but not to an extent to have a noticeable effect on peel strength.

Acknowledgements

Fortunately, my academic career is not soley my own accomplishment. If it was, I would not be writing this dissertation. So, it is with great joy and gratitude that I would like to express my thanks to those who have helped me along the way.

First, I would like to thank my advisor Dr. Taylor for directing my research during my graduate studies. His guidance, support, and patience have been invaluable in this process. Also, I would like to thank the other members of my research committee: Dr. John G. Dillard, Dr. James P. Wightman, Dr. Brian E. Hanson, and Dr. Mark R. Anderson who provided helpful suggestions and guidance during this work.

Special thanks are also due to Dr. James D. Rancourt who is always ready to listen or give advice. The numerous discussions we have had over the course of this work have been invaluable, especially concerning the area of transmission electron microscopy of bonded specimens. The same is true for Dr. Adley F. Rubira who always had helpful advice and encouragement.

Speaking of transmission electron microscopy, the micrographs presented here would not have been possible without the excellent work of James Hollenhead and Steve McCartney. I also wish to acknowledge the assistance of Frank Cromer for his instruction on X-ray photoelectron spectroscopy. I would also like to thank Dr. Dave Dillard

and Dwayne Rakestraw for training and use of the Instron.

I would also like to express my thanks to the Center for Adhesive and Sealant Science at VPI & SU and the Adhesive and Sealant Council for both funding this work and providing many opportunities to interact with others in the field. I also thank Dr. Terry St. Clair at NASA Langley Research Center for providing the BDSDA.

Finally, I need to thank my family. I thank my parents for all of their support and encouragement in not only this, but everything I do. I need to thank our dogs Candy and Amy who always let me know when I was not paying enough attention to them. They also kept me from losing that one valuable piece of information by sitting on it. Most importantly I thank my wife for her constant support and encouragement. Without her help, this would not be done. Lastly, I thank my son David whose arrival convinced me it was time to close this chapter of my life and move on.

Dedication:

To God:
The solvent in which this reaction takes place,

To my parents:
The reagents,

and to my wife and son:
The catalyst that kept the reaction going.

TABLE OF CONTENTS

List of Figures

List of Tables

List of Structures

I. INTRODUCTION

Adhesives have been in use for thousands of years. Archaeologists have discovered ancient arrows and spears assembled using natural resins, such as pitch [1]. In Thebes, carvings over 3300 years old showed the gluing of a thin piece of veneer to a plank of sycamore; while ancient Egyptians used a flour paste in the preparation of papyrus [2]. In fact, adhesives made from natural materials, such as animal and vegetable glues, were the only adhesives of major importance through the early part of this century. The poor resistance of these natural resins to moisture, mold growth, and other hazardous service conditions helped to inspire the search for new synthetic materials with superior properties [3].

The use of adhesives to join materials provides many advantages over mechanical methods, such as welding or riveting. Some of these advantages include the ability to join dissimilar materials, improved stress distribution within the joint, greater design flexibility, and often lower cost [4,5]. There are disadvantages, however, also

exist to the use of adhesives for joining materials, including the need for surface pretreatment, long curing times, difficulty of inspection and repair, and adhesive degradation due to environmental conditions [3,5]. For many applications, however, the advantages of using adhesives outweigh the disadvantages.

Adhesives have been used in the aircraft/aerospace industry since the first hot-air balloons, and structural adhesives have been used since the 1940s [6]. Most structural adhesive bonding was developed for defense purposes, from British aircraft in World War II to the modern F-16 and F-18 fighters. But adhesive bonding has found its way into commercial use. In the aircraft/aerospace industry, adhesive bonding produces structures that weigh less and are more aerodynamic than those using mechanical fastening techniques [6,7]. Adhesives possessing either insulative or conductive properties are important in the electrical/electronics market. The automotive industry uses adhesives for many diverse applications, including brake shoe bonding,

decorative trim, and even body assembly [8]. Other major areas of adhesive use are in construction and packaging [6].

While it is difficult to develop a method for classifying all adhesives, most can be grouped into one of three categories depending on their function. Structural adhesives are designed to bear large loads over small areas, such as in the automobile and aerospace industries. Laminating adhesives bear less load and cover a large area of the surface, such as in plywood and packaging. Pressure-sensitive adhesives (PSAs) can be used as either structural or laminating adhesives, but they are classified separately due to their ease of use and speed of bond formation [9].

Methods of testing adhesively bonded joints fall into two broad categories: destructive and non-destructive. Destructive testing is the most common and uses one of three classes of specimens. The cheapest and simplest standard test specimens include lap-shear, peel, and wedge among others. While they are cheap and simple, they often do not resemble an actual mechanical counterpart in the final product. The second type of specimen is representative of

one or more joints in the final product, which tests the adhesive under more realistic conditions. The third, and best, specimen is the final product itself which is often impractical to test due to economic factors [5].

Non-destructive testing can provide valuable information on the bonded joint by correlating the strength of the joint to some mechanical, physical, or chemical property which can be measured without damaging the joint. Most non-destructive tests, such as sonic testing or tapping, examine the cohesive strength of the adhesive and reveal voids in the bonded joint. Ultrasonic testing and radiography are also used [5, 7, 10]. A relatively recent development in non-destructive evaluations is the use of tagged adhesives. Clark and co-workers have examined the incorporation of magnetic particles in adhesive formulations for the purpose of assessing voids, degree of cure, and adhesive thickness [11-14].

One of the major questions concerning adhesive joints is the nature of the forces acting at the interface which prevent dissimilar materials from coming apart either during

testing or in actual use. According to Kinloch [4], four main theories of adhesion have been proposed:

a) mechanical interlocking,

b) diffusion theory,

c) electronic theory,

d) adsorption theory.

The theory of mechanical interlocking proposes that the adhesive functions by interlocking with surface irregularities on the substrate. For the most part, however, this method is not thought to play a dominant role.

The diffusion theory, as advocated by Voyutskii, relies on the interdiffusion of the adhesive and adherend. This theory is unlikely if the solubility parameters of the two materials are not similar.

The electronic theory of adhesion specifies that adhesive strength is due to the electrostatic attractive forces across the electrical double layer.

The adsorption theory is the most widely accepted theory of adhesion. In it, the van der Waals forces between the two materials are the major contributors to adhesive

strength. Included in this theory, are stronger types of interactions due to the acid-base nature of the adhesive and adherend [15, 16], as well as the formation of direct chemical bonds across the interface. The formation of direct chemical bonds would not only serve to increase the interfacial strength, but also help to make the interface more environmentally stable.

The objective of this work was two-fold. The first objective was to determine the chemical nature of the interaction between metal/metal complexes and thioether containing polyimides. Once that has been determined, then the second objective was to examine the effects of that interaction can be examined in adhesive situations between metal substrates and polyimide adhesives. It is proposed that certain metals, such as iron, catalyze the oxidation of thioether sulfur in the polyimide backbone, while others, i.e. aluminum, do not. The metal/sulfur interactions were characterized first by modifying free standing films with metal complexes. Once the nature of the interaction is known, then metal substrates will be examined which either

catalyze or do not catalyze the oxidation of thioether sulfur. Bonds synthesized with these metal substrates and polyimides either containing sulfur or not containing sulfur will be tested using the T-peel and wedge tests. It is believed that the metal catalyzed oxidation of thioether sulfur will increase interfacial strength and improve bond performance due to the formation of chemical bonds between the polyimide and the metal.

II. MODIFIER AND POLYMER INTERACTIONS IN METAL-MODIFIED POLYIMIDE COMPOSITES

INTRODUCTION

Polyimide films containing *in situ* generated metal/metal oxide particles have been studied for several years by Taylor and co-workers [17-28] in the attempt to synthesize materials with unique combinations of properties. Specific modified polyimides exhibit enhanced electrical [19], magnetic [20], and adhesive [21, 22] properties. For example, copper(II) [18, 23], cobalt(II) [19, 24], tin(II) [19], and iron(III) [20] salts and/or complexes were converted to copper metal, Co_3O_4, SnO_2, and Fe_2O_3, respectively, during the poly(amide acid) curing process. The modified polyimide composites were produced in this manner without affecting the polyimide chemically. Since polyimides exhibit weak donor properties and the monomeric dianhydrides and diamines contained, in most cases, poorly donating ether and ketonic functionalities, no interaction of metal ion and polyimide was ever apparent in these earlier studies.

Sulfur (thioether) containing monomers, however, have previously been implicated in metal-polyimide interaction. One of the dianhydrides used in several studies was 4,4'-bis(3,4-dicarboxyphenoxy)diphenyl sulfide dianhydride (BDSDA, Structure 1). Homogeneously dissolved dopants included cobalt(II) chloride [17, 24-26], silver nitrate [27, 28], and bis(trifluoroacetylacetonato)copper(II) [23]. The polyimide in these studies was synthesized from (BDSDA) and 4,4'-diaminodiphenyl ether (ODA, Structure 2). The presence of a metal additive in all three cases could be correlated via X-ray photoelectron spectroscopy with a distinct change in the chemistry of the thioether sulfur in the polyimide backbone [23, 24, 28]. These previous studies presented differing interpretations for this chemically altered polyimide thioether.

In the study with copper(II) [23], it was argued that copper(II) was chelated to the thioether sulfur of the polyimide. The metal was hypothesized to be in a mixed oxidation state. TEMs from this study showed the formation of very few metal/metal oxide particles compared to

Structure 1. 4,4'-Bis(3,4-dicarboxyphenoxy)diphenyl sulfide dianhydride (BDSDA)

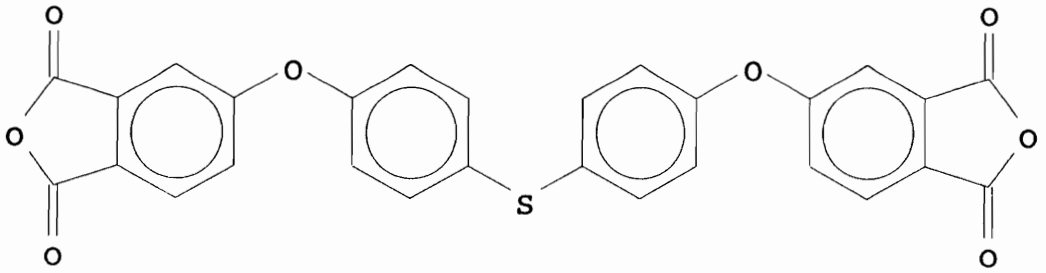

Structure 2. 4,4'Diaminodiphenyl ether (ODA)

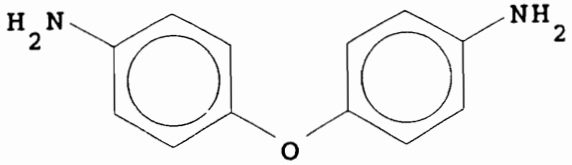

similarly prepared non-sulfur containing polyimides. Thus, it was hypothesized that the chelation of the copper to the thioether moiety caused the metal/metal oxide particles to exist in a dispersed state.

In the cobalt study [24], the sulfur was speculated to be catalytically oxidized by the cobalt to sulfoxide and/or sulfone. The cobalt chloride, meanwhile, was converted to Co_3O_4. This interaction was only observed on the atmosphere side of the film and not on the glass side. Coordination between the sulfur and cobalt was ruled out because it was suggested that if coordination were the cause, then it should be observed on both sides of the composite film. The chemical state of the glass side was not reported in the copper/polyimide composite [23]. TEMs of the cobalt/polyimide composites were not included so it was impossible to determine the exact particle distribution within the composite.

Both coordination and oxidation of sulfur were considered in the study of the silver/polyimide composites [28]. FT-IR reflectance spectra failed to show any band

attributable to either sulfone or sulfoxide. It was also observed that considerably more silver migrated to the atmosphere side of non-sulfur containing polyimide composites compared to those containing sulfur even though the glass transition temperature was 70°C less in the silver/BDSDA/ODA composite. Possible coordination was hypothesized as a reason for the reduced migration of Ag^{+}.

The dianhydride, BDSDA, without metal modification has also been used in several other studies. St. Clair and co-workers used this monomer in combination with either p-phenylene diamine or benzidene for the synthesis polyimides with a high degree of crystallinity [29]. They also investigated this dianhydride in conjunction with several diamines as a possible source of optically transparent polyimide coatings [30]. Crivello, *et al.*, have studied BDSDA in the synthesis of high temperature photoresist materials [31]. BDSDA was also one of the monomers examined by Takekoshi, et al., [32] in his study of thermal and physical properties of a series of polyimides. No chemical change in the thioether moiety was reported during

processing in any of these studies.

St. Clair and co-workers have also used BDSDA to prepare a series of thermoplastic polyimides [33-37]. BDSDA and 1,3-bis(aminophenoxy)benzene (APB, Structure 3) were reacted to yield a polyimide adhesive that contained both phenylene oxide and sulfide groups [33, 34]. This polymer exhibited the processability of polyphenylene oxides and sulfides while maintaining the thermal stability and solvent resistance of polyimides. The lap shear strength of this adhesive was reported to be quite high compared to other polyimides [34]. Another thermoplastic polyimide, designated 422, has been synthesized using equimolar amounts of *meta*-phenylene diamine and 4,4'-oxydianiline as the diamine component [35-36]. This polyimide found some application as a high temperature adhesive for bonding titanium and Celion 6000/LARC-160 composite, but this material was not compared to other adhesives. Again, no chemical change in the thioether was reported in these studies.

The only other study that made any note of a possible

Structure 3. 1,3-Bis(aminophenoxy)benzene (APB)

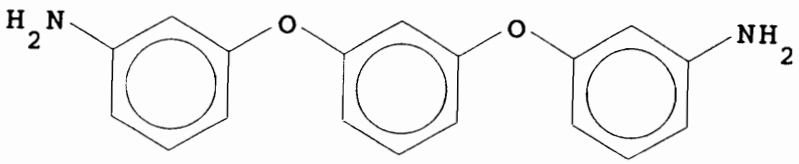

chemical change in the thioether was done by Burks and St. Clair [37] who examined the properties of polyimides synthesized from either BDSDA or its sulfone analogue ($BDSO_2DA$) and 3,3'-diaminodiphenyl sulfone ($DDSO_2$). Both nitrogen and air cured samples of BDSDA/$DDSO_2$ were investigated. They concluded that the thioether in both the fully air cured and nitrogen cured samples was oxidized to the sulfone moiety because they did not find any difference between the reflectance infrared spectra of these samples and that of $BDSO_2DA/DDSO_2$. Their observation of oxidized of thioether sulfur is contradictory to what has been found with other non-modified sulfur-containing polyimide films [24]. However, their interpretation of the spectra would be very complicated since a sulfone group from the amine monomer was present in the samples prior to oxidation.

This study will attempt to more accurately interpret the metal-sulfur interaction and resolve the differences in the interpretations of the previous studies. Several different metal complexes have been examined in this study to accurately identify the interaction between the metal and

thioether sulfur. Tris(2,4-pentanedionato)iron(III) ($Fe(acac)_3$, Structure 4) was the main additive used in this study since it had been shown not to interact chemically with non-sulfur containing polyimides [19]. Tris(1-phenyl-2,4-pentanedionato)iron(III) ($Fe(bzac)_3$, Structure 4) was used to examine the effect, if any, that the ligand had on the metal-catalyzed oxidation of sulfur. Tris(2,4-pentanedionato)aluminum ($Al(acac)_3$, Structure 4) was also examined as a non-transition metal additive comparable to $Fe(acac)_3$. The third modifier, bis(2,4-pentanedionato)vanadyl oxide ($VO(acac)_2$, Structure 5), has been shown to be a catalyst for the oxidation of thioether sulfur [38]. The interaction between the thioether and the metal additive has potential application in the field of adhesives. If this interaction occured between a sulfur-containing adhesive and a suitable metal substrate then interfacial strength could be enhanced by creating chemical bonds between the substrate and adhesive. Oxidation could also affect bond strength detrimentally, if the adhesive along the interface is degraded, creating a weak boundary

Structure 4. Tris(2,4-pentanedionato)iron(III) ($Fe(acac)_3$)
M = Fe; R = H

Tris(1-phenyl-2,4-pentanedionato)iron(III) ($Fe(bzac)_3$)
M = Fe; R = C_6H_5

Tris(2,4-pentanedionato)aluminum ($Al(acac)_3$)
M = Al; R = H

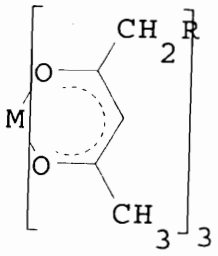

Structure 5. Bis(2,4-pentanedionato)vanadyl oxide ($VO(acac)_3$)

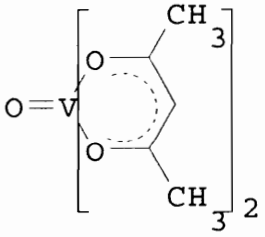

layer which would weaken the interfacial strength. Thus, it is important to fully understand this interaction.

EXPERIMENTAL

Materials

4,4'-Bis(3,4-dicarboxyphenoxy)diphenyl sulfide dianhydride (BDSDA) was obtained from NASA Langley Research Center (Hampton, VA), recrystallized twice from 2-butanone, and vacuum dried overnight at 120°C prior to use. Other dianhydrides examined included 3,3',4,4'-benzophenonetetracarboxylic acid dianhydride (BTDA, Structure 6), obtained from Allco Chemical Corp. (Galena, KS) and was vacuum dried at 120°C, and 3,3',4,4'-diphenylsulfone tetracarboxylic acid dianhydride (DSDA Structure 7), obtained from Chriskev, Inc. (Leawood, KS) which was vacuum dried at 110°C. Zone refined 4,4'-diaminodiphenyl ether (ODA) was obtained from Aldrich Chemical Co. (Milwaukee, WI) and was vacuum dried overnight at 70°C before use. The other diamine examined was 4,4'-diaminodiphenyl sulfone (ASD, Structure 8) obtained from

Structure 6. 3,3',4,4'-Benzophenonetetracarboxylic acid dianhydride (BTDA)

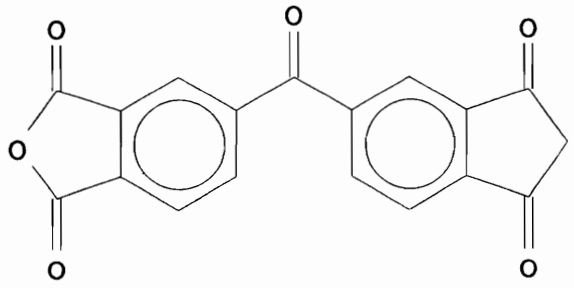

Structure 7. 3,3',4,4'-Diphenylsulfone tetracarboxylic acid dianhydride (DSDA)

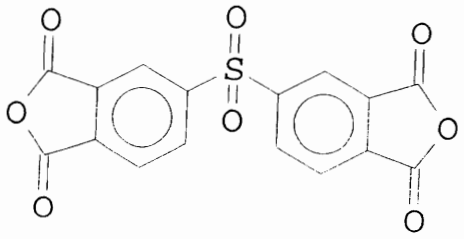

Structure 8. 4,4'-Diaminodiphenyl sulfide (ASD)

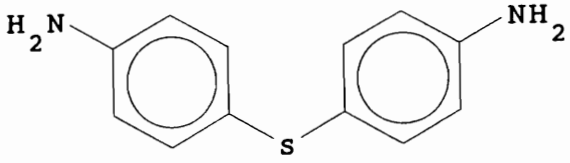

Mitsui Toatsu (Tokyo, Japan) and vacuum dried at 80°C overnight. N,N-Dimethylacetamide (DMAc) was obtained from Aldrich Chemical Co. and was stored under nitrogen and over molecular sieves. The iron additives used in this study were tris(2,4-pentanedionato)iron(III) ($Fe(acac)_3$), obtained from Amspec, Inc. (Gloucester, NJ), and tris(1-phenyl-2,4-pentanedionato)iron(III) ($Fe(bzac)_3$), obtained from the National Institute of Standards and Testing (Washington D.C.). Other additives examined included tris(2,4-pentanedionato)aluminum ($Al(acac)_3$) and bis(2,4-pentandionato)vanadium oxide ($VO(acac)_2$) both of which were obtained from Aldrich Chemical Co. All metal complexes were vacuum dried at 80°C overnight to remove moisture prior to use.

Synthesis

Poly(amide acid) solutions were made by reacting equal molar amounts of diamine and dianhydride in DMAc (11% w/w solids for BDSDA solutions and 18% w/w solids for BTDA and DSDA solutions) under a dry nitrogen atmosphere. The monomers were allowed to react for at least one hour in the

stirred solution. After one hour, modified poly(amide acid) solutions were made by adding the metal complex (20 mole% concentration) and stirred for at least one hour. The final metal concentration was approximately 2.0 wt% assuming complete imidization, complete conversion of the additive to the Fe_2O_3, and no residual solvent or ligand.

Free standing films were made by casting the modified and unmodified poly(amide acid) solutions onto a dust free glass plate at a thickness of 0.51 mm with a doctor blade. The film was then cured under either a dynamic air or nitrogen atmosphere at 80°C for twenty minutes and at 100°C, 200°C, and 300°C for one hour each. Upon cooling, the films were removed from the glass plate using a razor blade to lift off the film. The side exposed to the cure atmosphere will be referred to as the "atmosphere side" in the subsequent discussion. The "glass side" will be the side of the film which was in contact with the glass plate during the cure.

Measurements

X-ray photoelectron spectroscopy data were obtained

using a Perkin-Elmer Phi Model 5300 ESCA system equipped with a magnesium anode ($K\alpha$=1253.6 eV) operated at 400 W. The samples were attached to aluminum mounts using double stick transparent tape. The binding energies obtained from XPS spectra were all corrected by positioning the C1s photopeak of the aromatic polyimide backbone at 284.6 eV.

Transmission electron micrographs were taken with a Philips Model 420 scanning transmission electron microscope. The samples for TEM analysis were embedded in Polyscience ultralow viscosity resin and cured for eight hours at 70°C. A Reichert-Jung ultramicrotome and a microstar diamond knife were then used to obtain cross sections of the samples having thicknesses of between 500 and 800 Å. These sections were then placed on 200-mesh copper grids for analysis.

Thermal analyses were performed using a Perkin-Elmer Model TGS-2 thermogravimetric system (TGA) and a Perkin-Elmer Model DSC-4 differential scanning calorimeter (DSC). The instruments were used in conjunction with the Perkin-Elmer System 4 Thermal Analysis Data Station (TADS). TGA analyses were conducted at a heating rate of 10°C/min under

a dynamic air or nitrogen atmosphere and the results were used to determine the polymer decomposition temperature (PDT) (i.e. temperature at which 10% weight loss occurred). DSC analyses were conducted at a heating rate of 10°C/min under a nitrogen atmosphere to determine the glass transition temperature (Tg). Elemental analyses (iron and sulfur) were obtained by Galbraith Analytical Laboratories, Knoxville, TN.

Internal reflectance infrared spectra of the composite films in the 4000-400 cm^{-1} region were acquired using a Nicolet Model 510 FT-IR spectrophotometer. An attenuated total reflectance apparatus (ATR) with a zinc selenide crystal was used because the films were too thick for standard transmission mode. Each spectrum was the average of 1000 individual scans.

RESULTS and DISCUSSION

Physical Analysis of BDSDA/ODA Composite Films

Five films have been the focus of this investigation. Non-modified BDSDA/ODA films were cured in both air and

nitrogen atmospheres. Both films were pale yellow in color, very flexible, and creasible (Table I). Two 20 mole% $Fe(acac)_3$-modified composite films were also synthesized using air and nitrogen curing atmospheres. These two films were a deep red color. While the $Fe(acac)_3$-modified film cured in nitrogen was flexible and creasible like the non-modified films, the $Fe(acac)_3$-modified film cured in air was only flexible. This film could not be creased without breaking. The last composite film used $Fe(bzac)_3$ as the additive and was cured in air. It was also flexible and creasible like the non-modified films.

Thermal data are summarized in Table I for the five films. Non-modified films cured in either dry air or nitrogen lost only 50% of their weight upon reaching 900°C when tested in a dynamic flow of nitrogen (Figure 1). When the two non-modified films were tested in a dynamic flow of air, they lost in excess of 90% of their weight by 900°C (Figure 2). $Fe(acac)_3$-modified films cured in air (Figure 3) and nitrogen and the $Fe(bzac)_3$-modified film lost ~ 40% of their weight upon reaching 900°C in a nitrogen test

Table I. Physical and Thermal Properties of BDSDA/ODA Composite Films.

Film	Cure Atm	Color	Flexibility	PDT Air (°C)	PDT N_2 (°C)	Tg (°C)
1-Non-Mod	Air	Yellow	Creasible[a]	579	581	217
2-Non-Mod	Nitrogen	Yellow	Creasible	613	594	217
3-$Fe(acac)_3$	Air	Red	Bendable	442	553	261
4-$Fe(acac)_3$	Nitrogen	Red	Creasible	464	560	248
5-$Fe(bzac)_3$	Air	Red	Creasible	447	545	250

[a]Creasible refers to films that can be folded and creased twice in a perpendicular fashion without fracturing; bendable refers to films that can be folded but not creased without fracturing.

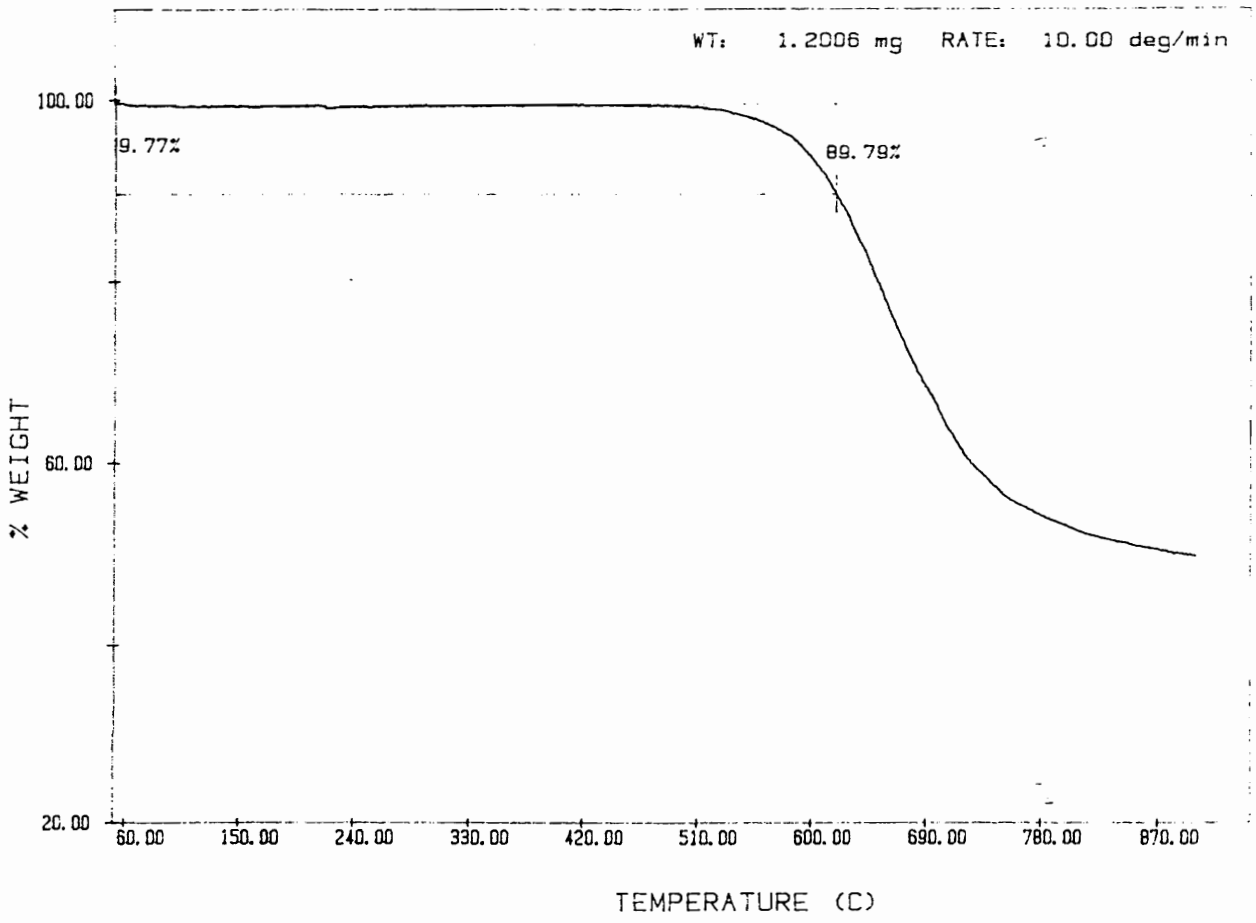

Figure 1. Thermogravimetric Profile of Air Cured Non-Modified BDSDA/ODA Film Tested in Nitrogen at 10°C/min.

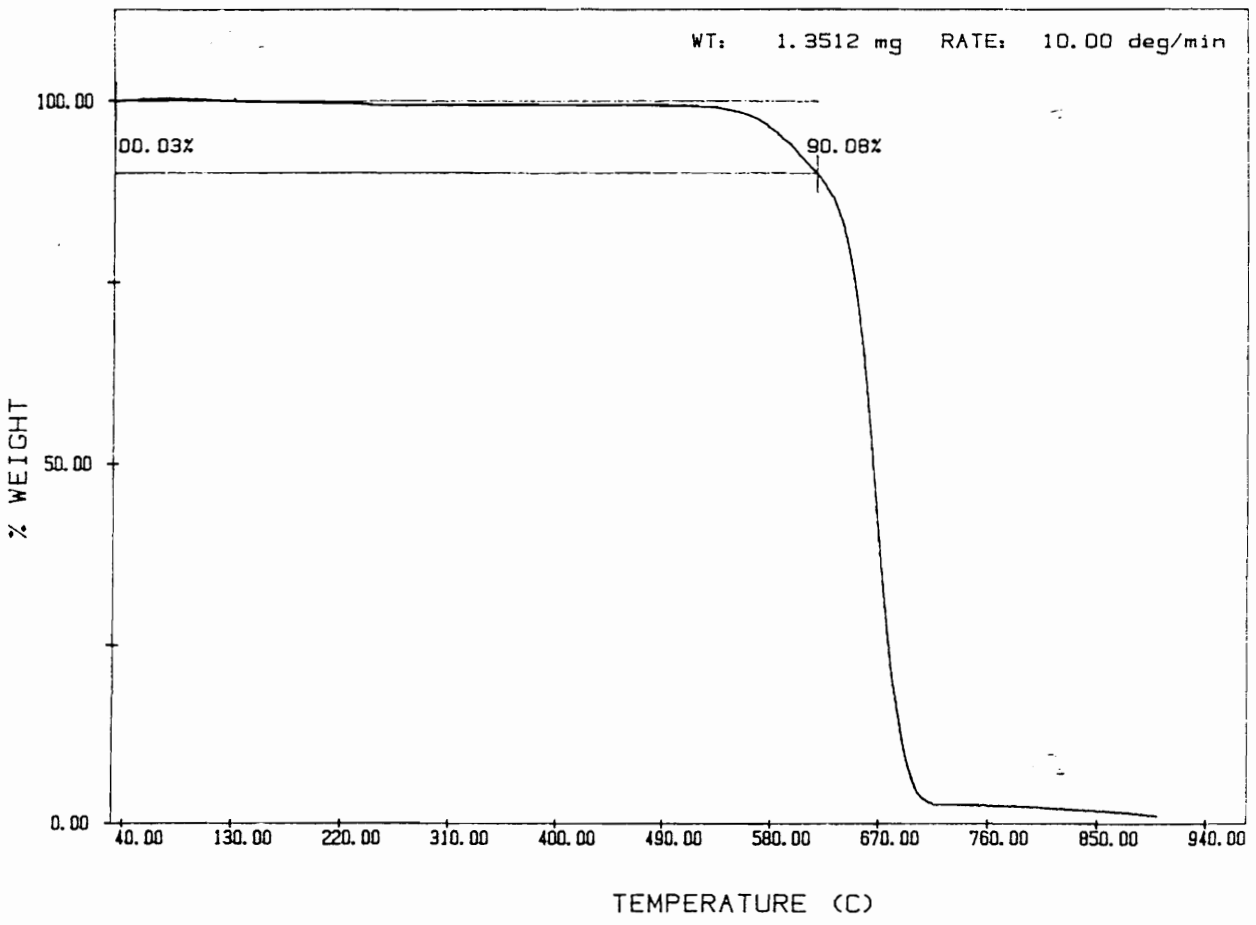

Figure 2. Thermogravimetric Profile of Air Cured Non-Modified BDSDA/ODA Film Tested in Air at 10°C/min.

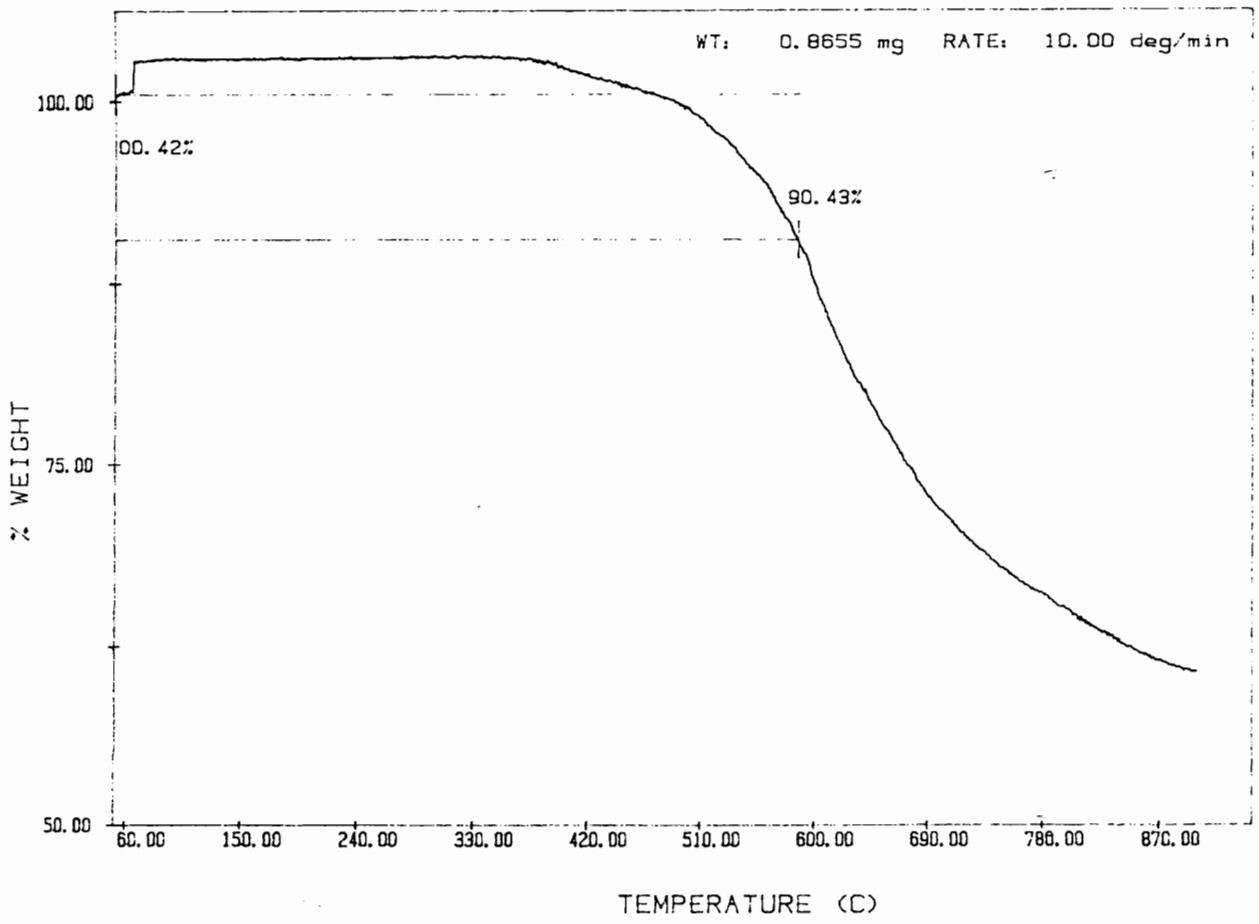

Figure 3. Thermogravimetric Profile of Air Cured $Fe(acac)_3$-Modified BDSDA/ODA Film Tested in Nitrogen at 10°C/min.

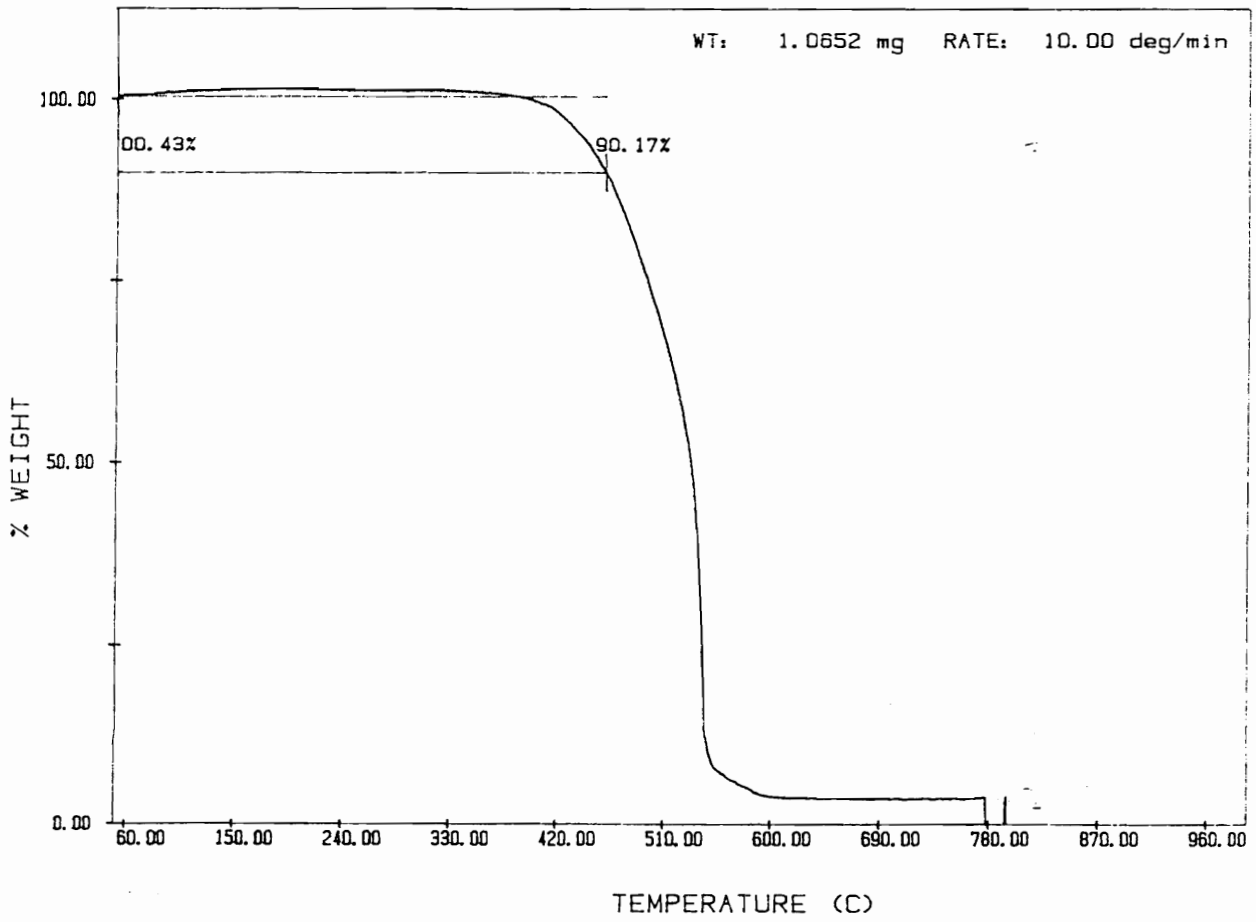

Figure 4. Thermogravimetric Profile of Air Cured $Fe(acac)_3$-Modified BDSDA/ODA Film Tested in Air at 10°C/min.

atmosphere. When these films were tested in air, however, they lost in excess of 95% of their weight by 900°C (Figure 4). The TGA plots were similar for the iron modified films, but the $Fe(acac)_3$-modified composite cured in nitrogen seemed slightly more stable with a PDT of 464°C compared to 442°C for the $Fe(acac)_3$-modified composite and 447°C for the $Fe(bzac)_3$-modified composite that were cured in air. They both showed rapid weight loss after the 10% mark was reached.

The effect of cure atmosphere on the PDTs of these four films was more noticeable when they were tested in air (Table I). When they were tested in nitrogen, the $Fe(acac)_3$-modified film cured in nitrogen was approximately 10° higher than both the $Fe(acac)_3$- and $Fe(bzac)_3$-modified films cured in air. This difference increased to 20° when tested in air. It was also apparent that iron-modification caused only a slight decrease (~ 30°C) in the PDT compared to the non-modified films when tested in nitrogen. The PDTs of the iron-modified composites measured in air, however, exhibited a significant reduction (~ 150°C) compared to the

non-modified films. This dramatic decrease in the PDT of metal modified/polyimide composite has been observed elsewhere, [20, 23] and the phenomena can probably be attributed to a metal-catalyzed oxidative decomposition pathway in the composite.

The Tg of the two non-modified films were identical (217°C) and correspond well with literature values (Table I) [32]. The Tg of the $Fe(acac)_3$-modified composites were higher than the non-modified films, 261°C for the air cured and 248°C for the nitrogen cured composites. The Fe(bzac)3-modified film possessed a similar Tg of 250°C. This increase in Tg has also been observed elsewhere, and the increase was similar to other $Fe(acac)_3$-modified polyimides [22]. The increase in Tg is probably due to the metal modifier serving as a filler resulting in a stiffer composite film. The Tg for the sulfone version of this non-modified polyimide is 260°C [32]. Thus, the increase in Tg could be due to the oxidation of the thioether moiety to a sulfone during the cure. For this oxidation to affect the Tg, however, it would have to occur completely throughout

the film. This conversion apparently did not occur throughout the film, as will be seen later, so oxidized sulfur would not be the prime cause of the increased Tg.

Elemental analysis was performed on the two non-modified films and on the two $Fe(acac)_3$-modified composites (Table II). If the iron was completely converted to one of its oxides, such as Fe_2O_3, FeO, Fe_3O_4, FeOOH, or even $Fe(OH)_3$, the weight percent of iron and sulfur would be approximately 2.0% and 4.6%, respectively. If the iron remained unconverted, *i.e.* as $Fe(acac)_3$, the expected weight percent of iron would be 1.8% and sulfur would be 4.2%. The actual weight percent of iron found was 1.94 ± 0.19% for the modified composite cured in nitrogen and 1.97 ± 0.20% for the modified composite cured in air. While these values were too close to differentiate between an iron oxide and $Fe(acac)_3$, it was apparent that no iron was lost during the curing process. The weight percent of sulfur; 4.66 ± 0.47% for the nitrogen cured composite and 4.56 ± 0.46% for the air cured composite; were also within the expected values which indicated that no polymer decomposition occurred and

Table II. Elemental Analysis of BDSDA/ODA Composite Films.

Film	wt % of Sulfur in Final Film		wt % of Iron in Final Film	
	actual	theoretical	actual	theoretical[a]
1	4.68	4.75	----	----
2	4.78	4.75	----	----
3	4.56	4.62	1.97	2.01
4	4.66	4.62	1.94	2.01

[a]Based on complete imidization, no residual solvent, and conversion to Fe_2O_3 in the case of iron-modified composites.

no sulfur was lost as SO_2.

Particle Distribution in BDSDA/ODA Composite Films

TEMs of the air cured $Fe(acac)_3$-modified polyimide (Figure 5) composite film revealed that a few large particles (60 nm) were scattered along the atmosphere side of the film forming a discontinuous surface layer, whereas only a few particles (80-100 nm in diameter) were observable in the bulk of the film. This observation is different from earlier work with non-sulfur containing polyimides and $Fe(acac)_3$ [20]. In Bergmeister's study [20], many particles (20-80 nm) were observed in the bulk of the film compared to the 10-15 particles observed in this study. Since the majority of iron added remained in the composite (>95%) in this study, it was hypothesized that the absence of a high population of iron-containing particles, observable by TEM, in the air cured composite film may be due to the iron dopant residing throughout the film as highly dispersed particles (< 10 Å). While this type of distribution is uncommon for metal-modified polyimides which do not contain a thioether moiety in the polymer backbone

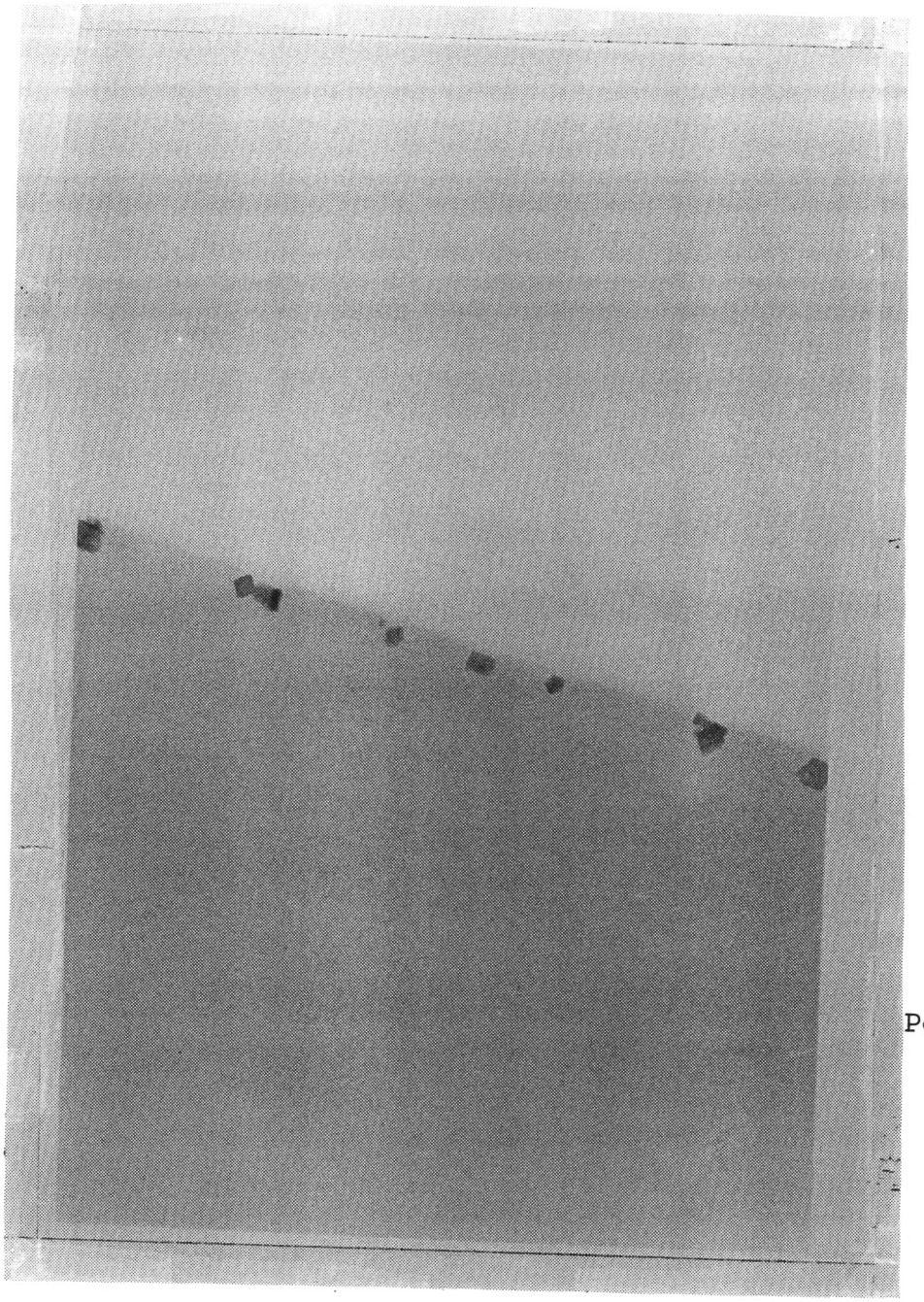

Figure 5. TEM of Atmosphere Side Surface of Air Cured $Fe(acac)_3$-Modified BDSDA/ODA Composite (106,000x).

[17], this distribution was observed in the work by Porta, *et al.* [23], using copper and this same sulfur containing polyimide. It was postulated in that study that the polyimide sulfur was binding to the metal modifier and thus, restricting its mobility. Unfortunately, the study by Boggess, *et al.* [24], did not include TEMs of the cobalt-modified BDSDA/ODA composites as an additional comparison, but the study with silver [28] did note that less silver migrated to the surface of the BDSDA/ODA composites compared to the BTDA/ODA ones. TEMs of the air cured $Fe(bzac)_3$-modified polyimide were similar to those of the $Fe(acac)_3$-modified polyimide but did not contain any particles along the atmosphere surface.

For $Fe(acac)_3$-modified films cured under a nitrogen atmosphere, a continuous atmosphere side surface layer (60 nm) was observed (Figure 6), but again, only a few particles (80-100 nm) were found in the bulk of the film. A continuous surface layer is probably formed in the nitrogen cured composite because the lack of molecular oxygen reduced the interaction between the sulfur and the iron during the

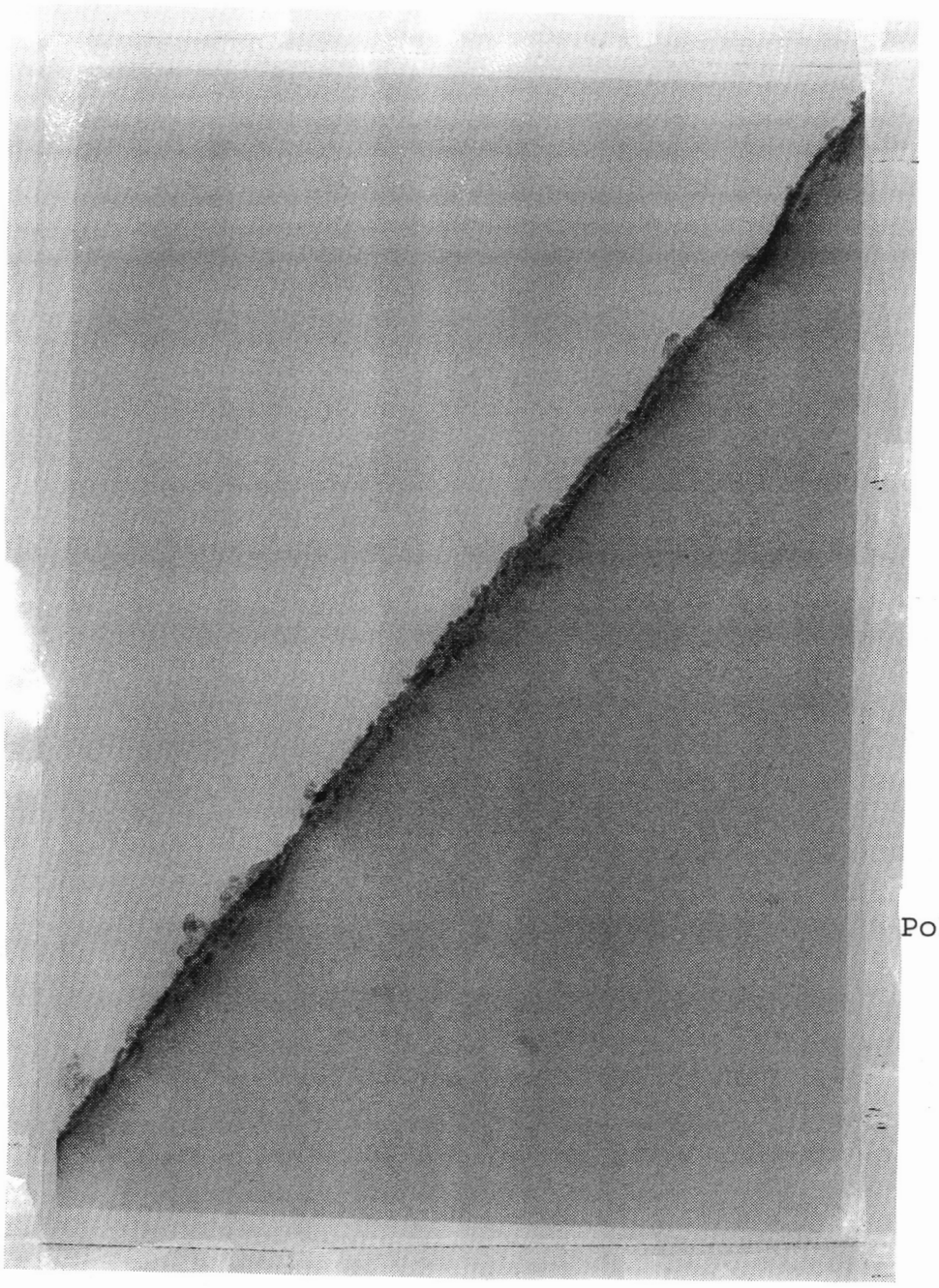

Figure 6. TEM of Atmosphere Side Surface of Nitrogen Cured $Fe(acac)_3$-Modified BDSDA/ODA Composite (106,000x).

formation of the iron oxide along the surface of the film, thus allowing the iron oxide more mobility.

Surface Characterization of BDSDA/ODA Composite Films

The chemical state of the elemental components of the polyimide and the iron additive along the film surface were examined by XPS. Non-modified films were also examined for purposes of comparison. The spectra were curve fitted to yield sets of photopeaks consistent with the types and relative concentrations of elements present.

On the atmosphere side of the non-modified air cured BDSDA/ODA film, the nitrogen 1s photopeak occured at 400.0 (±0.1) eV corresponding to the imide nitrogen [24]. The oxygen 1s photopeak (Table III) could be resolved into two peaks: (a) 533.4 (±0.1) eV for an ether oxygen and (b) 531.8 (±0.1) eV for an imide oxygen [24, 39] (Figure 7). The relative areas of these two peaks should have been in a ratio of 4:3 (imide:ether), but the ratio was closer to 3.2:3. The sulfur 2p photopeak could be fitted into the $2p_{1/2}$ and $2p_{3/2}$ components in the theoretical ratio of 1:2 and separated by 1.3 eV. The sulfur $2p_{3/2}$ binding energy of

Table III. Binding Energies and Relative Concentrations[a] of Oxygen, Sulfur, and Iron Species in the Composite BDSDA/ODA Polyimide Films.

Film	Oxygen						Sulfur			Iron
	Ether	Imide	Sulfone	Sulfoxide	Hydroxide	Oxide	Sulfone	Sulfoxide	Thioether	
1	533.4 (3.9)	531.8 (4.0)	-----	-----	-----	-----	-----	-----	163.3 (0.9)	-----
2	533.6 (3.8)	532.0 (4.0)	-----	-----	-----	-----	-----	-----	163.1 (1.1)	-----
3	533.2 (3.8)	532.0 (4.0)	531.9 (5.9)	-----	531.3 (2.8)	530.1 (2.8)	168.2 (1.5)	-----	-----	711.8 (2.7)
4	533.4 (3.8)	531.9 (4.0)	531.7 (2.2)	531.4 (0.5)	-----	530.2 (4.0)	168.2 (0.5)	165.8 (0.3)	163.3 (0.3)	711.2 (2.2)
5	533.3 (3.8)	531.9 (4.0)	531.8 (2.0)	-----	531.0 (0.3)	530.1 (0.2)	167.8 (0.4)	165.8 (0.1)	163.2 (0.2)	712.2 (0.3)

[a]Values in parentheses were the relative concentrations of all the various functionalities based on four imide oxygens.

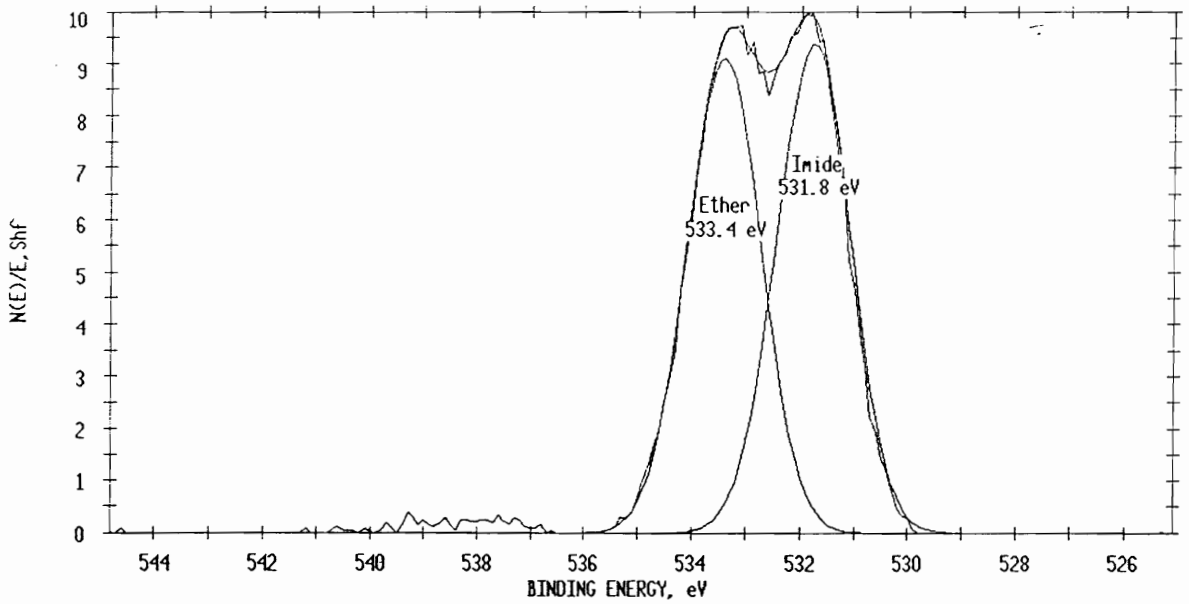

Figure 7. Oxygen 1s XPS Photopeak of the Atmosphere Surface of Air Cured Non-Modified BDSDA/ODA Film (Binding Energy Calibrated to C 1s = 284.6 eV).

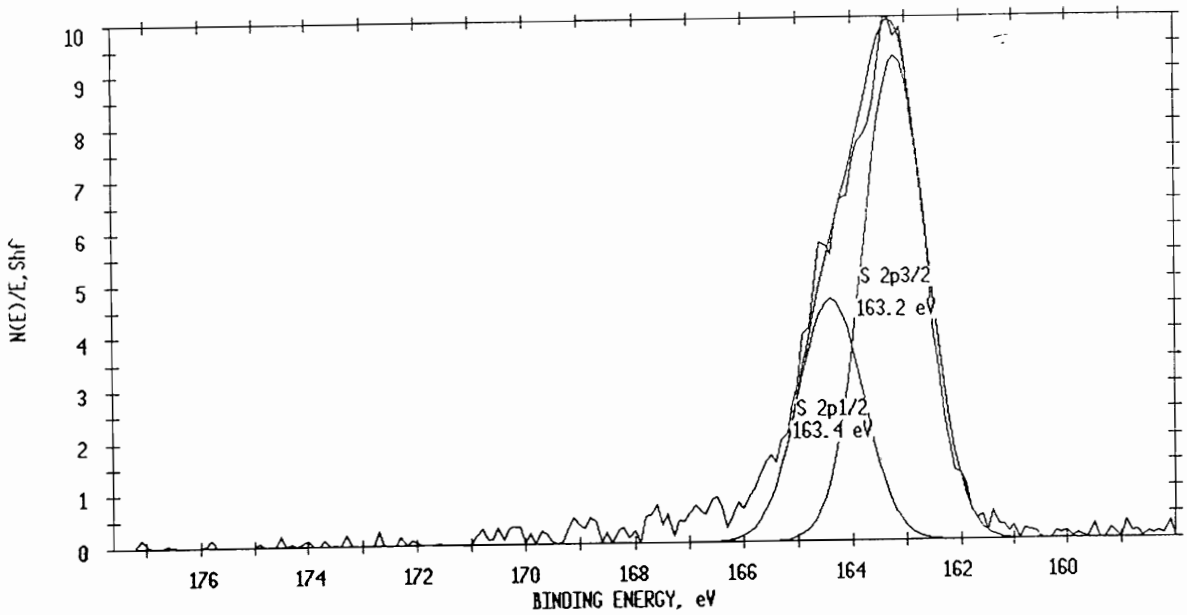

Figure 8. Sulfur 2p XPS Photopeak of the Atmosphere Surface of Air Cured Non-Modified BDSDA/ODA Film (Binding Energy Calibrated to C 1s = 284.6 eV).

163.3 (±0.1) eV corresponded to the thioether moiety [24, 40] of the BDSDA part of the polyimide (Figure 8). The glass side surface of this film yielded similar results, as did both sides of the non-modified nitrogen cured film.

No oxidation of the sulfur was evident on either surface of either non-modified film, which does not agree with the results of Burks and St. Clair [37], who reported that the thioether was oxidized to the sulfone based upon infrared spectra. Internal reflectance IR spectra were obtained for the atmosphere side of the air cured non-modified film to determine if any oxidation could be observed via this technique (Figure 9). Absorption bands characteristic of imide rings were observed at 1775, 1720, 1375, and 705 cm^{-1} [41]. Other adsorption bands were observed at 1240 and 830 cm^{-1} which represented an ether moiety [42] and parasubstituted phenyl rings, [41] respectively. Characteristic adsorption bands of sulfones, which occur at 1350-1300 cm^{-1} and 1160-1120 cm^{-1} [42], were not observed giving further evidence that the thioether sulfur was not oxidized in the non-modified films.

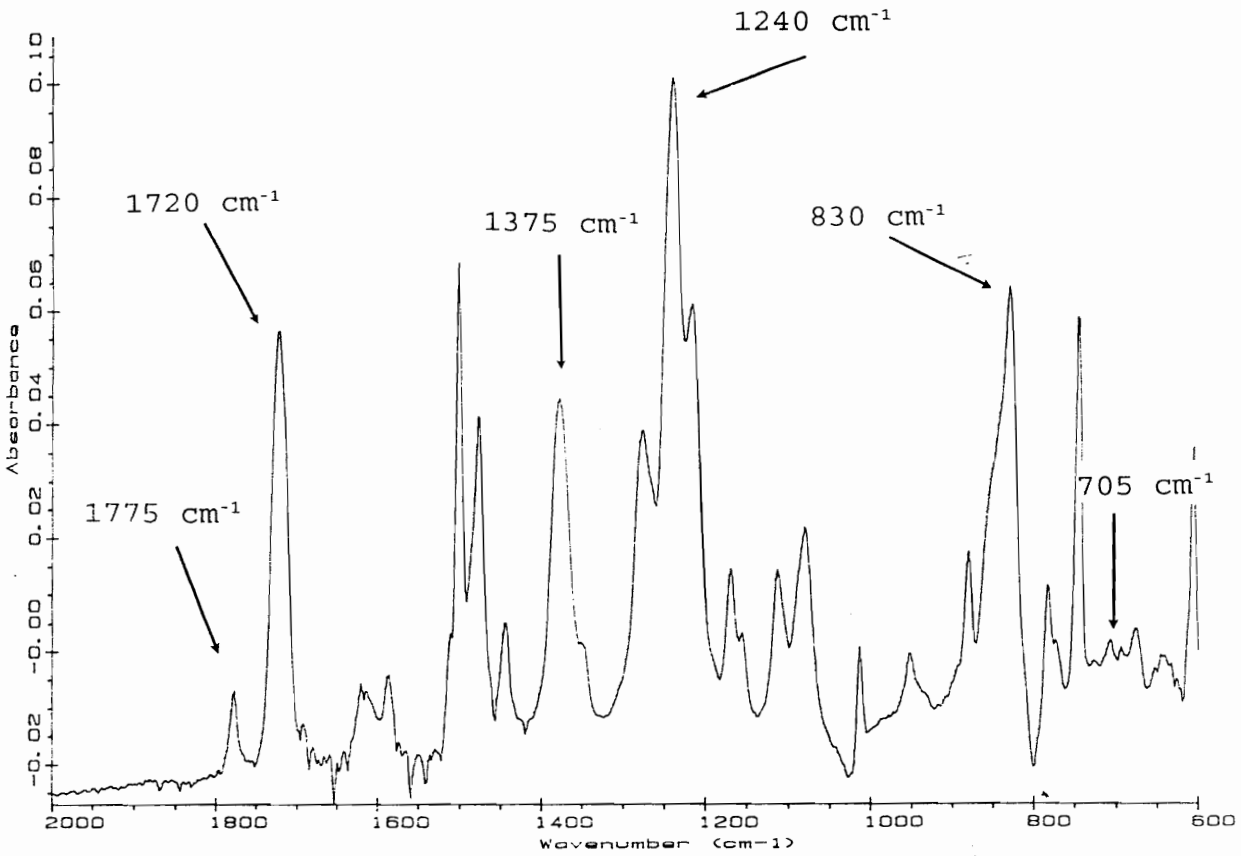

Figure 9. Internal reflectance Infrared Spectrum of Air Cured Non-Modified BDSDA/ODA Film.

The glass side surfaces of the iron-modified films appeared very similar to the non-modified films via XPS. No iron was detected on this surface of the modified films regardless of the additive or cure atmosphere used. The oxygen and sulfur photopeaks were similar to the photopeaks in the non-modified films, and no oxidized sulfur was evident.

The XPS data for the atmosphere sides of the air cured and nitrogen cured iron-modified films, however, were significantly different from the non-modified films and from each other in terms of the chemical state of the iron, sulfur, and oxygen. Thus, all further discussion of XPS data will refer exclusively to the atmosphere side of the films.

The chemical state of the iron seemed to be a function of cure atmosphere, while surface concentration was a function of the additive. In the air cured $Fe(acac)_3$-modified film, iron was detected on the surface with a $2p_{3/2}$ binding energy of 711.8 (±0.5) eV (Figure 10). The atomic concentration of iron detected was 2.9%. If the iron were

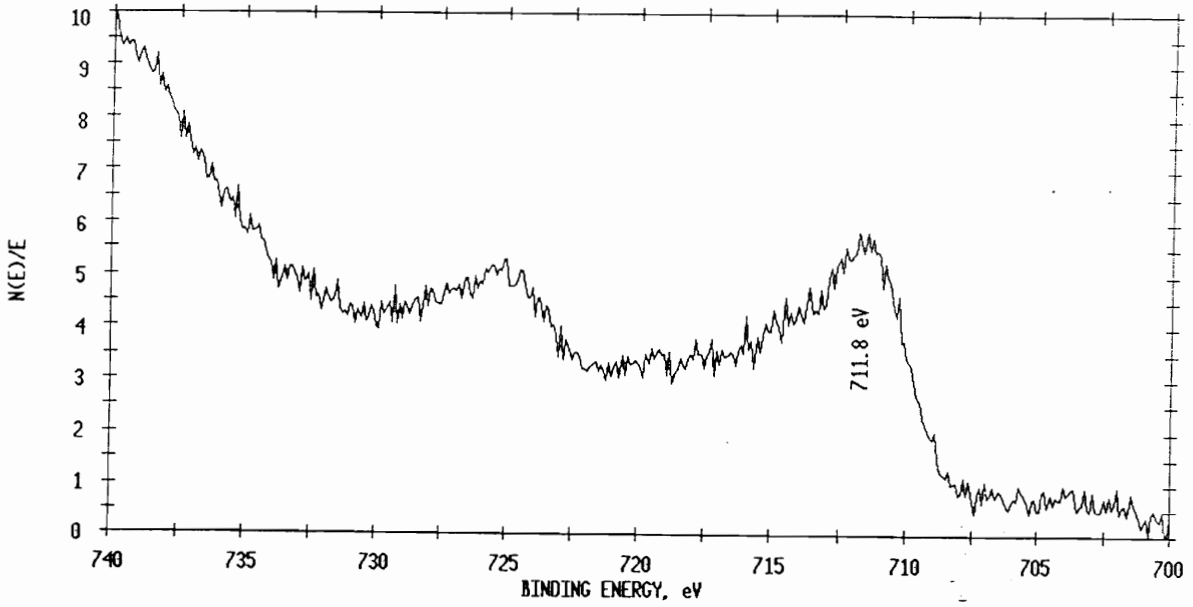

Figure 10. Iron 2p XPS Photopeak of the Atmosphere Surface of Air Cured $Fe(acac)_3$-Modified BDSDA/ODA Film (Binding Energy Calibrated to C 1s = 284.6 eV).

dispersed evenly throughout the film, then an atomic concentration of only 0.5% (one iron atom for every four polymer repeat units) would be expected, indicating a slight enrichment of iron along the atmosphere surface as corroborated by TEMs of that surface. The binding energy of the iron was indicative of iron in the +3 oxidation state [43, 44]. The main iron signal was too weak to ascertain any information from satellite structures with confidence. In the air cured $Fe(bzac)_3$-modified films the binding energy of the iron $2p_{3/2}$ photopeak was 712.0 (±0.1) eV, but the iron only had an atomic concentration of only 0.6% which agreed with the TEMs that showed no surface layer. Thus, changing the ligand from acac to bzac did not seriously affect the binding energy of the iron but did reduce the migration of iron to the surface. This phenomena is most likely due to the increased bulk of bzac compared to acac. In the nitrogen cured $Fe(acac)_3$-modified film (Figure 11), however, the iron $2p_{3/2}$ binding energy was 711.1 (±0.1) eV while the atomic concentration was 3.3%. Thus, cure atmosphere did not appear to profoundly affect the migration of iron to the

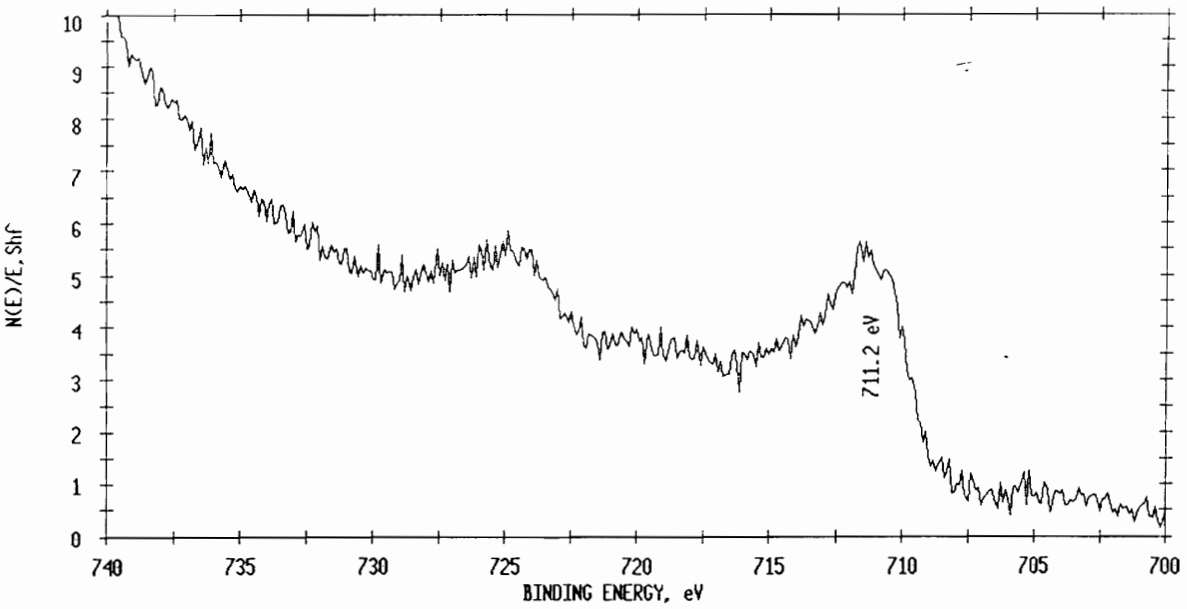

Figure 11. Iron 2p XPS Photopeak of the Atmosphere Surface of Nitrogen Cured $Fe(acac)_3$-Modified BDSDA/ODA Film (Binding Energy Calibrated to C 1s = 284.6 eV).

surface of the film since both air cured and nitrogen cured $Fe(acac)_3$-modified films had concentrations of approximately 3%.

On the other hand, difference in binding energies of the iron photopeaks in the films is probably due to the iron being in different forms of oxide. The iron in the nitrogen cured film had a binding energy similar to that of Fe_2O_3 (710.8 ± 0.2 eV) with a corresponding oxygen 1s oxide peak at 530.1 (±0.1) eV [44]. The ratio of oxide oxygen to iron in this film was 1.8:1 which was close to that of Fe_2O_3 (1.5:1) and similar to results found by Bergmeister [20] in other non-sulfur containing iron-modified polyimide composites. The iron in both the $Fe(acac)_3$- and $Fe(bzac)_3$-modified air cured films had $2p_{3/2}$ binding energies closer to that of FeOOH (711.7 ± 0.2 eV) with corresponding oxygen 1s oxide photopeaks at 530.2 (±0.1) eV (oxide) and 531.2 (±0.2) eV (hydroxide) [44]. The ratio of these oxygens to iron in these films was approximately 1:1:1 (iron:oxide:hydroxide) which is appropriate for FeOOH. The binding energies of the iron 3s and iron $3p_{3/2,1/2}$ photopeaks supported this

conclusion. In the nitrogen cured $Fe(acac)_3$-modified film, the iron 3s binding energy was 93.4 (±0.2) eV and the $3p_{3/2,1/2}$ binding energy was 55.6 (±0.2) eV which agreed with the conclusion that the iron was predominantly present as Fe_2O_3 [44]. On the other hand, the air cured $Fe(acac)_3$-modified composite had an iron 3s binding energy of 93.7 (±0.2) eV and a $2p_{3/2,1/2}$ binding energy of 56.1 (±0.2) eV which supported the assignment of iron in the form of FeOOH.

The other major difference between the atmosphere sides of the iron-modified and non-modified films involved the chemical state of the thioether sulfur. In the air cured $Fe(acac)_3$-modified film, practically all of the thioether sulfur had been converted to a species with a binding energy of 168.2 (±0.1) eV (Figure 12) similar to what was observed in the work of Boggess [24]. Several sulfur species have binding energies in this region, such as sulfone ($-SO_2-$), sulfonate ($-SO_3-$), or sulfate ($-SO_4-$) [45, 46]. New sulfur $2p_{3/2}$ peaks were also observed in the air cured $Fe(bzac)_3$-modified films at 165.8 (±0.1) eV and 167.8 (±0.1) eV that can be assigned to sulfoxide (-SO-) sulfur [36] and

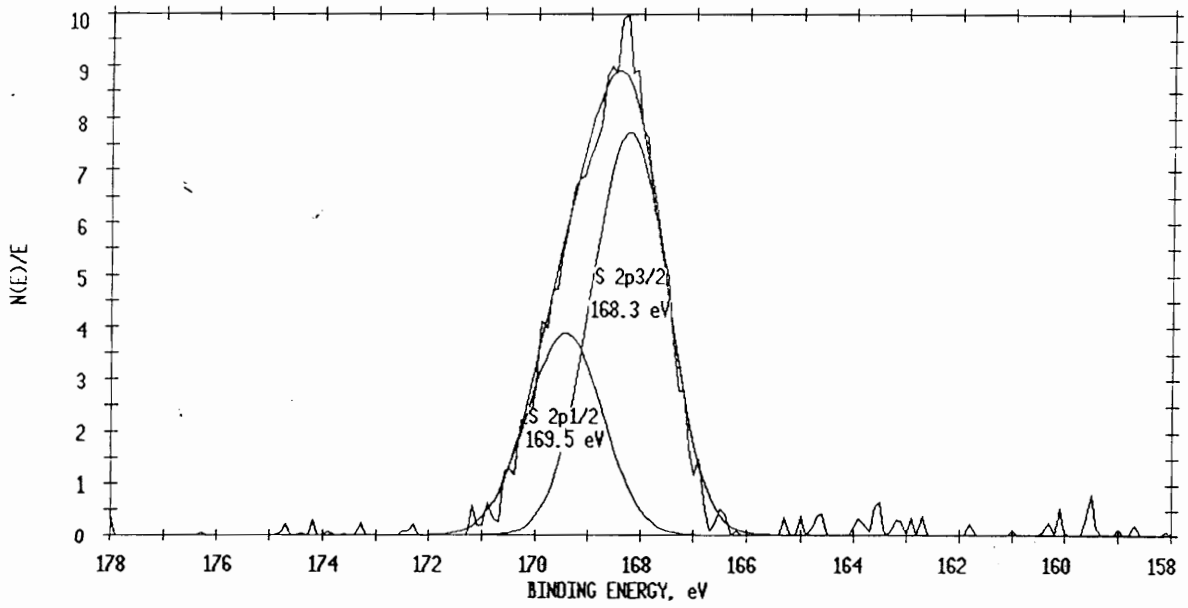

Figure 12. Sulfur 2p XPS Photopeak of the Atmosphere Surface of Air Cured $Fe(acac)_3$-Modified BDSDA/ODA Film (Binding Energy Calibrated to C 1s = 284.6 eV).

sulfone/sulfate sulfur [45, 46], respectively. The majority (55%) of the sulfur resided as in the sulfone/sulfate moiety while the original thioether sulfur constituted 32% of the total amount of sulfur. The sulfoxide sulfur comprised the remaining 13%. These same photopeaks were observed in the nitrogen cured $Fe(acac)_3$-modified films (Figure 13) but in different relative concentrations. As in the $Fe(bzac)_3$-modified films, approximately half of the sulfur was sulfone/sulfonate sulfur, but it had a binding energy similar to the air cured $Fe(acac)_3$-modified films (168.2 ($\pm$0.1) eV). The remainder of the sulfur was equally divided between thioether and sulfoxide sulfur. The total atomic concentration of sulfur was the same (2.1% $\pm$ 0.1%) for both $Fe(acac)_3$-modified films, which corresponded well with the expected atomic concentration of 2.0% for sulfur. The total atomic concentration of sulfur was slightly lower (1.5 $\pm$ 0.1%) in the $Fe(bzac)_3$-modified films.

The oxygen 1s photopeaks (Figure 14 and 15) were more difficult to curve resolve due to the amount of new oxygen species and the close proximity of their binding energies to

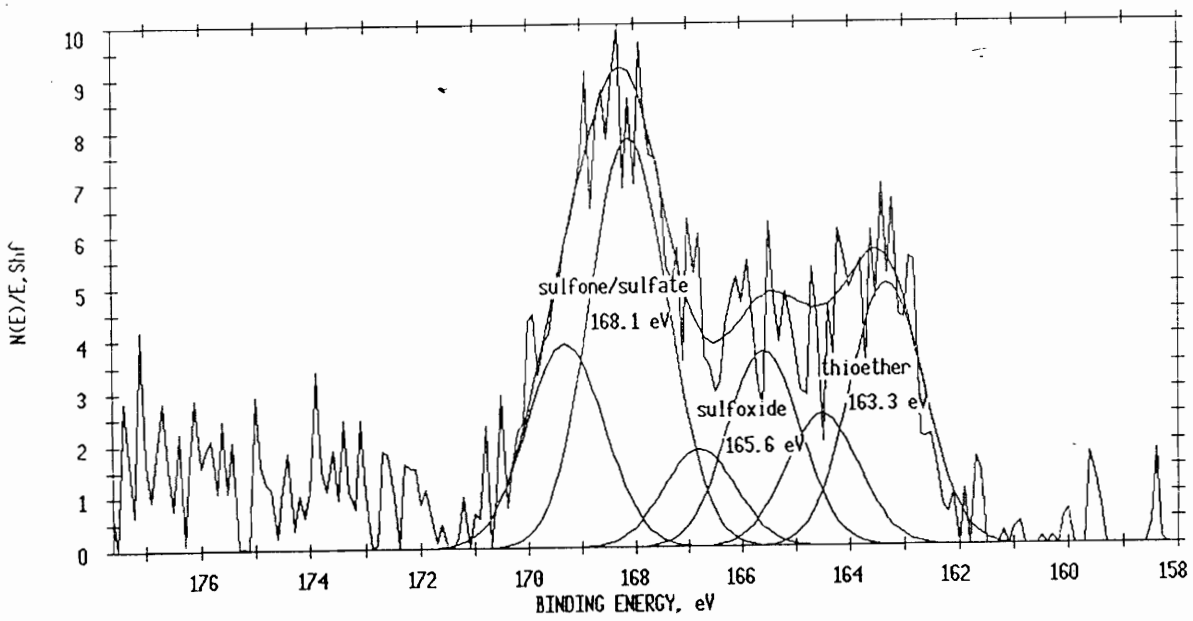

Figure 13. Sulfur 2p XPS Photopeak of the Atmosphere Surface of Nitrogen Cured $Fe(acac)_3$-Modified BDSDA/ODA Film (Binding Energy Calibrated to C 1s = 284.6 eV).

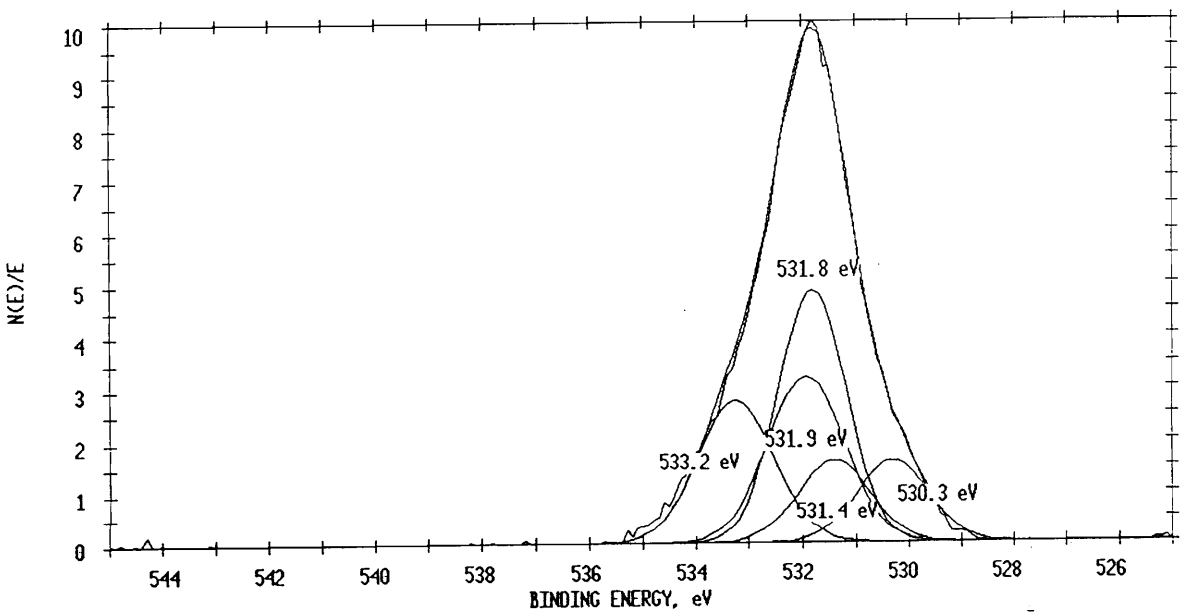

Figure 14. Oxygen 1s XPS Photopeak of the Atmosphere Surface of Air Cured $Fe(acac)_3$-Modified BDSDA/ODA Film (Binding Energy Calibrated to C 1s = 284.6 eV).

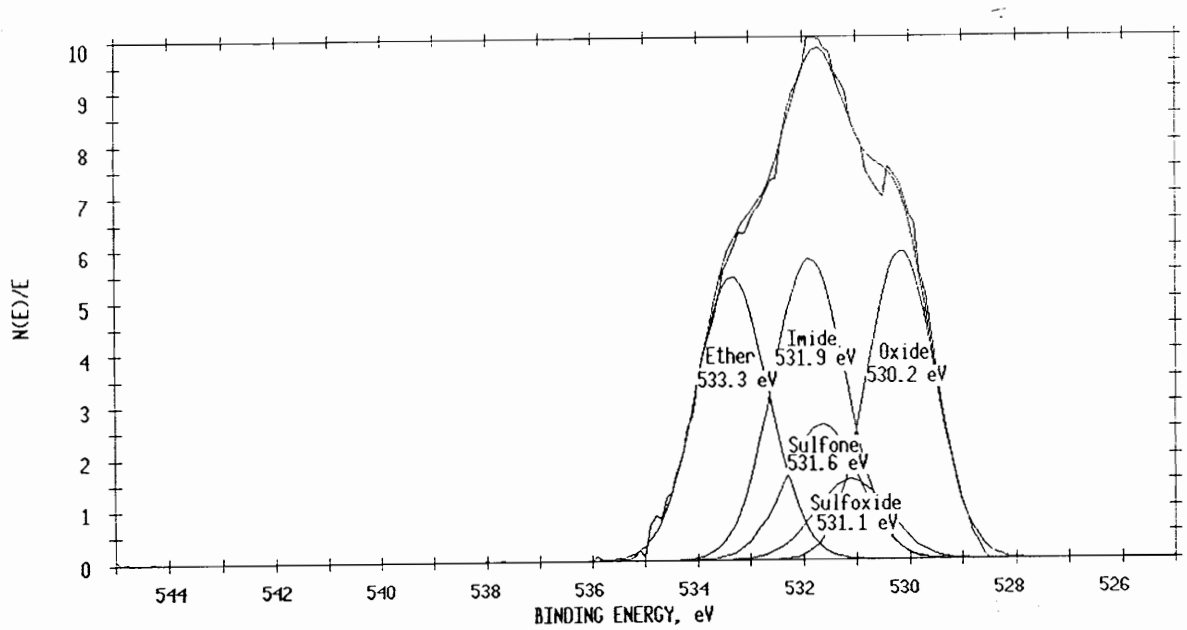

Figure 15. Oxygen 1s XPS Photopeak of the Atmosphere Surface of Nitrogen Cured $Fe(acac)_3$-Modified BDSDA/ODA Film (Binding Energy Calibrated to C 1s = 284.6 eV).

existing photopeaks and to each other. The process used in analyzing the oxygen photopeaks consisted of placing the ether (533.4 ± 0.1 eV) and imide (531.8 ± 0.1 eV) oxygen photopeaks in their known positions, peak widths, and relative concentrations as discussed for the non-modified films. The ether photopeak was placed first since its position was separated from the others to a degree that it was not seriously affected by them. Next, a photopeak was placed at 530.1 (±0.1) eV to represent the contribution from iron oxide [43, 44]. This photopeak was sufficiently separated from the other oxygen photopeaks so that it could be compared with the iron concentration. The final step was to locate the sulfone/sulfate oxygen, if present, at 531.7 (±0.1) eV [39, 45] and the sulfoxide oxygen at 531.2 (±0.1) eV [40] based on literature values. By using the concentrations of the different sulfur species, the concentrations of the corresponding oxygen species were inferred. In the air cured iron-modified films, an additional photopeak, equal in size to the oxide photopeak, was placed at 531.2 (±0.2) eV to represent the contribution

of the hydroxide oxygen of FeOOH. The values in parentheses in Table III are the relative concentrations of each element normalized to four imide oxygens. These new oxygen species contributed to the increase in the total atomic concentration of oxygen. The atomic concentration of oxygen was 30% for the air cured and 25% for the nitrogen cured $Fe(acac)_3$-modified films which is considerably greater than the expected atomic concentration of 14%. The air cured $Fe(bzac)_3$-modified films also had an increased oxygen content with an atomic concentration of 21%. In summary, the major difference between these films was in the relative amounts of oxide oxygen to sulfone/sulfate oxygen and the iron oxide produced. The sulfone/sulfate species was the major product in the air cured $Fe(acac)_3$- and $Fe(bzac)_3$-modified films along with FeOOH; while, iron oxide was more prevalent in the nitrogen cured films.

The most oxidized sulfur (binding energy of 168.2 eV) was difficult to assign due to the close proximity of several different sulfur species in this region. The sulfur to oxygen ratio for this species was approximately 1:4, but

the oxygen photopeak was also difficult to curve fit as mentioned earlier. Therefore, air cured non-modified and $Fe(acac)_3$-modified films using a sulfone containing monomer (DSDA) and ODA were examined to more fully characterize this phenomenon. The sulfone sulfur photopeak in the non-modified DSDA/ODA had a binding energy of 167.7 (±0.1) eV.

The iron in the $Fe(acac)_3$-modified DSDA/ODA seemed to be in a similar state as the air cured $Fe(acac)_3$-modified BDSDA/ODA, *e.g.* FeOOH, with a binding energy of 711.7 (±0.1) eV (Figure 16). The sulfur $2p_{3/2}$ photopeak in the iron-modified DSDA/ODA film had a binding energy of 167.5 (±0.1) eV, similar to that of the non-modified film, but was also broader than the sulfur photopeak of the non-modified film (Figure 17). When the curve fit for the non-modified sulfur photopeak was used with the $Fe(acac)_3$-modified sulfur photopeak, the left or higher binding energy side of the photopeak was not adequately covered. This area would be where sulfur that was more oxidized than sulfone would be located. Thus, this broadening could indicate further oxidation of sulfone to some sort of sulfonate or sulfate.

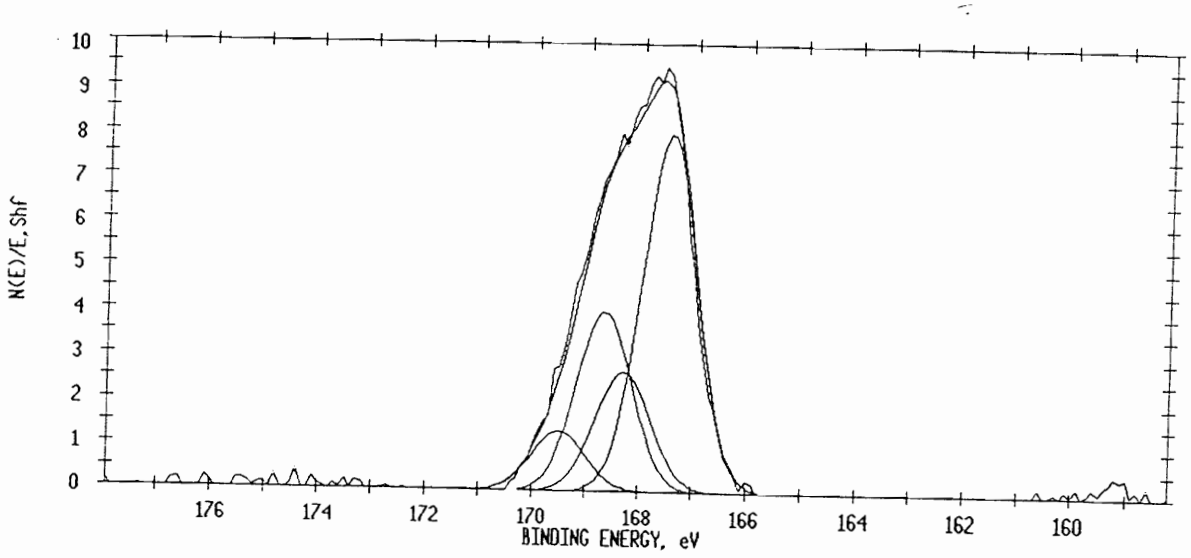

Figure 16. Sulfur 2p XPS Photopeak of the Atmosphere Surface of Air Cured $Fe(acac)_3$-Modified DSDA/ODA Film (Binding Energy Calibrated to C 1s = 284.6 eV).

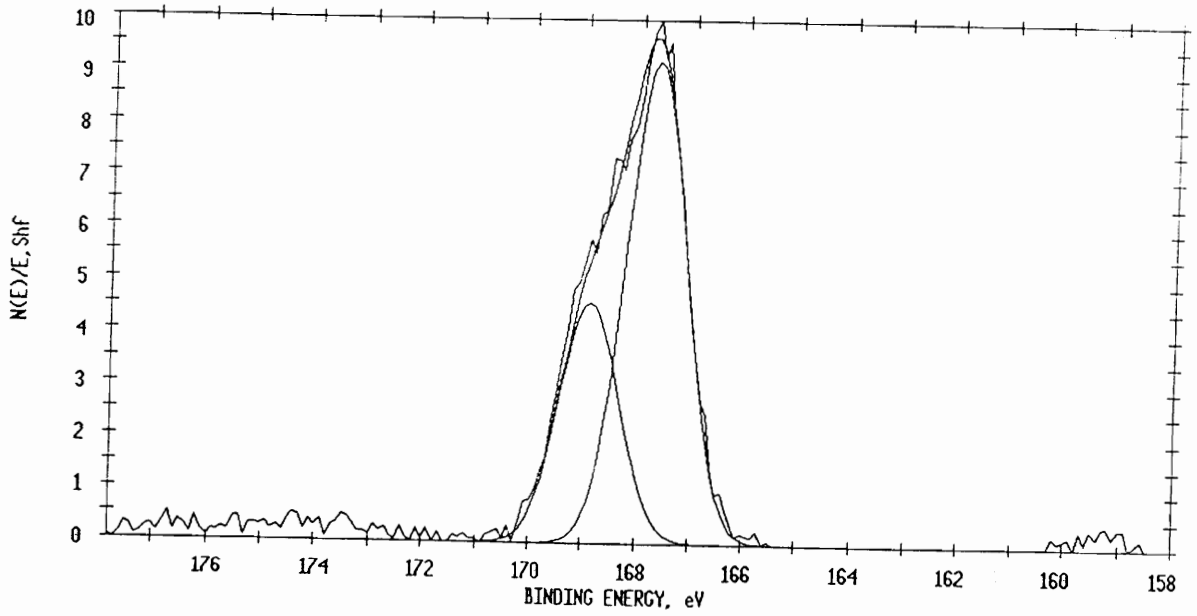

Figure 17. Sulfur 2p XPS Photopeak of the Atmosphere Surface of Air Cured Non-Modified DSDA/ODA Film (Binding Energy Calibrated to C 1s = 284.6 eV).

Internal reflectance IR spectroscopy was used to gain additional information on the chemical state of sulfur on the atmosphere side of the air cured and nitrogen cured $Fe(acac)_3$-modified BDSDA/ODA films. Similar adsorption bands were observed (Figure 18) as those described earlier for the non-modified films. Also, no adsorption bands indicative of sulfone were observed. A new band was observed at 1270 cm^{-1} in both composite films but was more prominent in the air cured film. The air cured $Fe(acac)_3$-modified film also had a new adsorption band at 1030 cm^{-1}. These bands corresponded to several possible species. A sulfate salt ($RSO_4^-M^+$) has a characteristic adsorption SO_2 stretching band in the region 1315-1220 cm^{-1} which often occurs as a doublet at ~1250 and ~1220 cm^{-1} [47]. A comparison of the air cured non-modified and $Fe(acac)_3$-modified spectra showed the disappearance of a valley in the 1220 cm^{-1} region that had been in the non-modified film (Figure 19). Also, an aromatic sulfate salt has a characteristic symmetric SO_2 stretch around 1040 cm^{-1} [47]. Sulfonic acid salts ($RSO_3^-M^+$) have characteristic adsorption

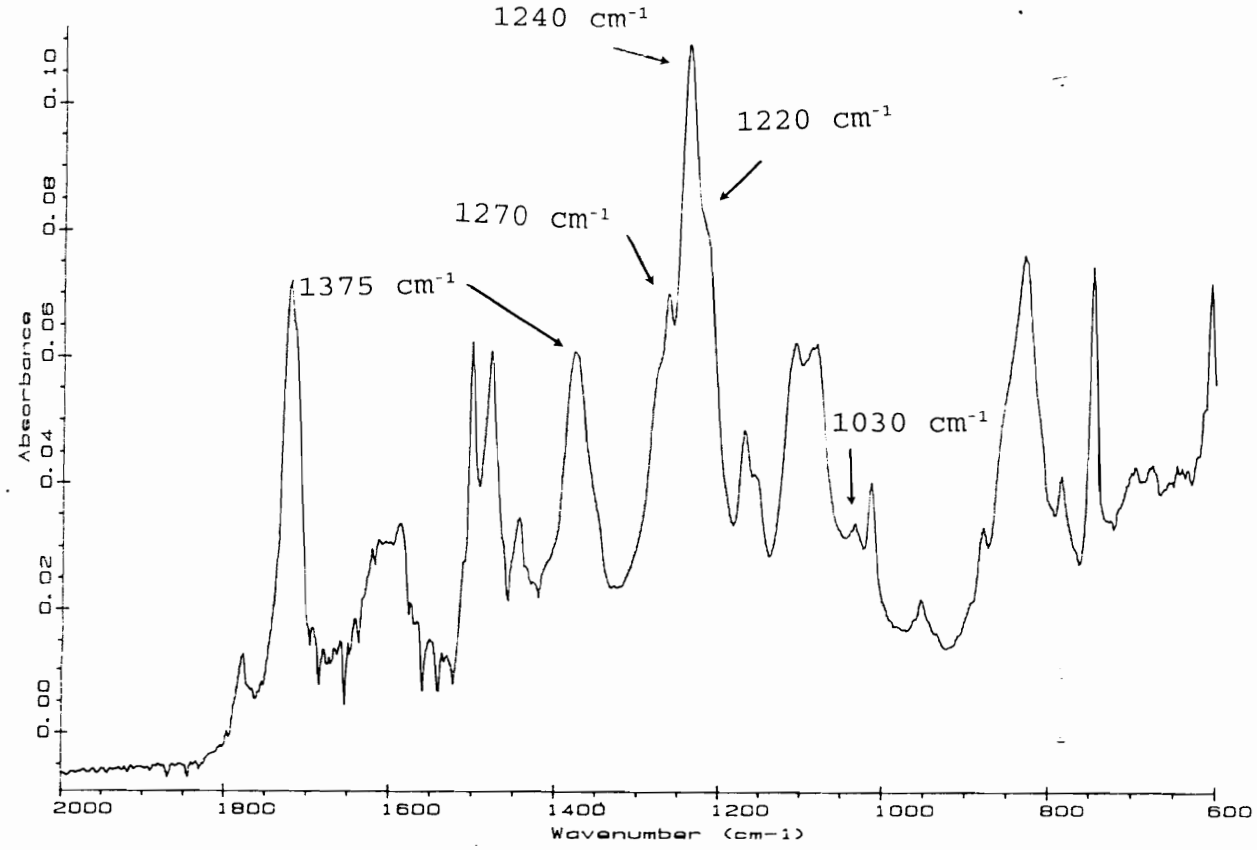

Figure 18. Internal reflectance IR Spectrum of Air Cured $Fe(acac)_3$-Modified Film.

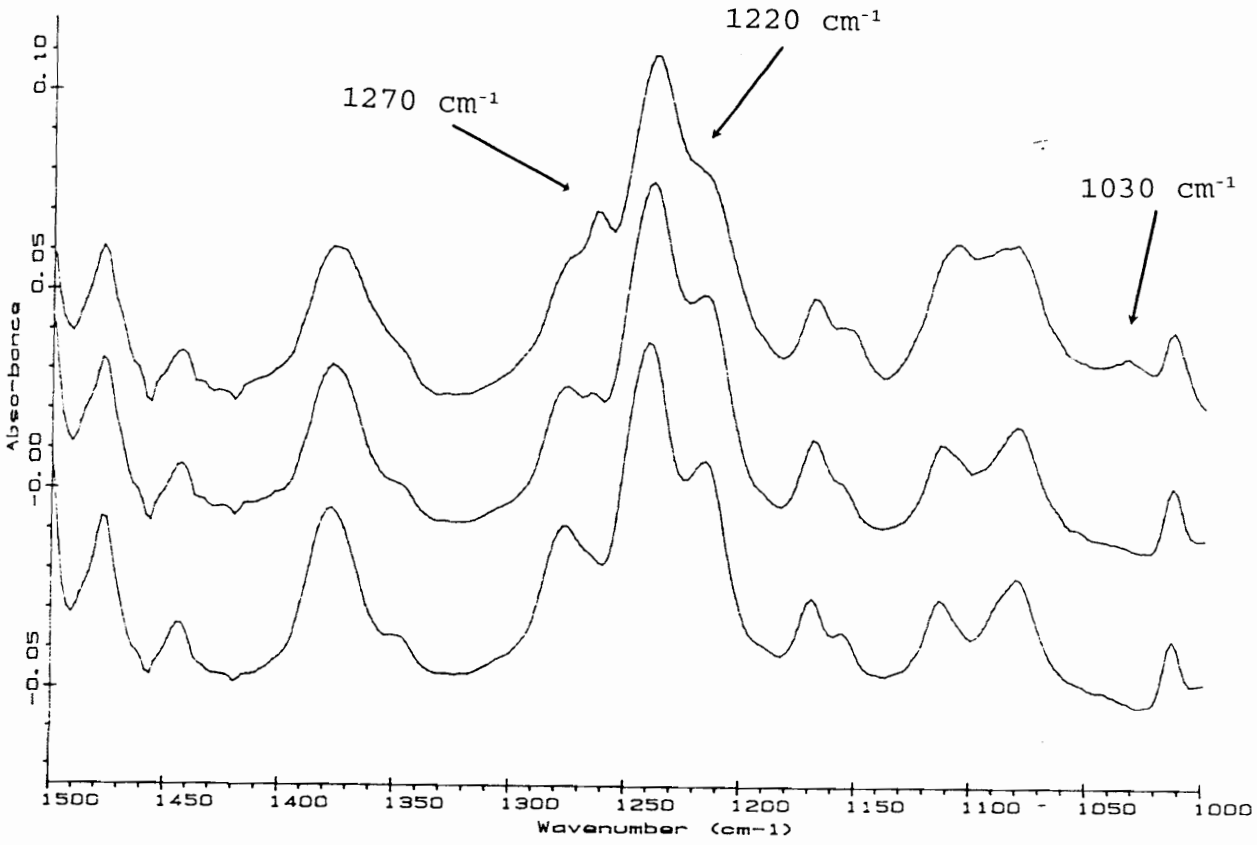

Figure 19. Internal reflectance IR Spectrum of Air Cured Non-Modified (bottom), Nitrogen Cured $Fe(acac)_3$-Modified (middle), and Air Cured $Fe(acac)_3$-Modified (top) BDSDA/ODA Films.

bands at 1250-1140 cm^{-1} (asymmetric SO_3 stretch) and 1070-1030 cm^{-1} (symmetric SO_3 stretch)[47]. The actual position of adsorption bands in both sulfate and sulfonic acid salts are strongly influenced by the metal ion. The adsorption band at 1030 cm^{-1} could also be due to a sulfoxide SO stretch which usually occurs ~1060 cm^{-1} in aromatic compounds [47]. A diffuse reflectance IR spectrum was collected for $Fe(acac)_3$ to make sure that these new peaks were not due to the additive (Figure 20). From a comparison of this spectrum and those for the $Fe(acac)_3$-modified films, it was apparent that no iron remains as $Fe(acac)_3$ along the surface of the film. Unfortunately, most adsorption bands corresponding to characteristic adsorption bands of Fe_2O_3 and FeOOH were not able to be identified. One adsorption band, however, that corresponds to γ-FeOOH occurs at 1026 cm^{-1} which could also explain the band at 1030 cm^{-1} in the air cured $Fe(acac)_3$-modified film [48].

Iron-BDSDA/ODA Interactions

From the XPS and IR data, it was evident that two

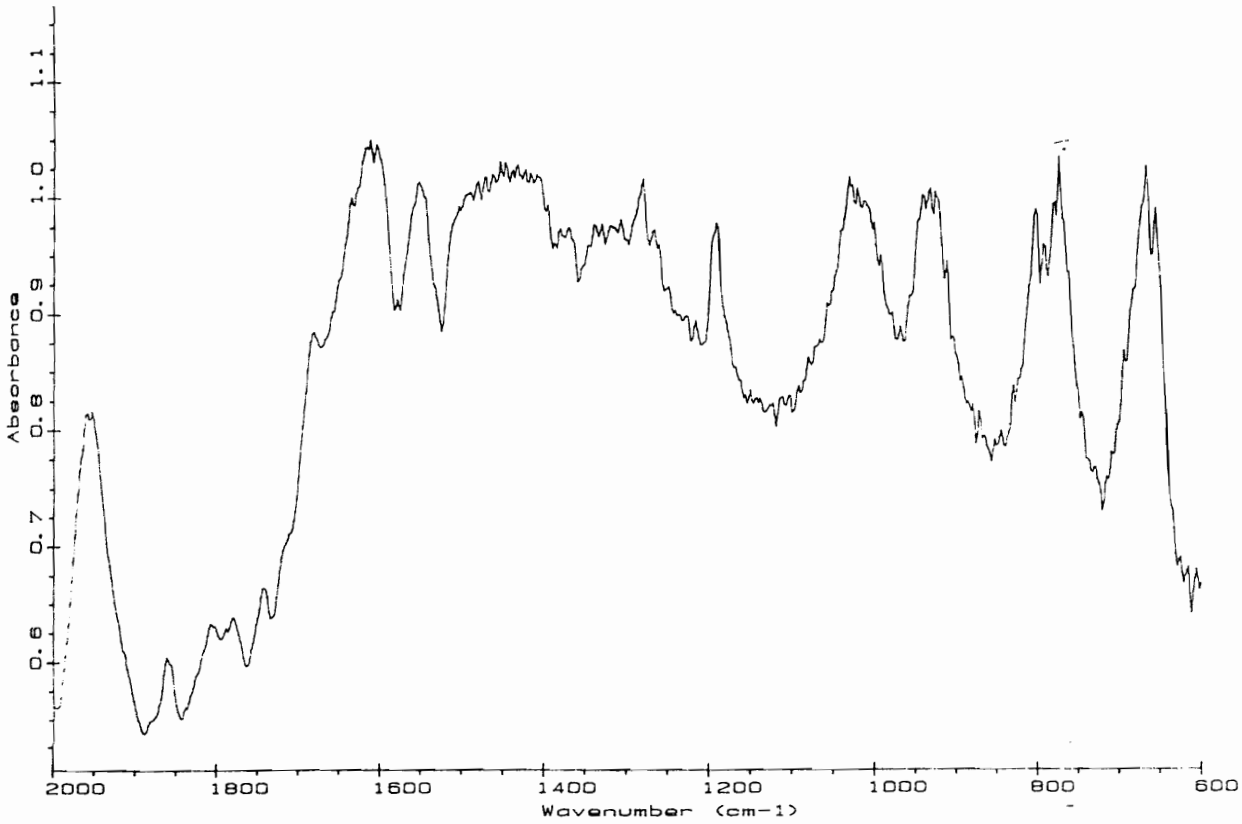

Figure 20. Diffuse Reflectance IR Spectrum of $Fe(acac)_3$.

reactions occurred along the atmosphere side during the thermal curing process: (a) conversion of the modifier to iron oxide and (b) oxidation of the thioether sulfur at least to sulfone and possibly either a sulfonate or sulfate. The extent to which both reactions were carried out appeared to be dependent on the cure atmosphere used.

It is hypothesized that during the cure the water of imidization reacted with the modifier to form $Fe(OH)_3$ as an intermediate and the corresponding Hacac or Hbzac. Such a reaction could occur through the following reaction:

$$Fe(acac)_3 + 3\ H_2O \text{ -------> } Fe(OH)_3 + 3\ Hacac$$

During this conversion, the thioether sulfur probably binds to the iron complex through a vacant ligand site and trapping the iron in place (Figure 21) [38]. In the work by Bergmeister [20], significant amounts of iron oxide had migrated to the surface as observed by XPS after only curing the non-sulfur containing composite to 100°C. In the air cured $Fe(acac)_3$-BDSDA/ODA composite, however, iron oxide and oxidized sulfur were not observed by XPS in the composite after curing to 200°C. No iron oxide particles were

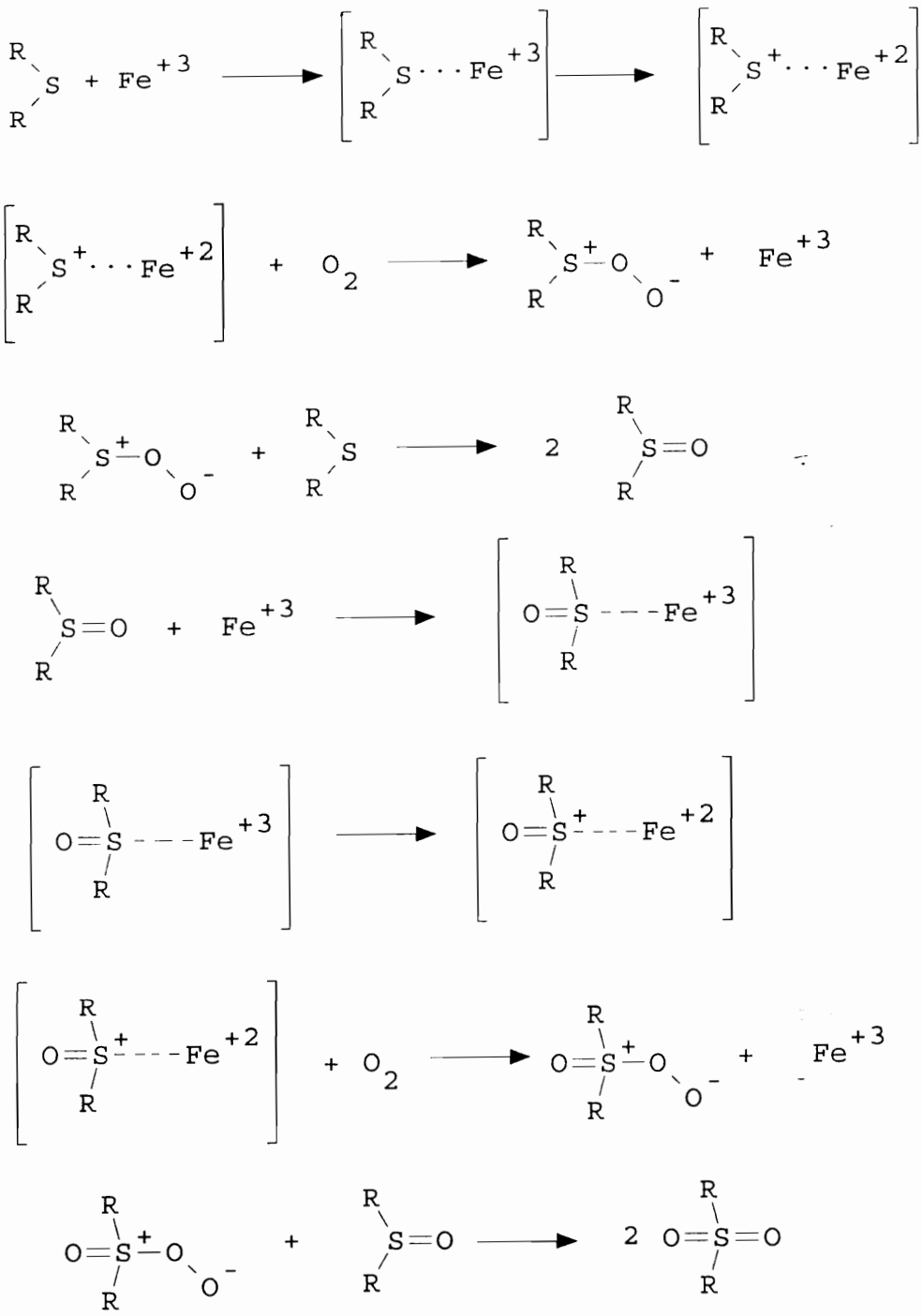

Figure 21. Mechanism of Iron Catalyzed Oxidation of Thioether Sulfur.

observed by TEM, either. Thus, it appeared that the sulfur trapped the iron on a molecular scale until the oxide was formed which could explain the lack of observable particles by TEM.

The oxidation of the thioether was probably caused by the transition metal catalyzed reaction with molecular oxygen. Both transition metal oxides and transition metal complexes, including $M(acac)_x$, catalyze this reaction [38, 49]. Apparently, the sulfur binds to the transition metal which activates the complex for attack by oxygen. Both water and molecular oxygen have been used as sources of oxygen for this reaction [38]. The only source of oxygen available to the nitrogen cured films would be from the water of imidization. Much less oxygen, therefore, would be available to participate in the oxidation of the sulfur than in the air cured films. Also, molecular oxygen would be much better at producing the oxidized product. Thus, the presence of the molecular oxygen is a probable explanation for why the thioether sulfur along the surface was completely oxidized in the air cured $Fe(acac)_3$-modified

film, while a mixture of products was the result in the nitrogen cured $Fe(acac)_3$-modified film. The air cured $Fe(bzac)_3$-modified film produced a mixture of products because there was no surface enrichment of iron to help catalyze the reaction as there was in the case of the $Fe(acac)_3$-modified film. Studies of silver-modified sulfur-containing polyimides by Rubira [50], have shown oxidation of the thioether sulfur along the glass side when silver metal was present on that side of the film. This feature was not observed here because no metal was observed on the glass sides of the films.

The different forms of iron oxide produced could be explained by the different cure atmospheres used. A possible explanation was that the oxidation of the sulfur by molecular oxygen, present in the air cure, created an ionic sulfonate/sulfate group that, in turn, coordinated to the iron during its conversion and prohibited the complete dehydration of the $Fe(OH)_3$ to form Fe_2O_3. Thus, the iron remained as FeOOH. Even after curing for an additional hour at 300°C, the iron was still present as FeOOH. In the

nitrogen cured iron-modified composite, however, the only source of oxygen was from the water of imidization. It appeared that the weaker oxidizing nature of water only oxidized the sulfur to a covalent sulfonate (RSO_3R) or sulfate (RSO_4R) which did not coordinate as strongly to the iron and did not prevent the conversion of $Fe(OH)_3$ to Fe_2O_3.

Other metal complexes were also examined to see how they would affect this oxidation. $VO(acac)_2$ is an excellent homogeneous catalyst for the oxidation of thioether sulfur [38]. Therefore, this complex was used in a polyimide composed of BTDA and ASD and cured in air to examine the effect of $VO(acac)_2$ and the possibility of oxidation of thioether sulfur in the diamine portion of the polyimide. Since $VO(acac)_2$ did not dissolve in the poly(amide acid), this composite also examined the effects of heterogeneous modification. The binding energy of the V 2p photopeak was 517.0 (±0.1) eV which indicated that it resided as V_2O_5 and not $VO(acac)_2$ which has a binding energy of 515.1 eV [51]. The binding energy of the sulfur (167.6 (±0.1) eV) indicated that it had been oxidized and was no longer thioether

sulfur. $Al(acac)_3$ was used as another modifier with BDSDA/ODA which was cured in air to examine the effects of a non-transition metal on the thioether sulfur. The Al 2p binding energy of 74.2 (±0.1) eV indicated that the modified was converted to Al_2O_3 and was no longer $Al(acac)_3$ (72.7 eV) [51]. Some of the sulfur was converted to sulfoxide (~20%) and sulfonate/sulfate (~10%) sulfur, but the majority (>70%) remained as the thioether sulfur (Figure 22). Thus, it appeared that non-transition metal complexes were not as active in catalyzing the oxidation reaction. The most likely reason for this reduction in catalytic activity for aluminum is due to its only having valent states of 0 and +3. Therefore, it was not able to go through the one electron reduction as the Fe^{3+} ion was able to do and had to proceed through a different pathway. Most likely, in the case of aluminum, a lone electron pair on the sulfur atom was shared by an empty orbital on aluminum in order to form the intermediate. This sharing of electrons weakened the C-S bond resulting in a homolytic cleavage and the formation of $R\cdot$ and $RS\cdot$ radicals. Molecular oxygen then reacted with

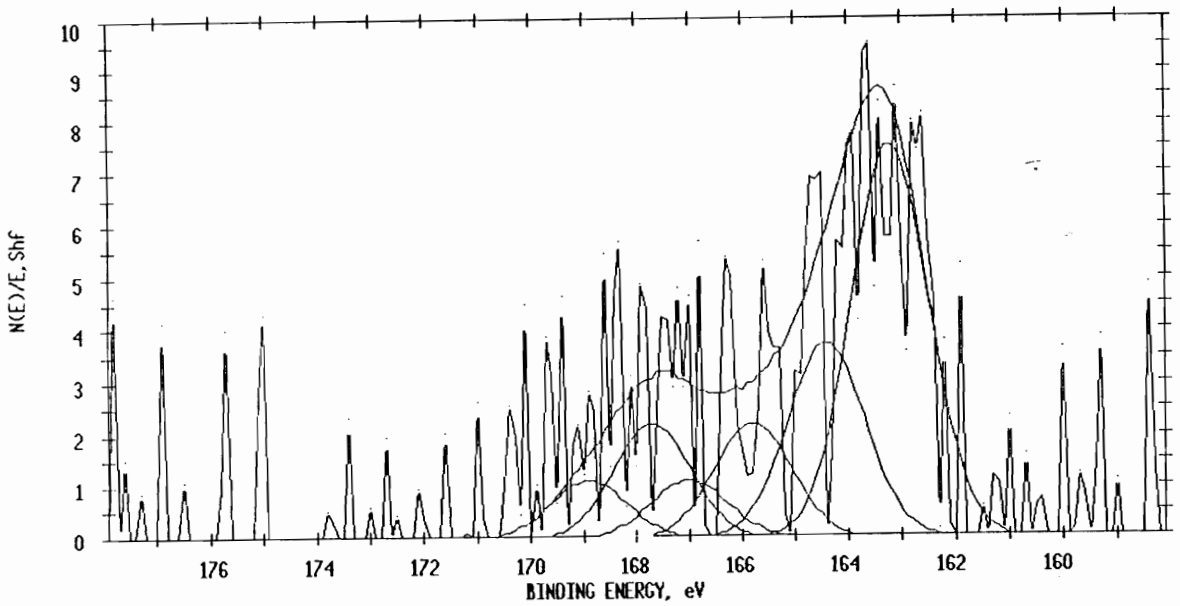

Figure 22. Sulfur 2p XPS Photopeak of the Atmosphere Surface of Air Cured $Al(acac)_3$-Modified BDSDA/ODA Film (Binding Energy Calibrated to C 1s = 284.6 eV).

these radicals to produce the oxidized products (Figure 23) [38].

From this interpretation of the data, the contradictory nature of the previous studies using copper [23], cobalt [24], and silver [28] can be explained. In the case of the copper, the surface sulfur, with a binding energy of ~168.6 eV, was mistakenly taken to be the thioether sulfur of the polyimide backbone. Thus, when a new sulfur photopeak was observed at ~163.4 eV after an argon ion etch, it was mistakenly assumed to indicate the copper was directly chelated to the sulfur. This interpretation was then used to explain the lack of particles in the TEMs. From the data in this present study with iron, it is apparent that all of the surface sulfur was oxidized to sulfonate/sulfate sulfur. Only after etching down into the film was the original sulfur observed. The metal-sulfur interaction which prevents the aggregation of particles could be direct chelation or some sort of M-O-S species. The conclusions in the study dealing with cobalt are mostly in agreement with this present study, but Boggess only hypothesized oxidation

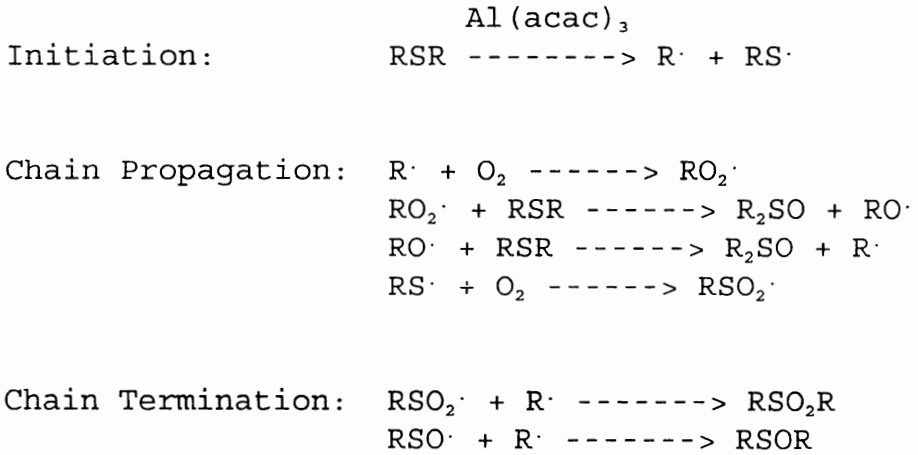

Figure 23. Mechanism of Aluminum Catalyzed Oxidation of Thioether Sulfur.

to sulfoxide and/or sulfone. Further examination by IR was not performed. In the study with silver, coordination of silver to thioether sulfur was assumed to be the explanation for the higher binding energy photopeaks of sulfur and the reduced silver migration. While oxidation of the sulfur was not ruled out, no adsorption bands attributable to either sulfoxide or sulfone were observed by IR. The IR spectra shown in this present study with iron do provide evidence of oxidized sulfur.

SUMMARY

XPS and internal reflectance data have shown that the presence of transition metal complexes correspond to the presence of oxidized sulfur in sulfur containing polyimides. Without the metal complex, sulfur is not oxidized and remains as thioether. The extent of oxidation is dependent on the cure atmosphere, metal, and ligand involved. An air cure corresponded to much more oxidation than a nitrogen cure which had much less oxygen. Transition metals, such as iron, vanadium, copper [23], cobalt [24], and silver [28], were better at catalyzing the oxidation than non-transition

metals such as aluminum. Also, bulkier ligands, such as bzac, prevented the metal from migrating through the polyimide which resulted in less oxidation.

This oxidation of sulfur in the polyimide backbone could be beneficial in adhesive situations. Since this oxidation has been observed on the glass side surface when metal is present, it would seem that this reaction could occur when sulfur-containing polyimides were used with transition metal substrates, such as steel or titanium. Granted, these substrates are not the same as the metal complexes, but metal oxides can also catalyze this oxidation [38, 49]. The resulting sulfonate/sulfate moiety could form stronger bonds to the metal substrate. The thioether itself may allow the polyimide to form stronger bonds to transition metal substrates since the thioether appeared to be responsible for keeping the iron particles dispersed on a molecular scale in the composites. It is also possible that this oxidation of the thioether sulfur could damage the polyimide resulting in the formation of a weak boundary layer at the interface.

III. NON-DESTRUCTIVE ANALYSIS OF ADHESIVE MODIFIER LOCATION VIA TRANSMISSION ELECTRON MICROSCOPY

INTRODUCTION

It has been shown that the *in situ* generation of metal/metal oxide particles in polyimide films enhances the electrical [19], magnetic [20], or adhesive [21, 22] properties of the polyimide. It had also been hypothesized that the formation of a concentration gradient of a suitable metal species in the polyimide adhesive near the adhesive/adherend interphase would also enhance adhesive strength [52, 53]. More specifically, one of the weaknesses in any bond structure is the abrupt change in physical properties between the organic polymeric adhesive and the inorganic metallic adherend in the interphase region. A concentration gradient should reduce the change in physical properties that occurs between the metallic adherend and the polymeric adhesive. An inherent problem for examining this hypothesis, however, is determining where the actual metal/metal oxide particles reside in the bond itself. Several methods including transmission electron micrographs

(TEM) of simulated bonds [52] and X-ray photoelectron spectroscopy (XPS) of failed bond surfaces [53] have been used in the attempt to determine if the concentration gradient was formed within the adhesive. Neither of these methods was successful in demonstrating the presence or absence of a concentration gradient of metal/metal oxide particles within an actual bond.

Previous work studying the *in situ* generation of metal/metal oxide species in thin polyimide films has greatly benefitted from the use of TEM [21-22, 52, 54-57] which permitted the examination of particle size and location within the free standing film. Simulated bonds [52] have been studied wherein modified polyimides were cured in the oven to 200°C on glass plates and then "bonded" between two pieces of Kapton® in a hot press to 300°C under pressure. TEM was performed on these samples, but the particle distribution was not necessarily similar to what exists in an actual bond with metal adherends.

Still, TEM is one of the best methods to examine particle distribution. The problem associated with

performing TEM on metal interfaces, however, is the thickness of the metal. The metal has to be very thin in order to be ultramicrotomed without damaging the knife. To overcome this problem, samples have normally been prepared in one of three general methods: 1) deposition of a thin layer of metal onto a polymeric substrate, 2) deposition of a polymer layer onto a thin metal substrate, or 3) cutting or ion milling of the sample.

Deposition of metal onto the polymer is a common technique used frequently in the microelectronics industry. This technique was used in a study by Silvain and co-workers for examining the interface between aluminum and polyethylene terephthalate (PET) [58]. In Silvain's study, an aluminum layer (50-60 nm in thickness) was vapor deposited onto a PET film. These composites were examined via TEM and 180° peel test were performed. They found that smaller aluminum grain sizes corresponded to increased peel strength. Metal deposition onto polyimide surfaces has also been studied. Ho and co-workers have examined the deposition of titanium, aluminum, nickel, and copper onto

pyromellitic dianhydride-oxydianiline (PMDA/ODA) polyimide films [59-63]. The metal in these studies was deposited onto the surface of the polyimide film in a layer up to 50 nm thick. Ultraviolet photoemission spectroscopy (UPS), XPS, and TEM were used to study these interfaces. The thickness of the metal layer was no problem for TEM analysis. The method of formation of the interface, however, was very different from the formation of a metal-polymer interface in a structural adhesive where the polymer is coated onto solid metal.

TEM analysis has also been performed on polyimide-metal composites where the polyimide was applied to the metal. Studies by Kim and co-workers have examined the interface between PMDA/ODA and copper [64-67]. The polymer-on-metal interfaces were produced by spin coating the poly(amide acid) onto 25 μm thick copper foil. The copper foil had previously been covered with a thin (200-500 nm) layer of copper [64-66], chromium [66], nickel [66], or gold [66] through vapor deposition. Thin layers of palladium, platinum, or chromium were investigated as passivation

layers [67] because copper was shown to react with the poly(amide acid) during the thermal curing. These studies also showed that peel strength was much greater when the polyimide was cast on metal rather than when the metal was deposited onto the polyimide [66]. The thickness of the sample, however, was such that it presented no problem for ultramicrotoming.

Larger metal substrates were used in studies by Crompton [68] and Adema and co-workers [69]. In these studies, samples were prepared via cutting and ion milling until they reached a thickness which could be ultramicrotomed. The study by Crompton examined the interface between aluminum and single-part heat-curing epoxies, but no correlation was made with adhesive strength. Adema and co-workers [69], on the other hand, only studied the effects of the interface on electrical performance. These studies [68,69] used somewhat larger substrates, but no correlation was made between TEM results and adhesive strength.

The study described here examines the application of

TEM analysis to complete bond systems. Samples have been prepared using the same procedure as samples for adhesive tests. The bonds consisted of high purity (99.99%) aluminum foil with a polyimide adhesive. A solution of NaOH was used to etch the foil to a thickness suitable for ultramicrotoming. TEMs of these samples showed the entire bond line from one interface to the other. Information about the particle size and spatial distribution of the modifier was obtained and compared with the adhesive strength afforded by the modified polyimides.

EXPERIMENTAL

Materials

The dianhydrides used in this study were BDSDA and BTDA. ODA and APB were the diamines used. The only modifier used was $Fe(acac)_3$, and the solvent was DMAc. These materials were treated as discussed in the previous chapter. High purity aluminum foil (99.99%) aluminum foil (0.10 mm thick) was used as the adherend.

Synthesis

Poly(amide acid) solutions were made as described in Chapter II.

Bonding

The aluminum substrates were pretreated via a chemical etch that consisted of immersing the aluminum in an aqueous 5% NaOH (w/w) bath for thirty seconds at room temperature followed by a rinse with deionized water. The aluminum was then immersed in a 10% HNO_3 (w/w) solution for ten seconds, rinsed with deionized water, and air dried.

The bond samples were prepared by casting the poly(amide acid) solution at a thickness of 0.051 mm onto two pieces (4" x 6") of the pretreated aluminum foil. These coated substrates were then cured under a dynamic air atmosphere at 80°C for 20 minutes and at 100° and 200°C for an hour each under either a dynamic air or nitrogen atmosphere. Next the coated substrate were placed, adhesive sides together, in a Carver Hot Press. The specimen was heated to 200°C under contact pressure. The system was then heated for an hour each at 200° and 300°C under 500 psi.

The press was then allowed to cool to room temperature under pressure. Samples to be prepared for TEM were cut (2" x 2") from the bonded foil; the rest of the bonded sample was cut into 0.5 cm strips for peel testing.

Preparation of TEM Samples

The 2"x2" bond squares was immersed in a 1.25N NaOH solution at 50°C for approximately 35 minutes. After this time the bond sample, which was then approximately 50 microns in thickness, was rinsed with distilled water. The actual TEM specimen was removed from the center of the sample in order to eliminate any effects of the etch occurring along the edge of the bonded sample.

Measurements

Peel strength was determined using the T-peel test on a Model 1123 Instron tensile tester with a 5 kN load cell at a cross head rate of 100 mm/min. TEMs were taken with a Philips Model 420 Scanning Transmission Electron Microscope. The samples for TEM analysis were embedded in Polyscience ultra low viscosity resin and cured for eight hours at 70°C. A Reichert-Jung ultramicrotome and a microstar diamond knife

were then used to obtain sections of the samples between 500 and 800Å. These sections were then placed on 200-mesh copper grids for analysis.

RESULTS AND DISCUSSION

Bond TEMs

The particles which formed in the iron-modified BDSDA/ODA bonded aluminum specimens were considerably different from those seen in the iron-modified BDSDA/ODA free standing films. It was shown in Chapter II that particles in the iron-modified BDSDA/ODA free standing films formed either a discontinuous or continuous surface layer with a thickness of 60 nm on the atmosphere side depending on whether the film was cured in air or nitrogen, respectively (Figures 5-6). Very few if any particles were seen in the bulk of the film or on the glass side of the film. The glass side of the film would be analogous to the polyimide/aluminum interface in the bonded specimen. Therefore, judging by the free standing films, no concentration gradient or even **any** particles would be

expected at the interface in the bonded specimen. TEM analysis of the bonded specimen, however, did indicate the formation of particles along the interface (Figures 24-25). These particles were 5-10 nm in diameter and were distributed evenly throughout the bond (Figures 26-27). Thus, the particle formation in the bonded specimen was very different from that seen in the free standing film. If the surface layers observed in the free standing films (Figures 5-6) had been observed in the bonded specimens, then a layer of particles would have been seen at the center of the bond (Figure 28). This layer was not observed in the TEMs of the bond cross sections (Figures 29-30). Unlike the free standing films, however, little difference was observed between bonds that had been precured in air and in nitrogen.

The extra hour in the curing cycle for the bonds could have been responsible for the increased number of particles. Therefore, an iron-modified BDSDA/ODA bond was prepared which omitted the 200°C stage in the press; thus, seeing the same thermal curing cycle as the free standing films. No difference was observed between the TEMs of this specimen

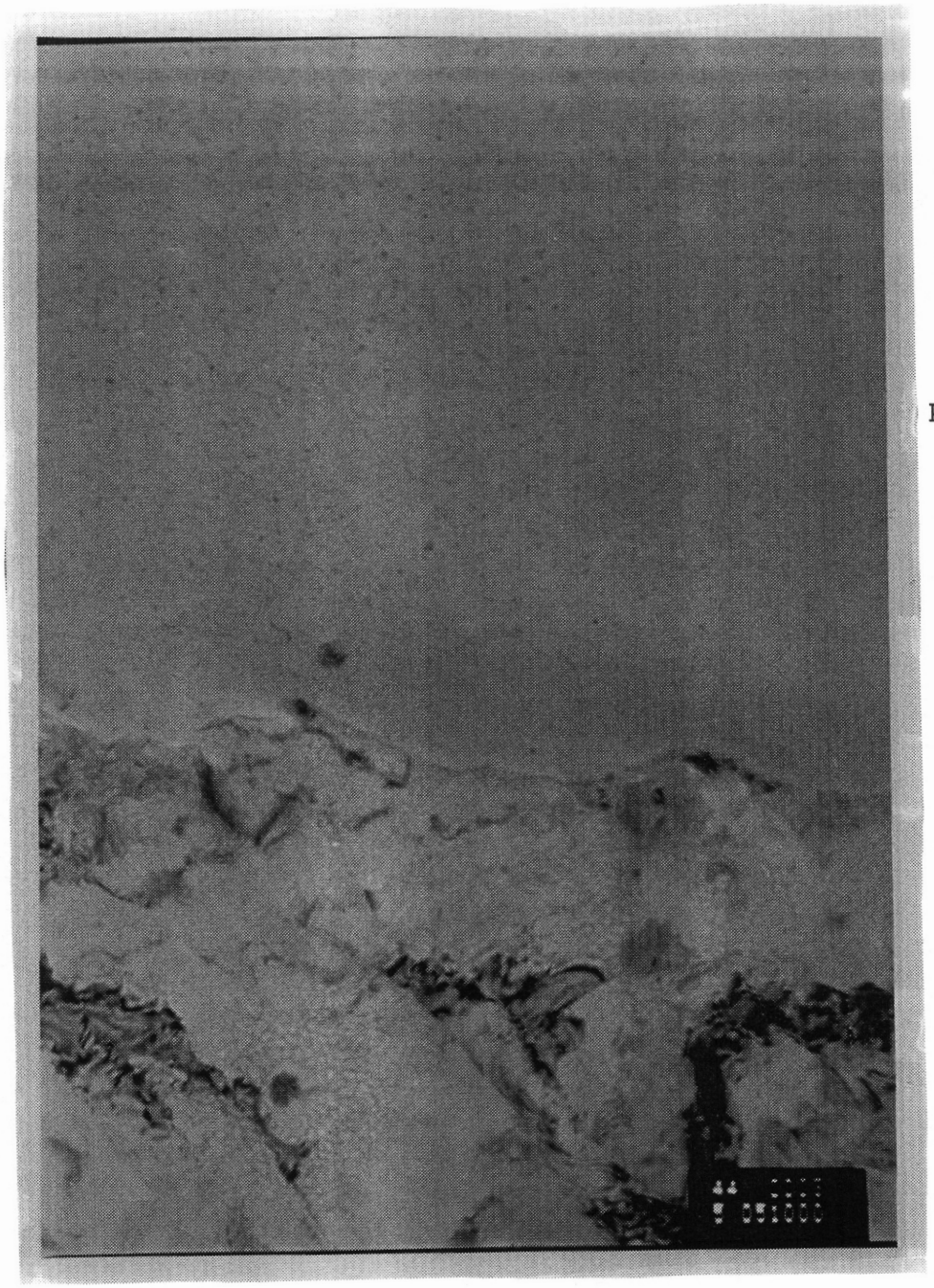

Figure 24. TEM of BDSDA/ODA-Aluminum Foil Interphase of Bond Precured in Air (91,100x).

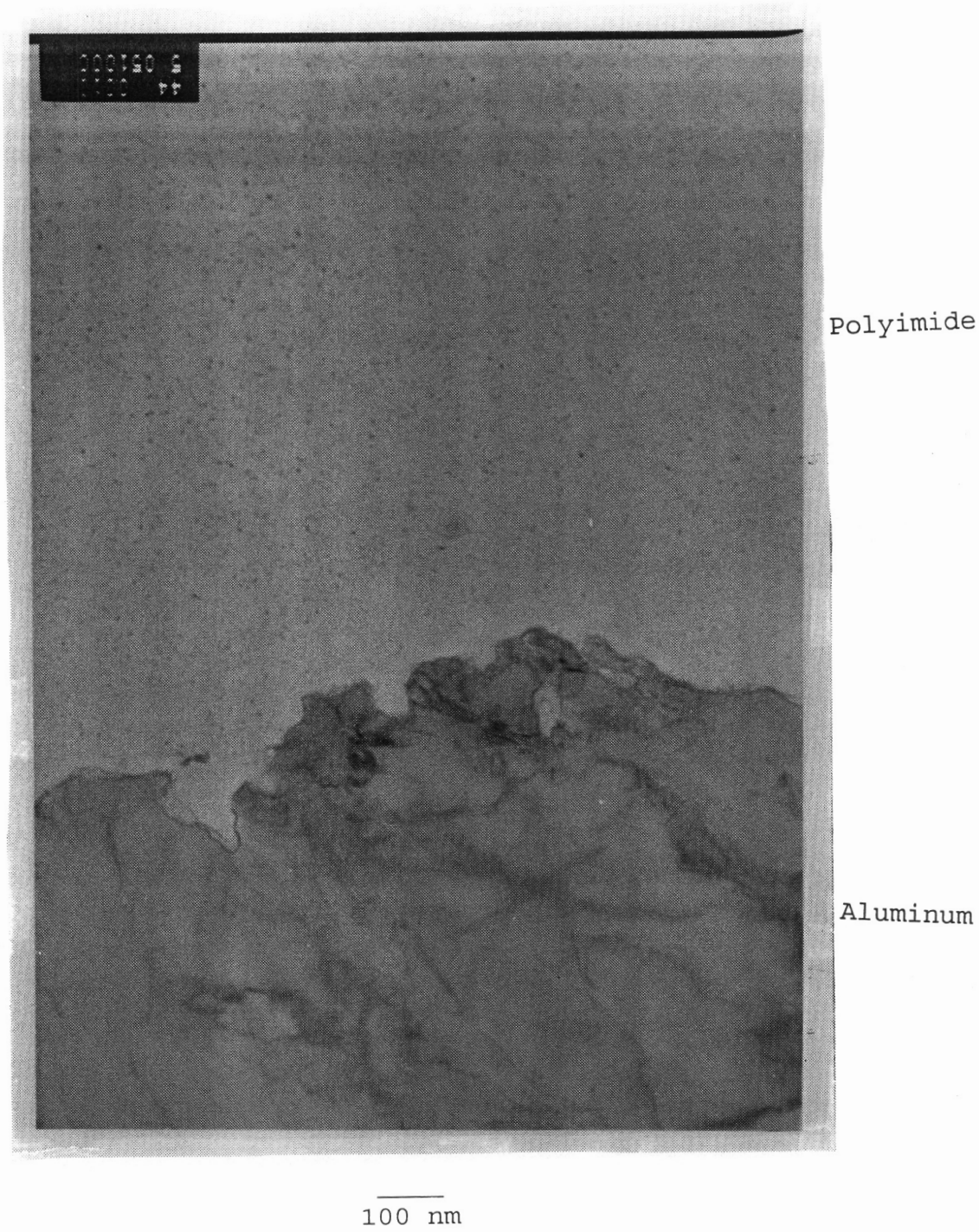

Figure 25. TEM of BDSDA/ODA-Aluminum Foil Interphase of Bond Precured in Nitrogen (91,100x).

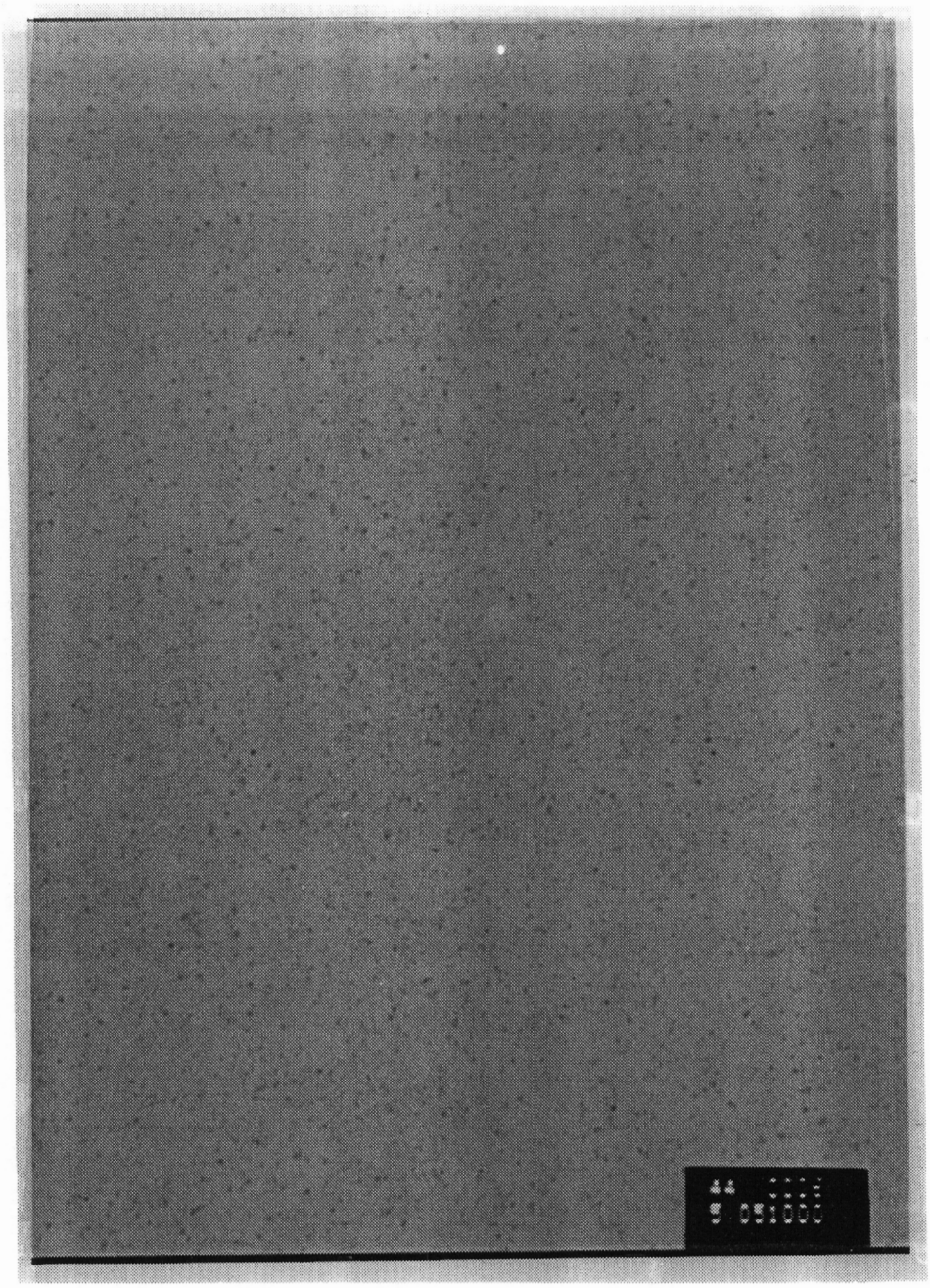

Figure 26. TEM of Bulk BDSDA/ODA Adhesive of Bond Precured in Air (91,100x).

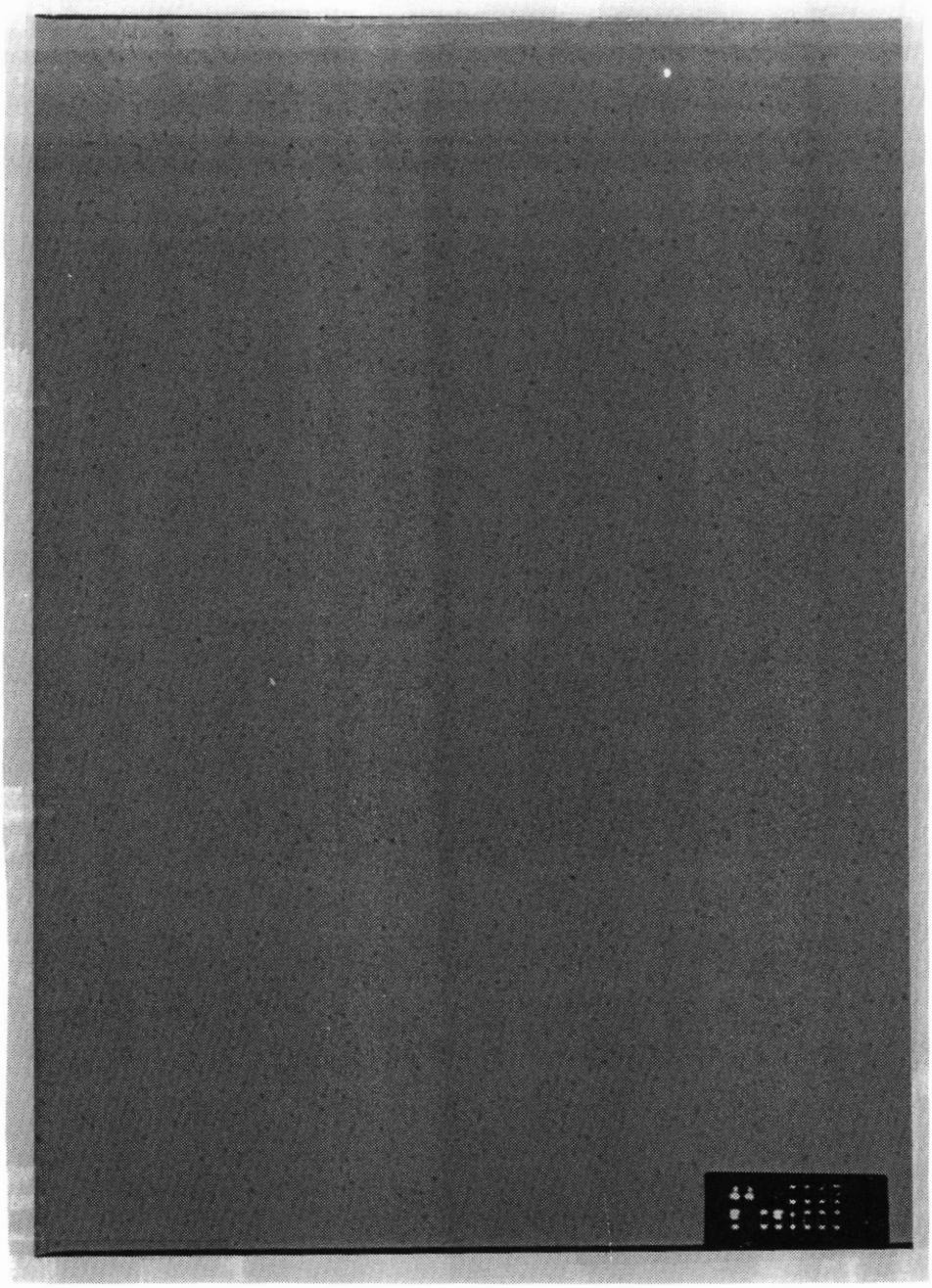

Figure 27. TEM of Bulk BDSDA/ODA Adhesive of Bond Precured in Nitrogen (91,100x).

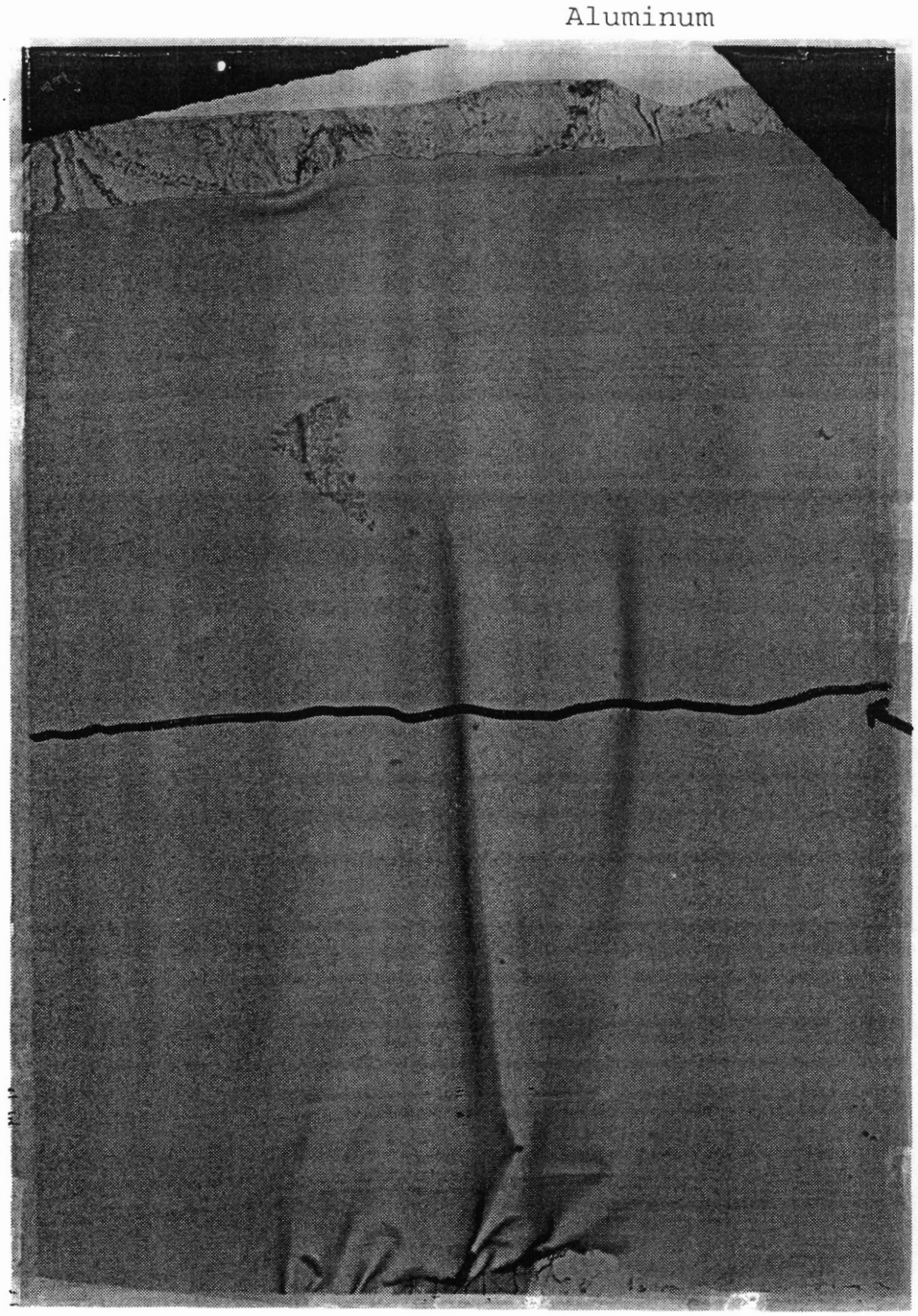

Figure 28. Hypothetical TEM of Bond Cross-Section if Polyimide Adhesive Displayed Metal/Metal Oxide Surface Layer as in Free Standing Film.

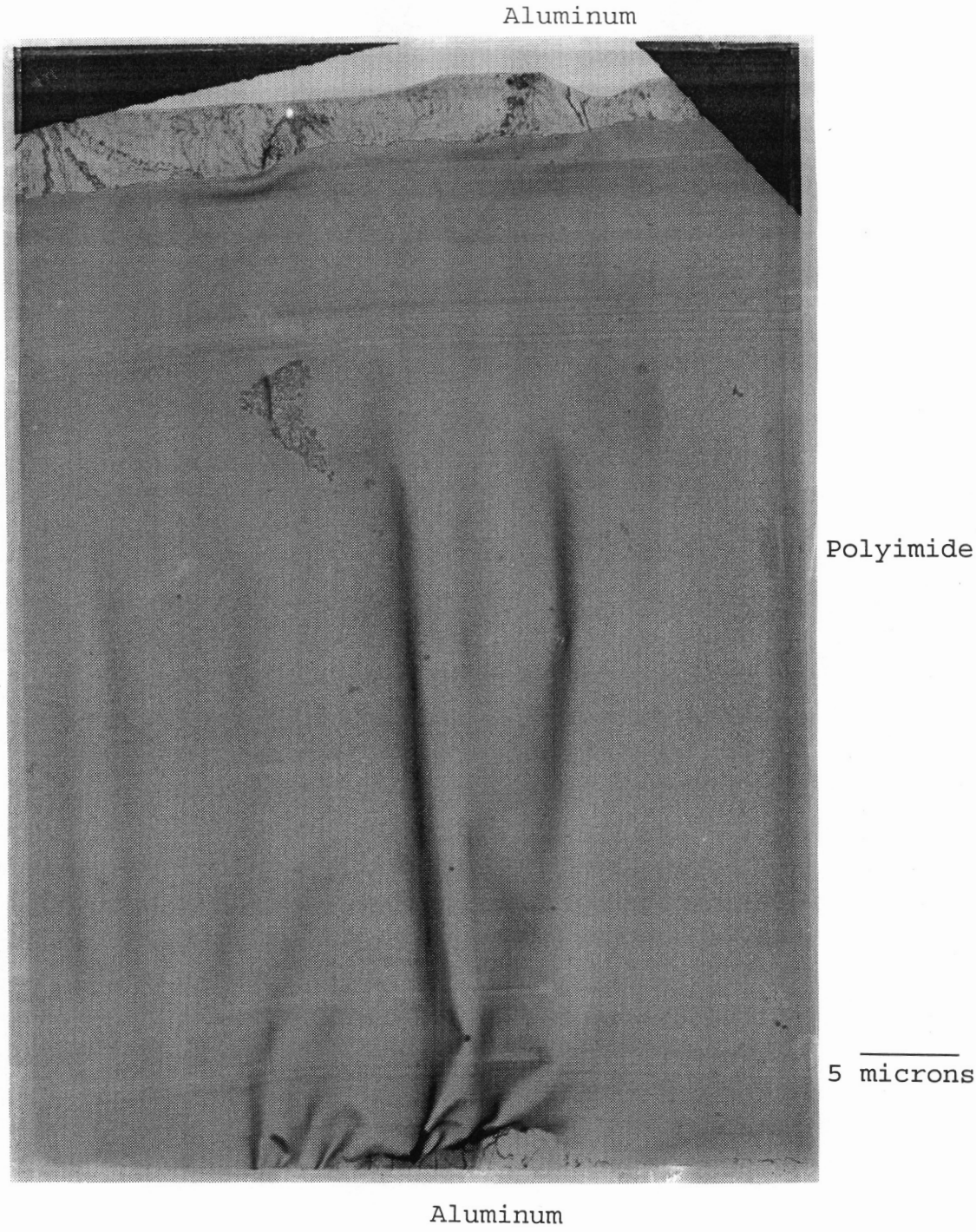

Figure 29. TEM of BDSDA/ODA-Aluminum Foil Bond Cross-Section Precured in Air (3100x).

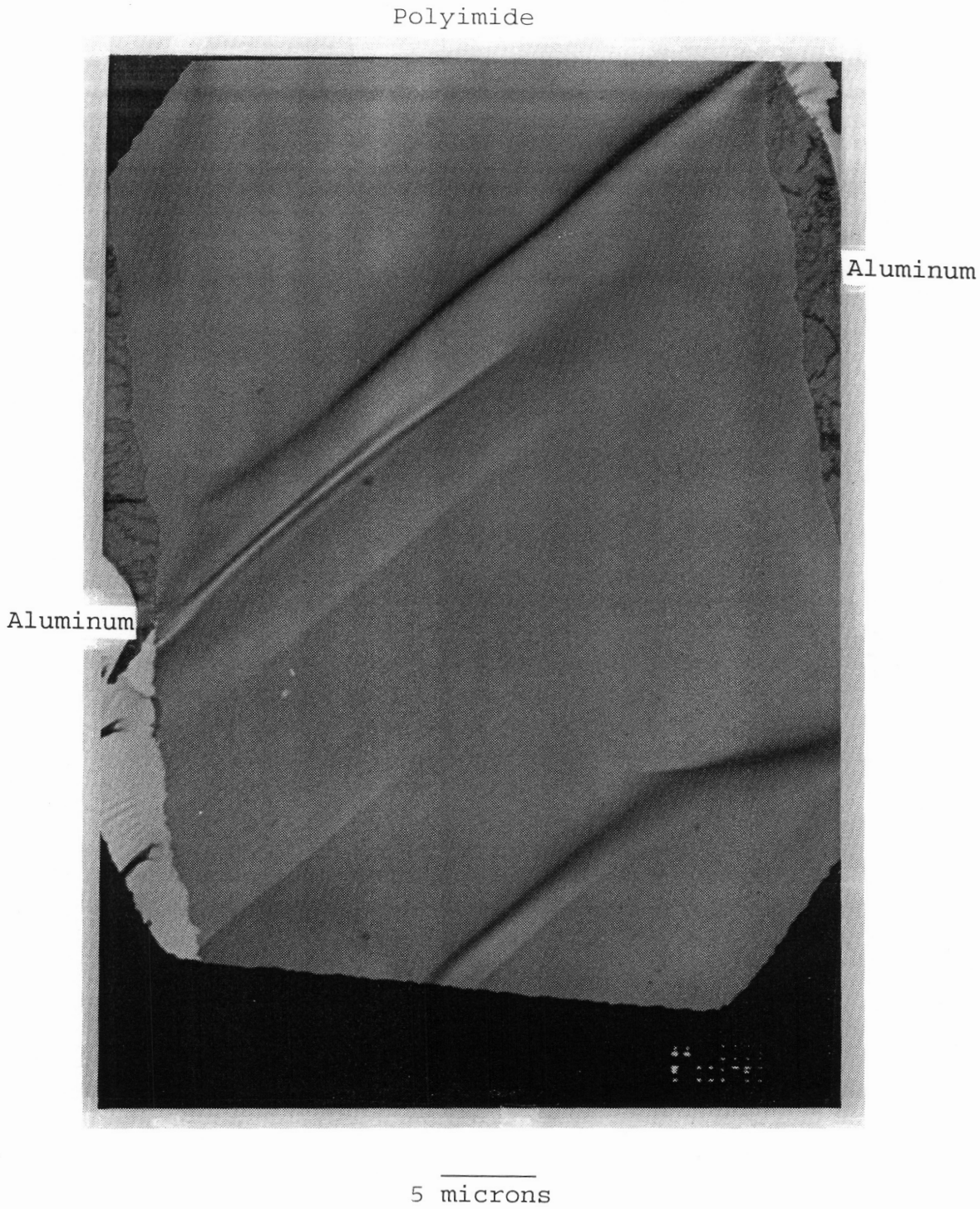

Figure 30. TEM of BDSDA/ODA-Aluminum Foil Bond Cross-Section Precured in Nitrogren (3100x).

(Figure 31) and the longer heated bonded specimen (Figures 24-25). Also, an iron-modified free standing BDSDA/ODA film was cured for an extra hour at 200°C, thus mimicking the thermal cure for the bonded specimen. This sample (Figure 32) had both a surface layer similar to the previously discussed free standing film and particles that were up to 5 nm in diameter. From these two samples it appeared that both the extra hour in the curing cycle and the pressure used during the bonding were responsible for the increased formation of particles, although the bonded samples never developed surface layers. Since no surface layer, or even any particles, was evident in the free standing film cured to 200°C, as discussed earlier, its absence was not suprising in the TEMs of the bonds.

TEMs of iron-modified bonds using non-sulfur containing polyimides provided interesting differences depending on the Tg of the polyimide. The iron particles in modified bonds synthesized with BTDA/ODA (Figure 33), a high Tg polyimide (285°C), were approximately 20-30 nm in diameter. Also, instead of appearing like the spherical particles seen in

Figure 31. TEM of BDSDA/ODA-Aluminum Foil Interphase of Bond Precured in Air but with No 200°C Stage in the Press (217,000x).

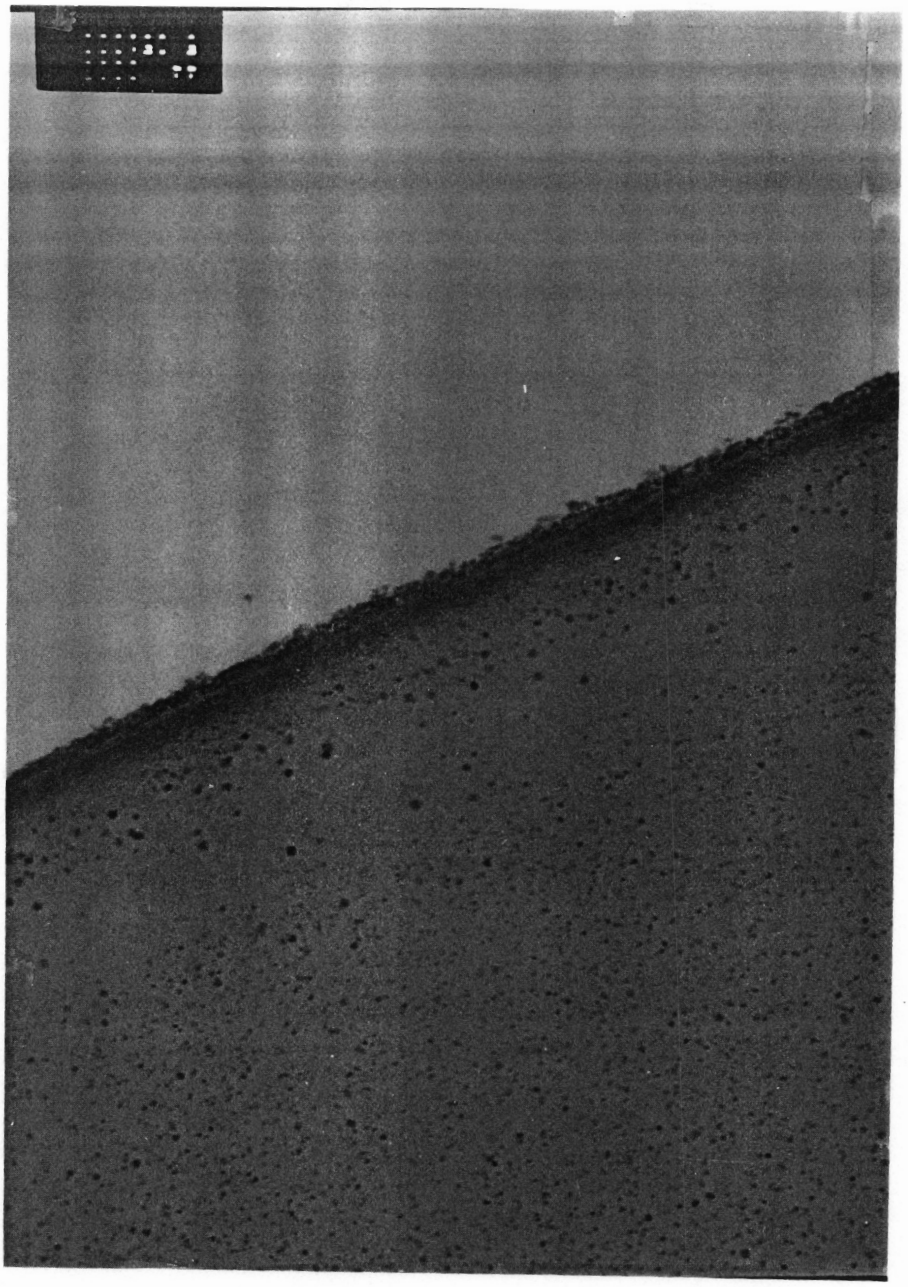

Figure 32. TEM of Iron-Modified BDSDA/ODA Free Standing Film Cured for an Additional Hour at 200°C (91,100x).

the BDSDA/ODA bonds, the particles appeared cubic. In the low Tg polyimide BTDA/APB (198°C) (Figure 34), the particles were mostly amorphous with diameters of 10-20 nm, although some were observed as large as 240 nm in diameter.

Peel Tests of Iron-Modified Bonds

The T-peel strength (Table IV) of the non-modified BDSDA/ODA polyimide did not vary much with pre-cure atmosphere, 6.45 ± 3.01 N/cm for air and 7.28 ± 1.47 N/cm for nitrogen. The same is true for the iron-modified BDSDA/ODA polyimide which had a T-peel strength of 5.13 ± 0.67 N/cm when pre-cured in air and 4.89 ± 1.08 N/cm when pre-cured in nitrogen. Thus, even though cure atmosphere had a significant impact on the iron-modified free standing films, it did not seem to significantly affect T-peel strength. Upon further examination of the data, these results were not suprising. The coated substrates were only precured to 200°C under the different atmospheres. After that, they were put into the press where they were all exposed to the same conditions. Since earlier work in Chapter II has shown that no oxidation at the surface or

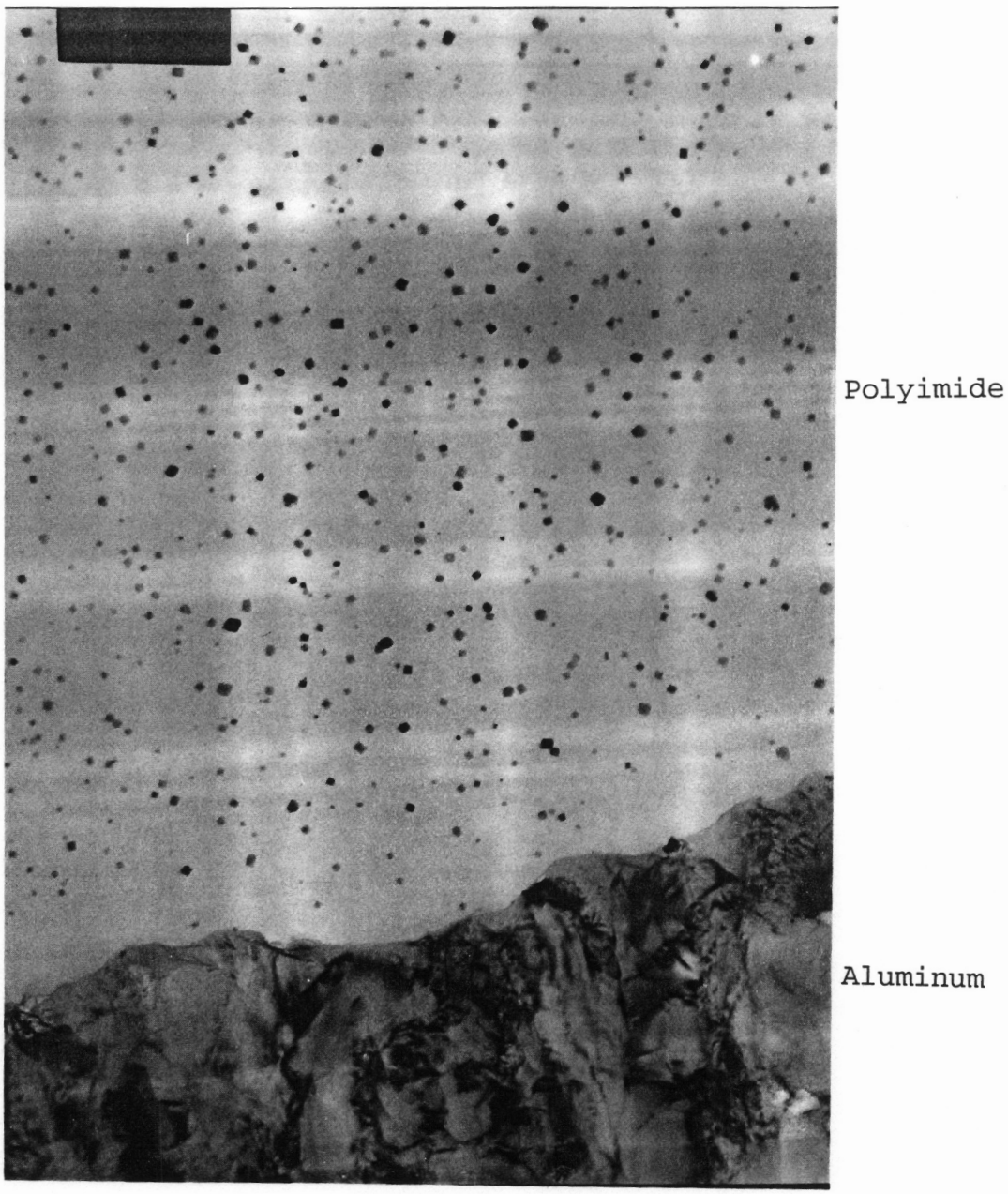

Figure 33. TEM of BTDA/ODA-Aluminum Foil Interphase of Bond Precured in Air (91,100x).

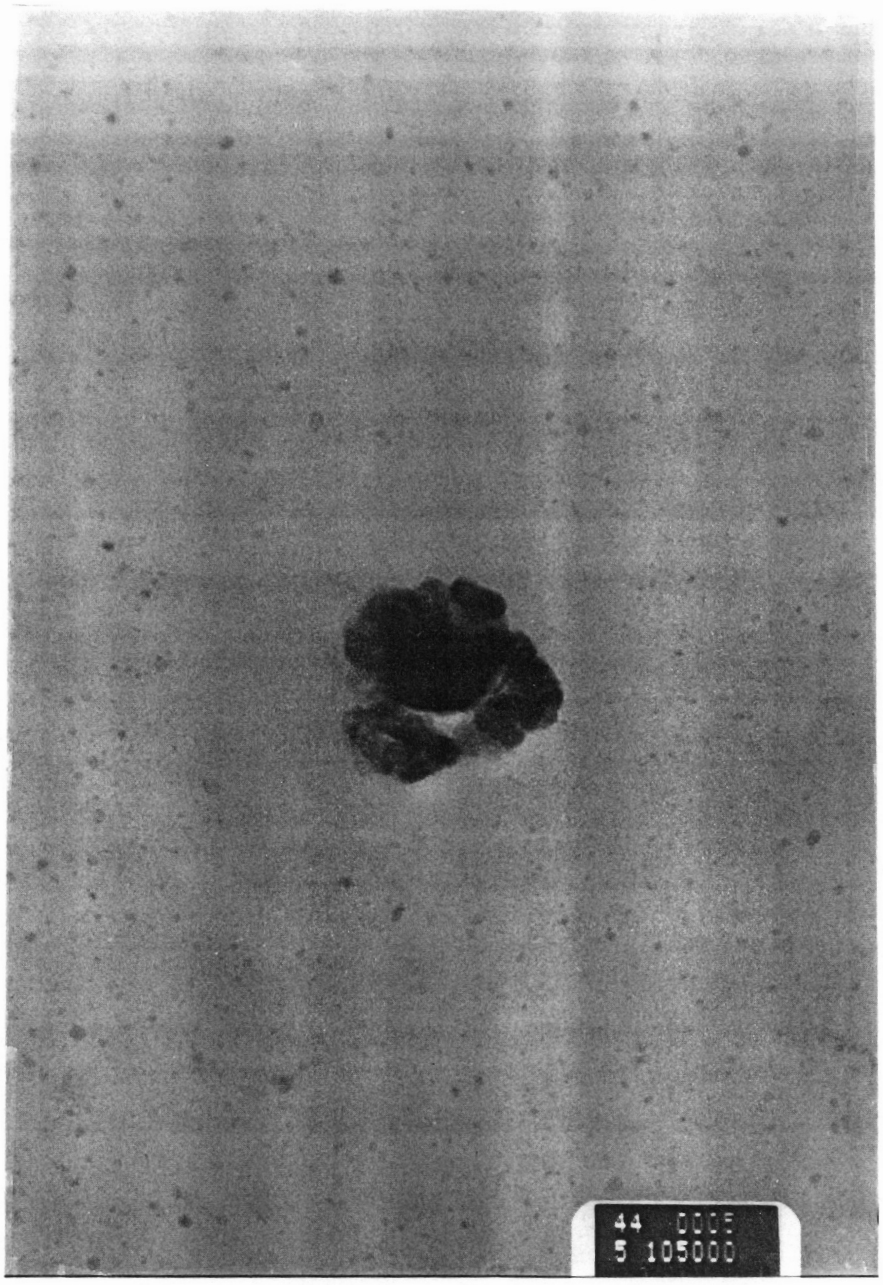

50 nm

Figure 34. TEM of Bulk BTDA/APB Adhesive of Bond Precured in Air (151,000x).

Table IV. T-Peel Strength of Iron-Modified and Non-Modified Polyimide/Aluminum Foil Bonds.

Polyimide	Iron-Modified	Cure Atmosphere	Peel Strength (N/cm)
BDSDA/ODA	No	Air	6.45 ± 3.01
BDSDA/ODA	No	Nitrogen	7.28 ± 1.47
BDSDA/ODA	Yes	Air	5.13 ± 0.67
BDSDA/ODA	Yes	Nitrogen	4.89 ± 1.08
BTDA/APB	No	Air	5.54 ± 0.70
BTDA/APB	No	Nitrogen	5.31 ± 0.98
BTDA/APB	Yes	Air	1.39 ± 0.47
BTDA/APB	Yes	Nitrogen	1.55 ± 0.37
BTDA/ODA	No	Air	3.74 ± 0.88
BTDA/ODA	Yes	Air	2.52 ± 0.41

200°C, those changes must occur after that point when they are in the press. Therefore, precure atmosphere should not have any significant effect on T-peel strength.

As expected the precure atmosphere did not have any significant effect on the T-peel strength of the non-modified BTDA/APB, either, which had a T-peel strength of 5.54 ± 0.70 N/cm for air and 5.31 ± 0.98 N/cm for nitrogen. These results were similar to the sulfur containing BDSDA/ODA which had a similar Tg. The results were markedly different for the iron-modified BTDA/APB, however. Whereas the iron-modified sulfur containing BDSDA/ODA retained approximately 75% of the strength of the non-modified polyimide, the iron-modified BTDA/APB lost approximately 75%. Its T-peel strength for the air precure was 1.39 ± 0.47 and 1.55 ± 0.37 for the nitrogen precure.

On the other hand, the non-modified BTDA/ODA was weaker than the lower Tg polyimides with a T-peel strength of only 3.74 ± 0.88 N/cm for the air precure. The BTDA/ODA polyimides were only tested with an air precure. While the non-modified BTDA/ODA performed worse than the other non-

modified polyimides, the iron-modified BTDA/ODA performed significantly better than the iron-modified BTDA/APB. It retained 67% of the non-modified T-peel strength (2.52 ± 0.41 N/cm).

The TEM results proved helpful in analyzing possible causes for the difference in the amount of peel strength lost among the three polyimides. Among the three samples, BDSDA/ODA and BTDA/ODA showed the greatest retention in peel strength compared to the non-modified polyimides. The modifier particles, as observed via TEM, possessed similar particle sizes, 5-10 nm for the BDSDA/ODA and 10-20 nm for the BTDA/ODA. Even though they were shaped differently, the particle size remained fairly constant throughout the adhesive in each case. With the BTDA/APB, however, more variation was noticed. The particles were spherical and, for the most part, 10-20 nm in diameter as in the BDSDA/ODA adhesive. It was observed, however, that much larger particles were also formed (up to 240 nm in diameter). Therefore, instead of having a uniform size distribution and serving as a filler, the larger particles served to localize

the stress within the bond causing it to fail under less load. Thus, it appeared that correlations could be drawn between peel strength and TEM analysis of modified adhesive bonds.

SUMMARY

TEM provided a means of directly analyzing the location of modifier particles in an actual bonded specimen. It was successful in showing that the formation of particles was quite different between the bond and free standing film. Also, this technique could be applied to other metal joints where etching processes are available, e.g. steel and copper, and other types of modifiers. At low magnification, the entire bond was viewed which allowed for the inspection of gross characteristics, such as voids or large aggregations of modifier particles. At high magnification, the actual bond line can be examined. One drawback to this technique is the method of samping. Observations from a TEM of one site might not necessarily be representative of the whole bond. Therefore, many TEMs need to be viewed from

several different areas in the bond.

IV. POLYIMIDE ADHESIVES AND ALUMINUM

INTRODUCTION

Few studies have examined the adhesion of polyimides to aluminum substrates because the upper temperature limit on use is not very different than that for aluminum itself. Those that have used aluminum as an adherend were usually examining factors other than metal-polymer interactions. One example was the study by Driscoll and Walton which used aluminum 2024 alloy adherends to determine the lap shear strength of a variety of different commercial polyimides [70] including 4000TF, AI-10, Eccobond 104, PMR-15, Matrimid 5292, Compimide 896, Kerimid 601, Compimide 453, BTL 94-606, Epoxy/PMDA, BTL 94-396, BPA-BMI, and Matrimid 5218. Other studies included attempts to create a graded interface region between an aluminum adherend and either BTDA/APB or BTDA/ODA polyimide adhesive [52, 53]. These studies used $CoCl_2$ [52, 53] and tris(2,4-pentanedionato)aluminum [52] as modifiers to create a concentration gradient of metal particles along the interface. The modified adhesives in these studies possessed lower peel strengths than the non-

modified adhesive as determined by the floating roller peel test. None of these studies, however, examined the possibility of interaction between the metal adherend and the polymeric adhesive.

The previous chapter examined the effect of an iron modifier the T-peel strength of several polyimides. The study described here will examine the effects of Tg and the presence of sulfur on polyimide adhesives bonded to aluminum. No iron modification is examined. Both sulfur and non-sulfur containing polyimides possessing either high or low Tg have been examined using aluminum adherends. Aluminum was studied first because it was shown earlier not to catalyze the oxidation of the thioether sulfur completely in the sulfur containing polyimdies. Therefore, no metal catalyzed oxidation of the surface was likely which would affect bond strength. Surface analysis of failed bond specimens was used to determine the chemical state and composition of the interfacial regions. These data were then correlated with bond strength and the mechanism of bond failure. This chapter describes work only with aluminum.

The next chapter will outline the findings with steel adherends.

Experimental

Materials

Again, BDSDA and BTDA were the two dianhydrides used. ODA, APB, and ASD were used as the diamines, and DMAc was used as the solvent. The reagents were treated as discussed in Chapter II. High purity aluminum foil (99.99%) aluminum foil (0.004" thick) and Al 6061 aluminum coupons (6" x 1" x 0.25") were used as adherends.

Synthesis

Poly(amide acid) solutions were made as discussed in Chapter II.

Bonding

The aluminum substrates were pretreated by either an acetone wipe or a chemical etch. The etching process and the preparation of T-peel specimens were the same as described in Chapter III.

The wedge samples were prepared by casting the

poly(amide acid) solution onto twelve coupons leaving one inch free along one end. The solution was cast at twice the thickness described for the peel specimens. The coated coupons were precured in a similar fashion as the peel samples. After the precure, the six sets of two coupons each were placed into the hot press and bonded as described above. After bonding, the coupons were taken from the press and numbered one to six (left to right) with the odd numbered bonds being stored in the desiccator and the even numbered bonds being stored under water during testing. All bonds were stored at room temperature.

Measurements

Peel strength was measured as described in Chapter III. The wedge test was performed by inserting a 0.13" wedge into the bond to a distance of 0.25". The initial crack growth was measured as was the subsequent crack growth as a function of time.

X-ray photoelectron spectroscopy data were obtained in the same manner as Chapter II.

Results and Discussion

Four polyimides were used to bond aluminum to aluminum in this study. Two were low Tg polyimides; one containing sulfur (BDSDA/ODA, 217°C) and one not containing sulfur (BTDA/APB, 198°C). The other two were high Tg polyimides; sulfur containing (BTDA/ASD, 285°C) and non-sulfur containing (BTDA/ODA, 285°C). From the previous work in Chapter II, it was hypothesized that the aluminum from the substrates would only catalyze the oxidization of thioether sulfur in the sulfur containing polyimides to a minor extent.

Two tests were selected to examine the effects, if any, of high/low Tg. The T-peel test was chosen to compare these polyimides due to the simplicity of the test and its emphasis on interfacial strength; while the wedge test was chosen because of its emphasis on bond durability. While the stress situation in the peel test is difficult to assess, the peel test has often been used to compare the relative strengths of adhesives and the effects of surface pretreatment [71, 72].

Peel Tests

The T-peel results of several repetitions have been tabulated in Table V. The peel strength of the NaOH etched BTDA/APB bonds (5.21 ± 0.82 N/cm) corresponded well with that found by Horning (5.3 N/cm)[52] for the same polyimide and pretreatment even though he used the floating roller peel test. Comparisons with the other values were not found in the literature. Standard deviations for the peel strengths were good for most of the samples especially the acetone wiped BTDA/ODA, BTDA/ASD, and BDSDA/ODA specimens. Though the standard deviations for some of the sets might not be very good, the deviation within a single preparation was good (Table VI). The NaOH etched specimens, overall, had larger standard deviations. This increase was probably due to variations in the time between the etch and the casting of the poly(amide acid) solution and a reduction of solution strength after repeated etchings. These differences would account for changes in peel strength between preparations but would not affect different samples within a single bond preparation.

Table V. T-Peel Strength and Mode of Failure in the Polyimide/Aluminum Foil Bonds

Polyimide	Tg	Sulfur	Wiped Bonds		Etched Bonds	
			T-Peel Strength (N/cm)	Failure Mode	T-Peel Strength (N/cm)	Failure Mode
BTDA/APB	Low	No	3.85 ± 0.42	Oxide	5.21 ± 0.82	Adhesive
BDSDA/ODA	Low	Yes	2.88 ± 0.15	Oxide	6.64 ± 2.27	Adhesive
BTDA/ODA	High	No	0.38 ± 0.10	Oxide	3.40 ± 1.55	Mixed Mode
BTDA/ASD	High	Yes	1.04 ± 0.09	Oxide	1.63 ± 0.57	Mixed Mode

Table VI. T-Peel Strength of Single Preparations of Polyimide/Aluminum Foil Bonds.

Polyimide	Pretreatment	Number of Samples	Peel Strength (N/cm)
BDSDA/ODA	Acetone Wiped	9	2.88 ± 0.15
BDSDA/ODA	NaOH Etched	5	6.20 ± 0.19
BTDA/APB	Acetone Wiped	12	3.85 ± 0.42
BTDA/APB	NaOH Etched	12	5.54 ± 0.70
BTDA/ASD	Acetone Wiped	6	1.04 ± 0.09
BTDA/ASD	NaOH Etched	7	1.38 ± 0.51
BTDA/ODA	Acetone Wiped	6	0.38 ± 0.10
BTDA/ODA	NaOH Etched	6	3.74 ± 0.88

Upon examination of the results of the T-peel test of the aluminum polyimide bonds, several factors were notable. One, for a given polyimide, the bonds made using etched aluminum adherends were significantly stronger than those using only acetone wiped aluminum adherends. The enhanced strength of the etched aluminum bonds was most likely due to the reduction or removal of a weak oxide layer at the surface prior to bonding. Surface analysis of the NaOH etched aluminum foil by XPS lent evidence to support this idea that significantly more aluminum metal (71.2 ± 0.1 eV [51]) was present on that surface (Figure 35) than on the acetone wiped aluminum surface (Figure 36). Surface analysis of the failed bonded surfaces (Figures 37-40) corroborated this hypothesis that the acetone wiped aluminum bonds were weaker due to a poorly attached oxide layer at the surface. The atomic concentration of carbon in Figures 37-40 has been divided by four in order to make the smaller sulfur and nitrogen concentrations more noticeable. The atomic concentration of total aluminum (both oxide and metal) on the failed surfaces of the etched aluminum bonds

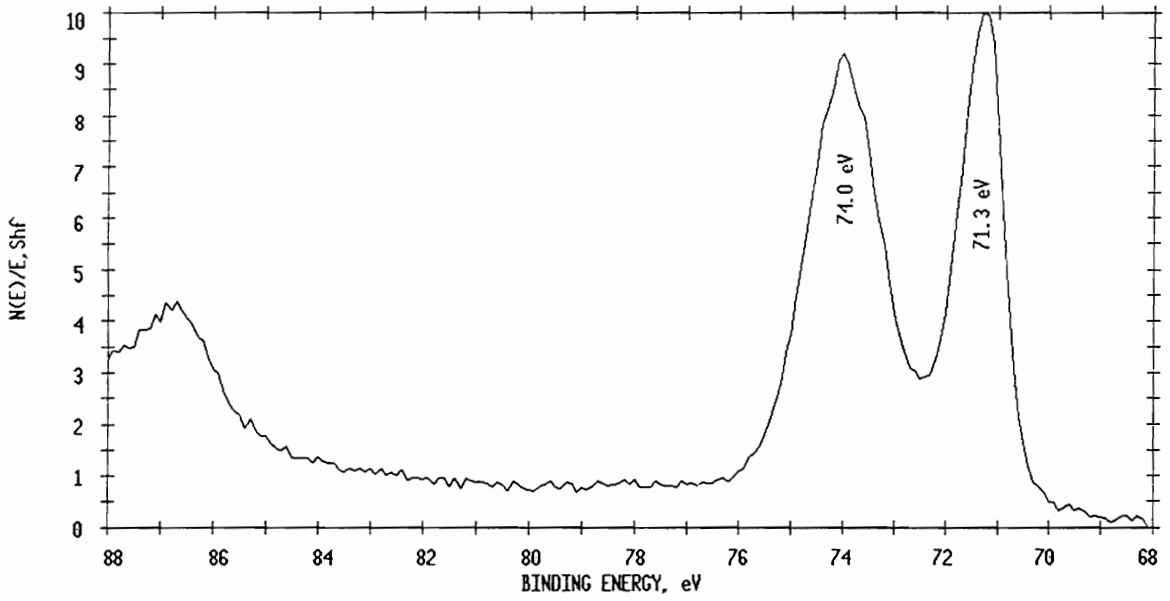

Figure 35. Aluminum 2p XPS Photopeak of NaOH Etched Aluminum Foil (Binding Energy Calibrated to C 1s = 284.6 eV).

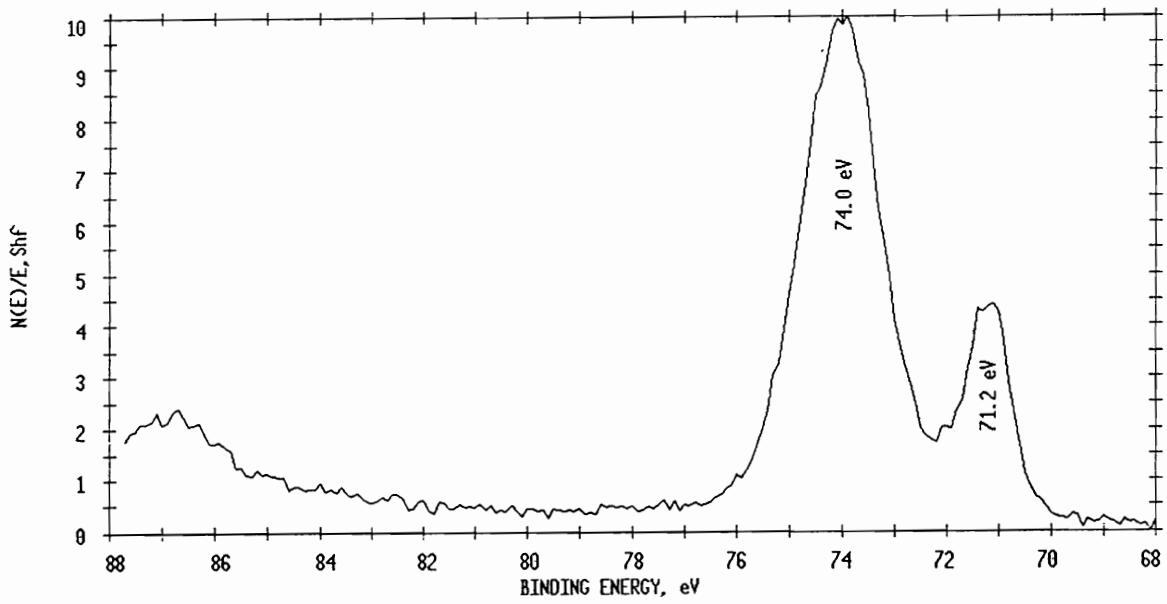

Figure 36. Aluminum 2p XPS Photopeak of Acetone Wiped Aluminum Foil (Binding Energy Calibrated to C 1s = 284.6 eV).

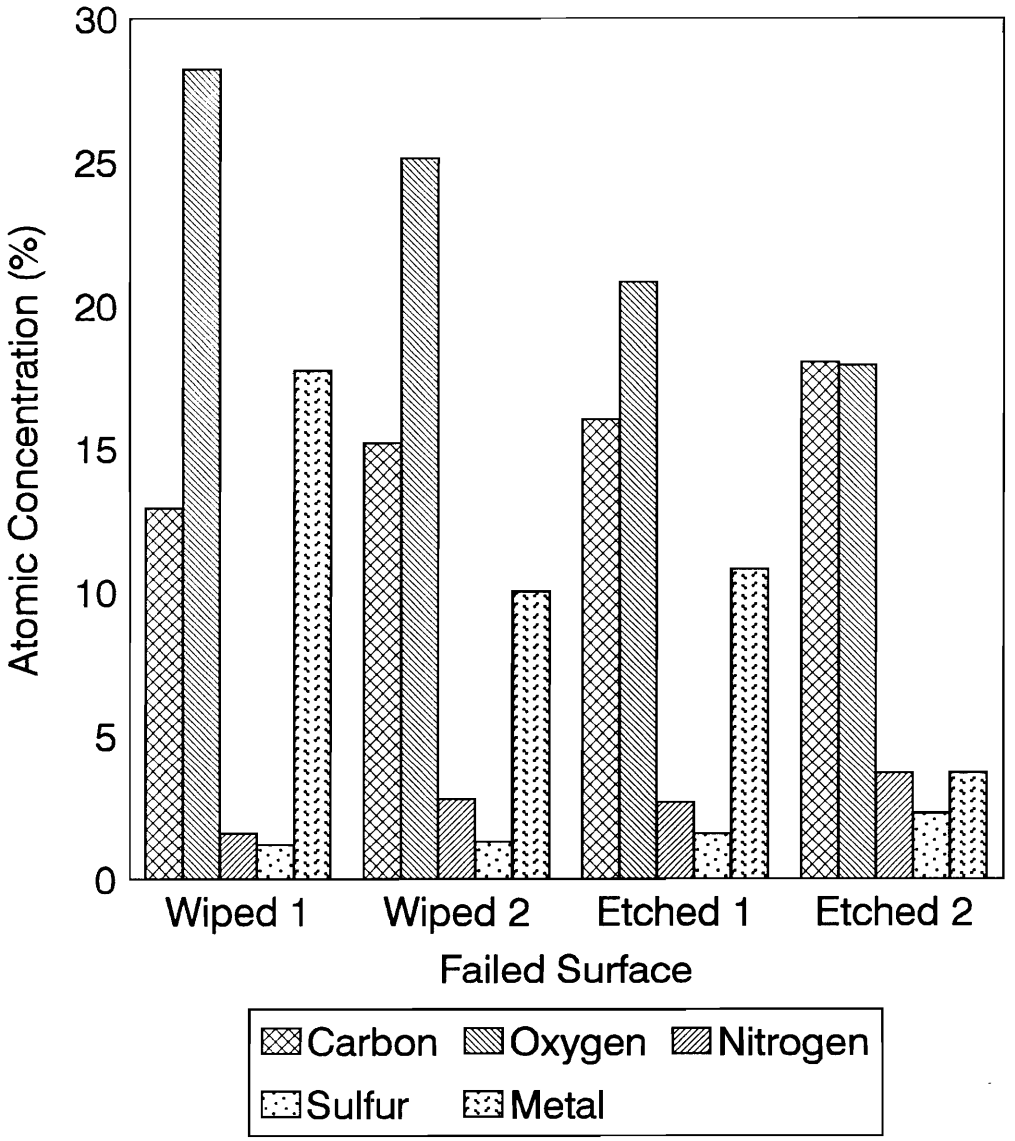

Figure 37. Atomic Concentrations of Failed BDSDA/ODA/Aluminum Peel Bond Surfaces (Carbon concentration/4).

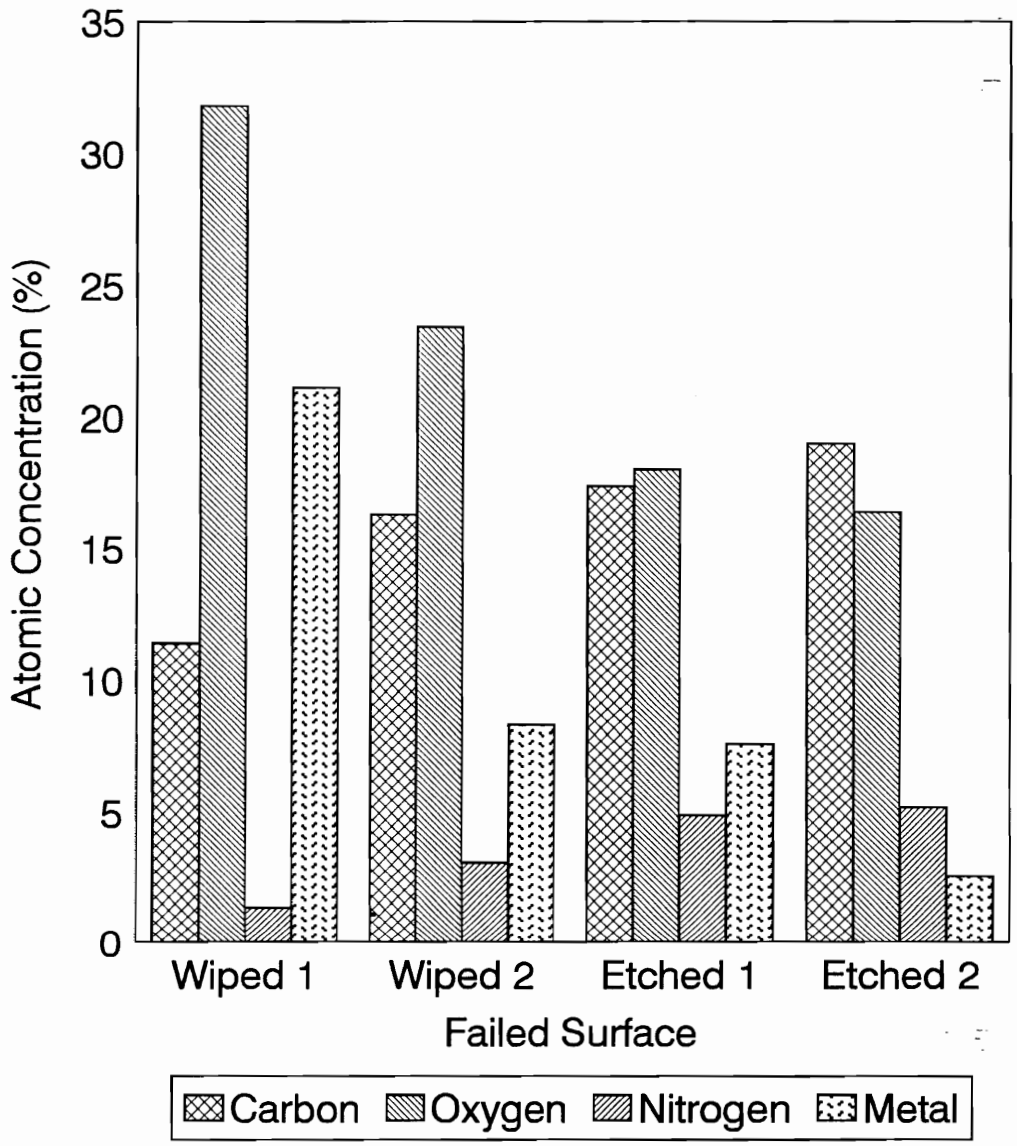

Figure 38. Atomic Concentrations of Failed BTDA/APB/Aluminum Peel Bond Surfaces (Carbon concentration/4).

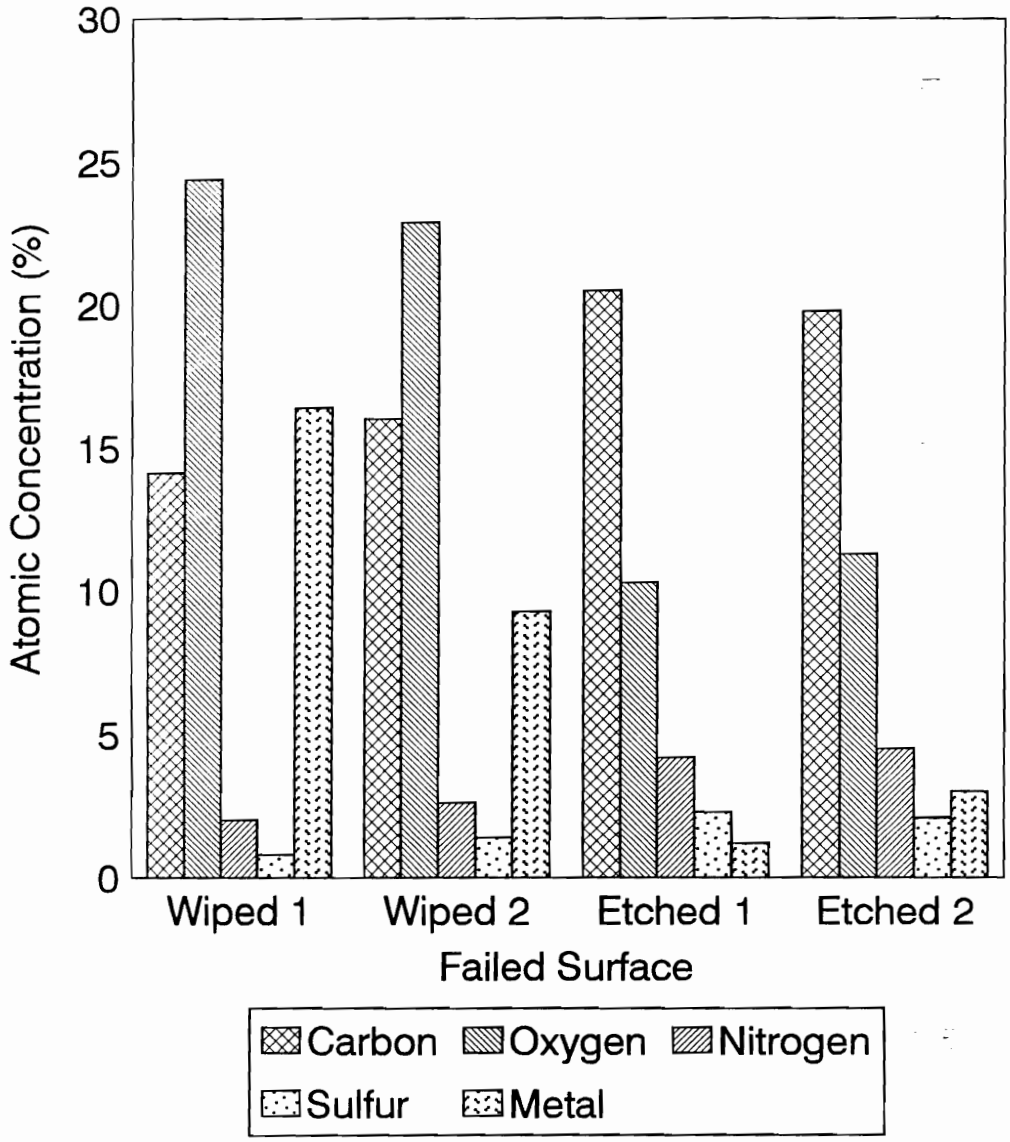

Figure 39. Atomic Concentrations of Failed BTDA/ASD/Aluminum Peel Bond Surfaces (Carbon concentration/4).

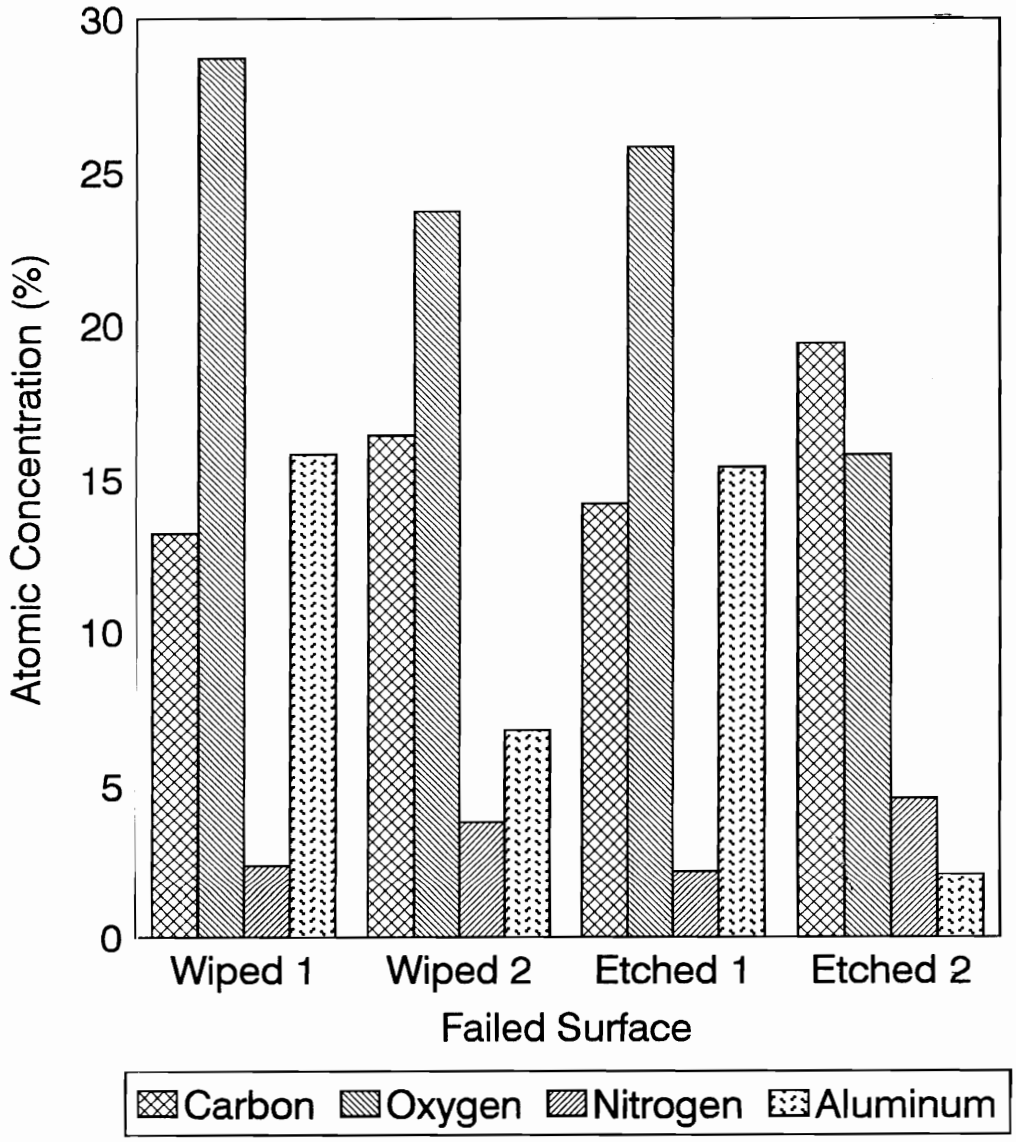

Figure 40. Atomic Concentrations of Failed BTDA/ODA/Aluminum Peel Bond Surfaces (Carbon concentration/4).

was consistently lower within a given adhesive system than the acetone wiped aluminum surfaces. The increased aluminum on the failed acetone wiped surfaces seemed to indicate that those bonds failed within the oxide layer of the aluminum surfaces. The etched substrates, on the other hand, have less of the oxide layer present. One failed surface of the etched bonds consistently had only a small (2-3 atomic%) amount of aluminum compared to the wiped failed surfaces. The presence of such a small amount of aluminum on one surface would seem to indicate that these bonds failed more within the polyimide portion of the interphase region compared to the oxide region.

Another noticeable feature was the similarity of peel strengths between the polyimides with similar Tg. Some difference was to be expected since the polyimides were not exactly the same. No evidence could be detected for metal-sulfur interactions in the sulfur containing polyimides which was as expected because aluminum did not significantly catalyze sulfur oxidation. The sulfur 2p photopeak from the failed surfaces (Figure 41) had a binding energy of 163.2 eV

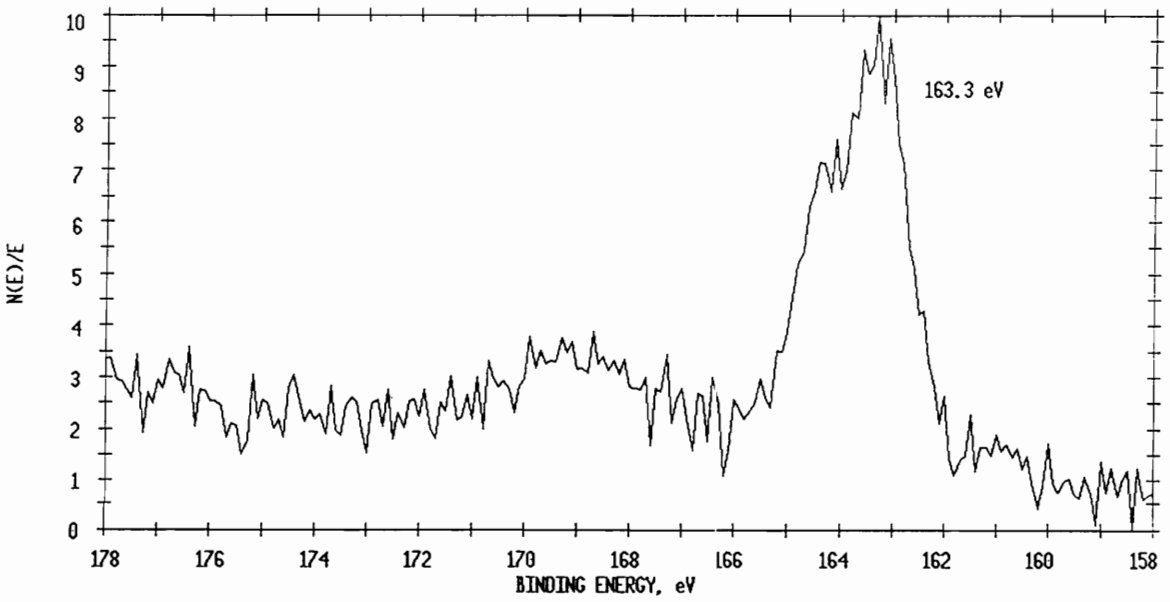

Figure 41. Sulfur 2p XPS Photopeak of Failed Peel Bond Surface (Binding Energy Calibrated to C 1s = 284.6 eV).

which also indicated that the sulfur remained in the thioether form [40].

It was also interesting to note that the low Tg polyimides possessed higher peel strengths than the high Tg polyimides for a given surface pretreatment. One possible explanation was that the processing conditions, *i.e.* the precure and press temperatures, were not high enough to allow sufficient intermingling of the two adhesive coats to produce a strong bond in the high Tg case. If this had been the case, then the locus of failure would be expected to occur cohesively within the adhesive itself. Surface analysis of the failed surfaces (Figures 39-40), however, indicated that the locus of failure was primarily along the interface. The most likely answer for this observation was the rigid polyimide backbone that contributed to the high Tg of these polyimides. These stiff chains would be less likely to dissipate energy and be more likely to fail under lower stresses.

Wedge Tests

Wedge tests were also performed under dry (Table VII)

Table VII. Crack Growth and Mode of Failure in the Polyimide/Al 6061 Wedge Bonds Tested in a Dry Environment.

Polyimide	Tg	Sulfur	Wiped Bonds			Etched Bonds		
			Initial Crack Length (mm)	Crack Growth (mm)	Failure Mode	Initial Crack Length (mm)	Crack Growth (mm)	Failure Mode
BTDA/APB	Low	No	51 ± 9	18 ± 7	Cohesive	Failed	-----	Cohesive
BDSDA/ODA	Low	Yes	48 ± 8	5 ± 6	Adhesive	59 ± 7	38 ± 1[a]	Mixed Mode
BTDA/ODA	High	No	114 ± 1	Failed	Adhesive	110 ± 5	Failed	Mixed Mode
BTDA/ASD	High	Yes	Failed	-----	Mixed Mode	Failed	-----	Cohesive

[a]After 11 days

Table VIII. Crack Growth and Mode of Failure in the Polyimide/Al 6061 Wedge Bonds Tested in a Wet Environment.

Polyimide	Tg	Sulfur	Wiped Bonds			Etched Bonds		
			Initial Crack Length (mm)	Crack Growth (mm)	Failure Mode	Initial Crack Length (mm)	Crack Growth (mm)	Failure Mode
BTDA/APB	Low	No	51 ± 9	Failed	Cohesive	Failed	-----	-----
BDSDA/ODA	Low	Yes	48 ± 8	29 ± 11	Oxide	59 ± 7	42 ± 7[a]	Oxide
BTDA/ODA	High	No	114 ± 1	Failed	Cohesive	110 ± 5	Failed	Cohesive
BTDA/ASD	High	Yes	Failed	-----	-----	Failed	-----	-----

[a]After 11 days

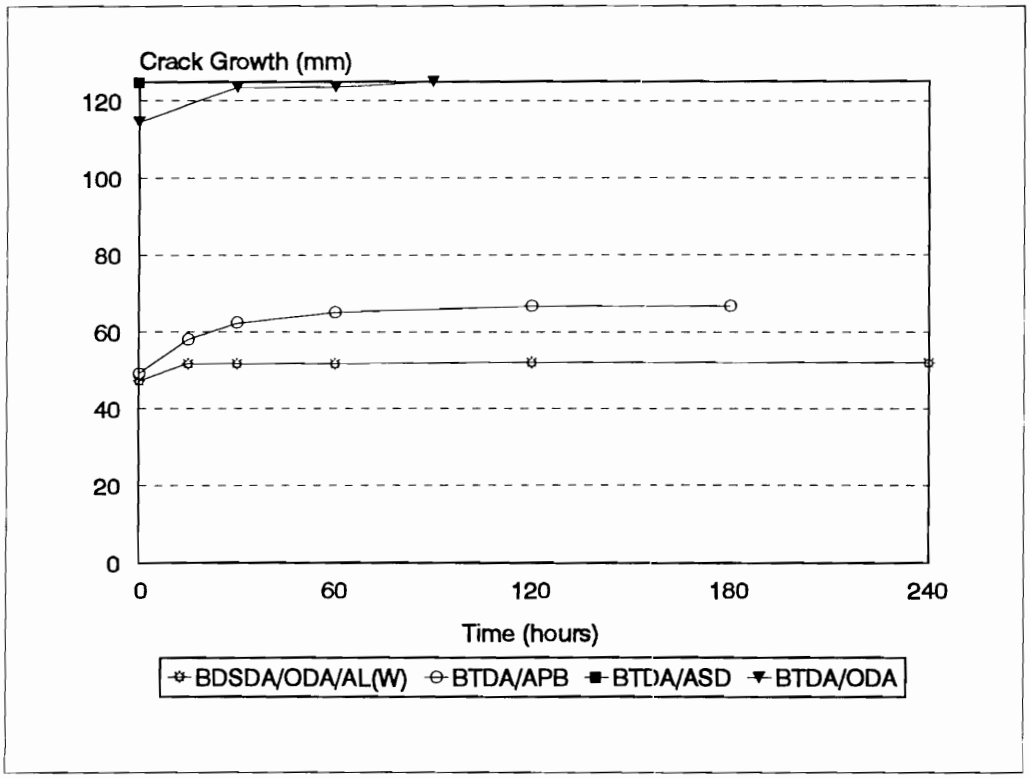

Figure 42. Crack Growth in Acetone Wiped Polyimide/Aluminum Wedge Bonds Tested in a Dry Environment at Room Temperature.

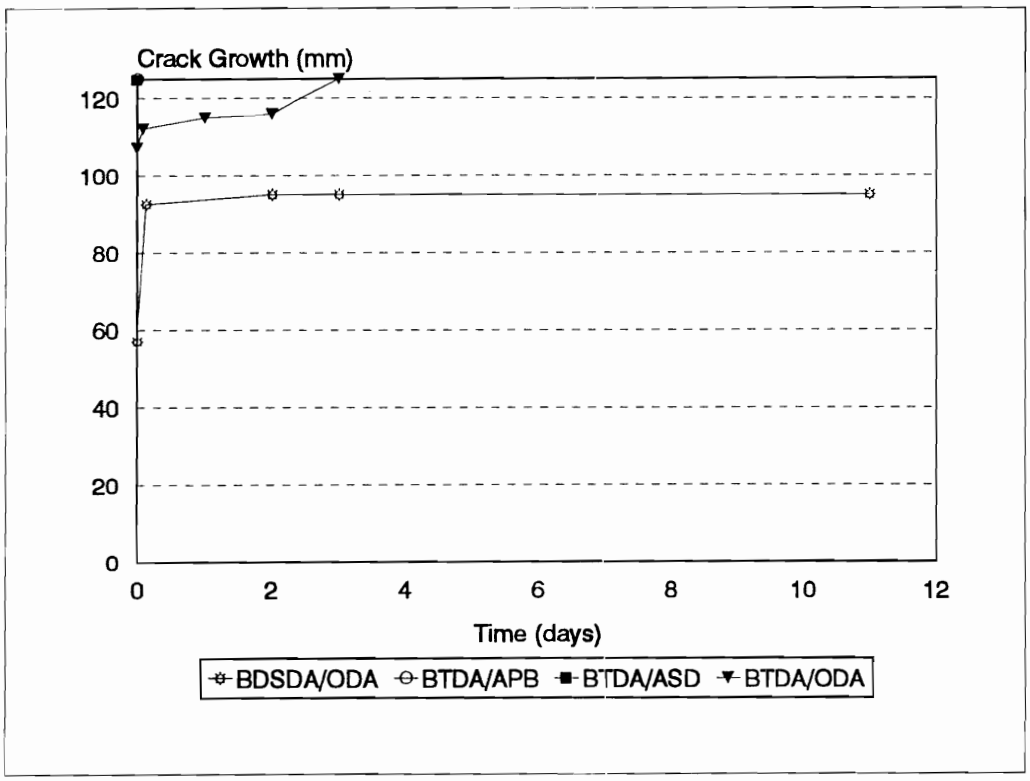

Figure 43. Crack Growth in NaOH Etched Polyimide/Aluminum Wedge Bonds Tested in a Dry Environment at Room Temperature.

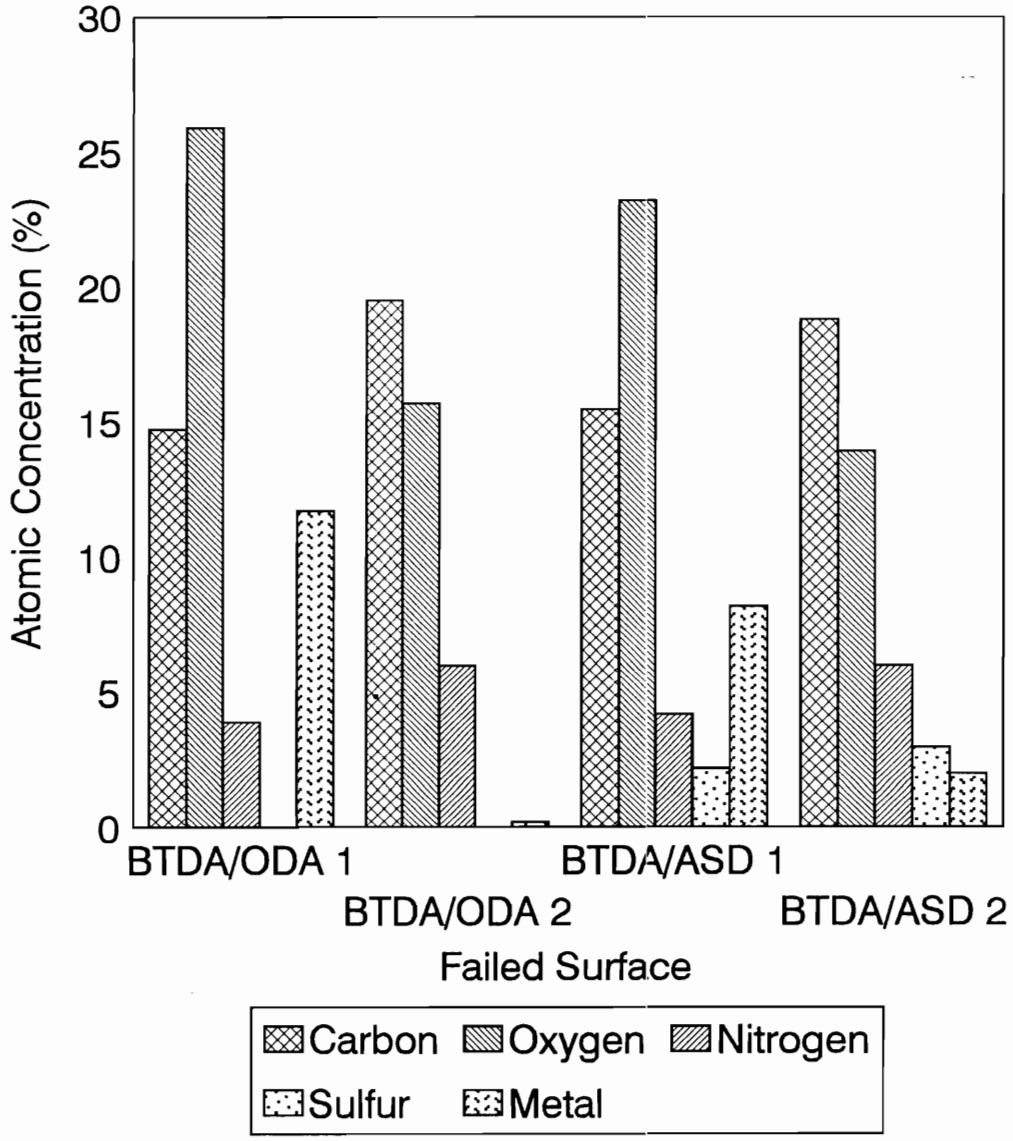

Figure 44. Surface Atomic Concentrations of Failed Acetone Wiped High Tg Polyimide/Aluminum Wedge Bonds Tested in a Dry Environment.

and wet (Table VIII) environments using these four polyimides with both surface pretreatments. The BTDA/ASD (Figures 42-43) bonds failed upon insertion of the wedge no matter what pretreatment was used. Thus environmental conditions were not a factor in this case. The surface pretreatment did, however, seem to affect the locus of failure in the BTDA/ASD specimens. Surface analysis (Figure 44) indicated that the acetone wiped Al6061 specimens failed in mixed mode. Some aluminum (8.2 atomic% and 2.0 atomic%) was present on both failed surfaces in addition to the polyimide components. The presence of polyimide, or lack of it, was determined from the concentration of nitrogen, and sulfur when it was present in the polyimide, since carbon and oxygen were also observed on the cleaned substrates. The NaOH etched Al6061 specimens failed cohesively within the adhesive (Figure 45). Less than 1 atomic% of aluminum was present on either surface.

The BTDA/ODA specimens also failed quickly , but not as quickly as the BTDA/ASD specimens. The acetone wiped specimens, both wet (Figure 46) and dry (Figure 42), failed

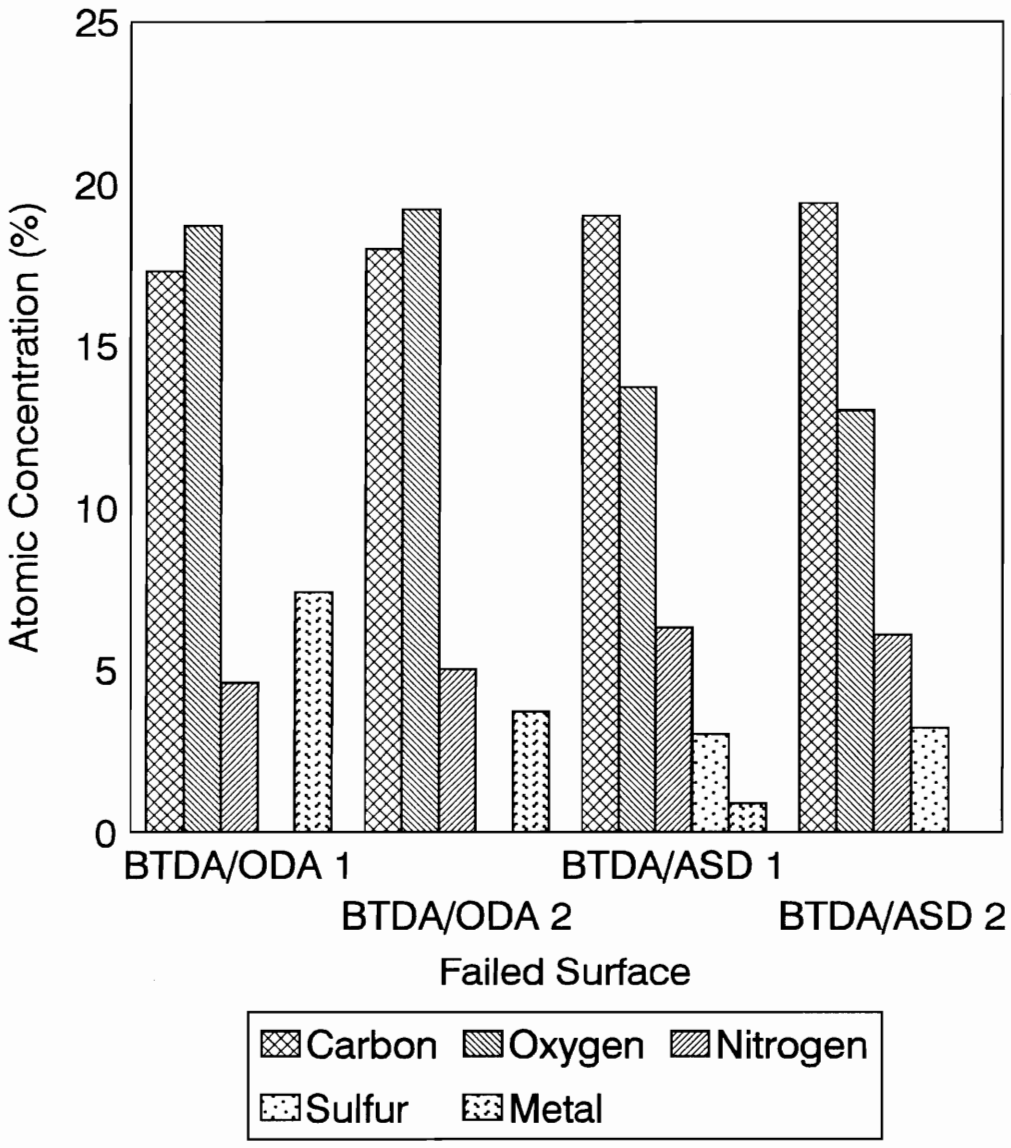

Figure 45. Surface Atomic Concentrations of Failed NaOH Etched High Tg Polyimide/Aluminum Wedge Bonds Tested in a Dry Environment.

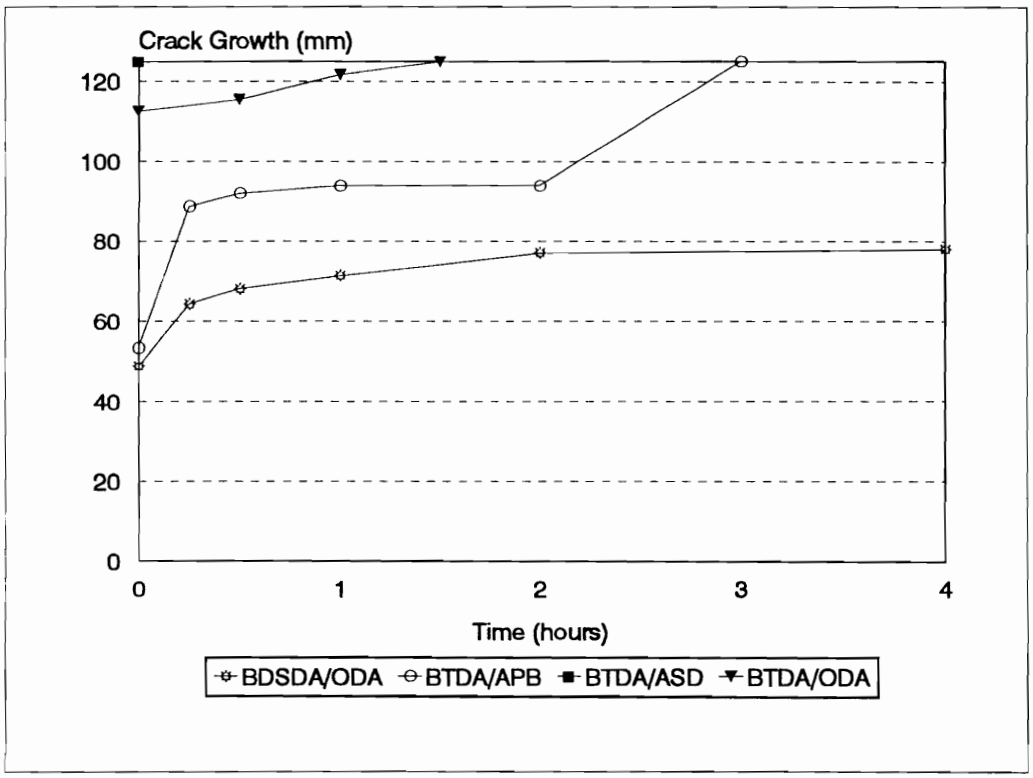

Figure 46. Crack Growth in Acetone Wiped Polyimide/Aluminum Wedge Bonds Tested in a Wet Environment at Room Temperature.

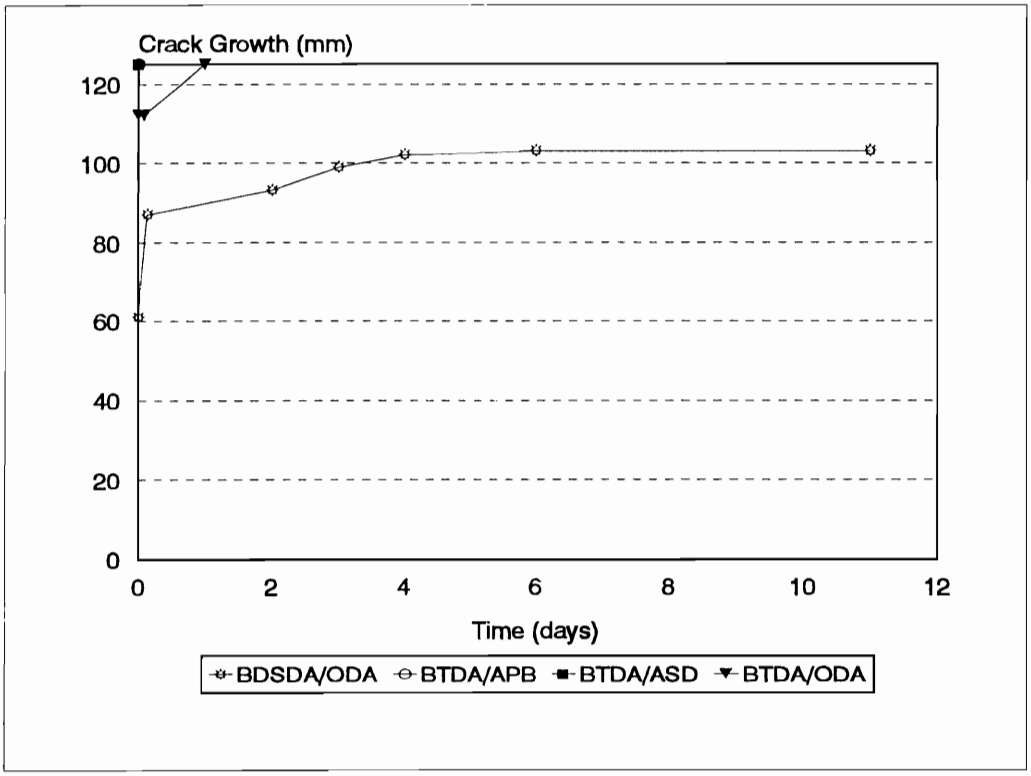

Figure 47. Crack Growth in NaOH Etched Polyimide/Aluminum Wedge Bonds Tested in a Wet Environment at Room Temperature.

within ninety minutes, while the etched specimens (Figures 43 and 47) failed within two hours. Again, the specimens seemed to fail too quickly for environmental conditions to have much of an effect on crack growth, although it did seem to affect how it failed. The surface pretreatment also affected the locus of failure. The dry wiped BTDA/ODA bonds failed adhesively (Figure 44), as determined by XPS, since one side had a considerable amount of aluminum (11.7 atomic%); while, the other side had practically none (0.2 atomic%). The dry etched BTDA/ODA bonds appeared to fail in mixed mode (Figure 45) since sizable amounts of both aluminum and polyimide were found on both surfaces. The wet wiped BTDA/ODA bonds were assumed to fail cohesively since only 1 atomic% aluminum was found on either surface (Figure 48).

As in the peel tests, the low Tg polyimides generally performed better than the high Tg polyimides in the wedge specimens. The wiped BTDA/APB bonds had an initial crack length of 51 mm ± 9 mm. The wet wiped bonds (Figure 46) failed after three hours, while the dry wiped bonds (Figure

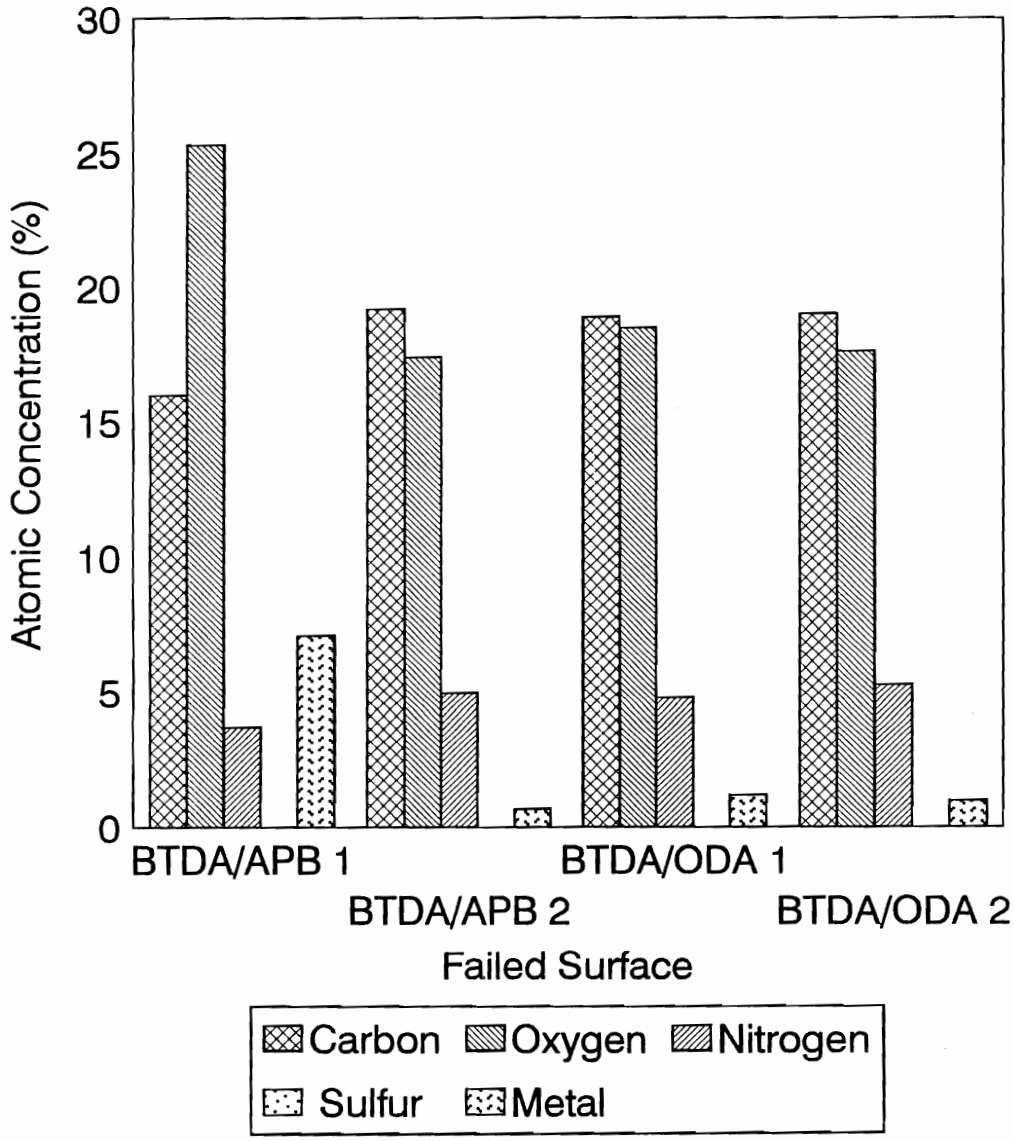

Figure 48. Surface Atomic Concentrations of Failed Acetone Wiped BTDA/ODA/Aluminum and BTDA/APB/Aluminum Wedge Bonds Tested in a Wet Environment.

42) appeared to stop after a crack growth of 18 mm ± 7 mm after three hours. Surface analysis of both the wet and dry wiped BTDA/APB bonds indicated that they failed cohesively (Figures 49 and 50). The NaOH etched BTDA/APB bonds all failed within a few minutes (~ 2 min) of inserting the wedge and failed cohesively via XPS (Figure 48).

Overall, the BDSDA/ODA bonds performed the best in the wedge test. The bonds using acetone wiped substrates had an initial crack growth of 48 mm ± 8 mm, which was not significantly different from the BTDA/APB acetone wiped bonds. After four hours, however, the average crack growth was only 5 mm ± 6 mm for the acetone wiped BDSDA/ODA bonds tested in a dry environment. The acetone wiped BDSDA/ODA bonds tested in a wet environment had an average crack growth of only 29 mm ± 11 mm and had not failed after four hours. The NaOH etched BDSDA/ODA bonds were not significantly worse with an initial crack length of 59 mm ± 7 mm. The NaOH etched BDSDA/ODA bonds tested in a dry environment, however, had an average crack growth of only 38 mm ± 1 mm after eleven days. The acetone wiped BDSDA/ODA

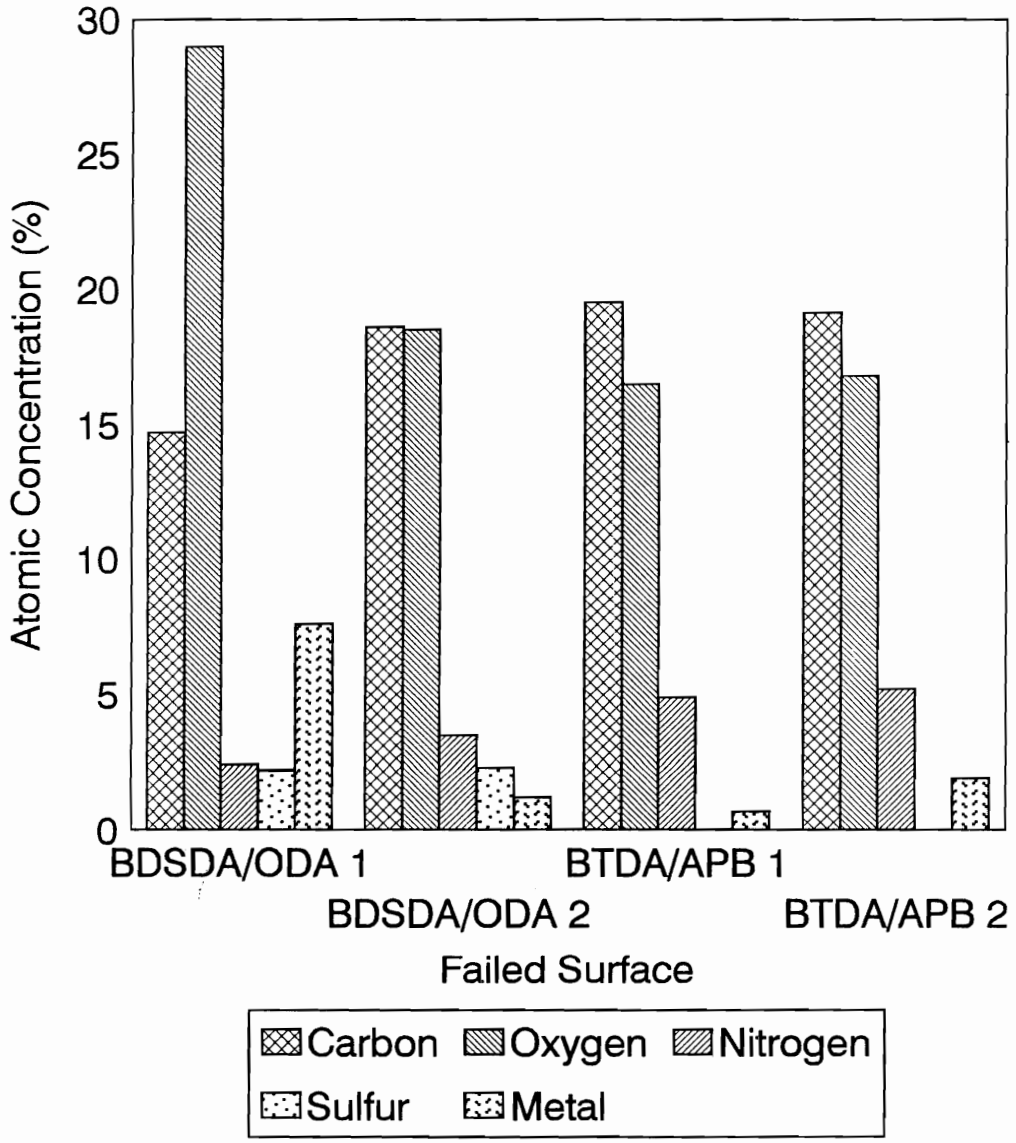

Figure 49. Surface Atomic Concentrations of Failed Acetone Wiped Low Tg Polyimide/Aluminum Wedge Bonds Tested in a Wet Environment.

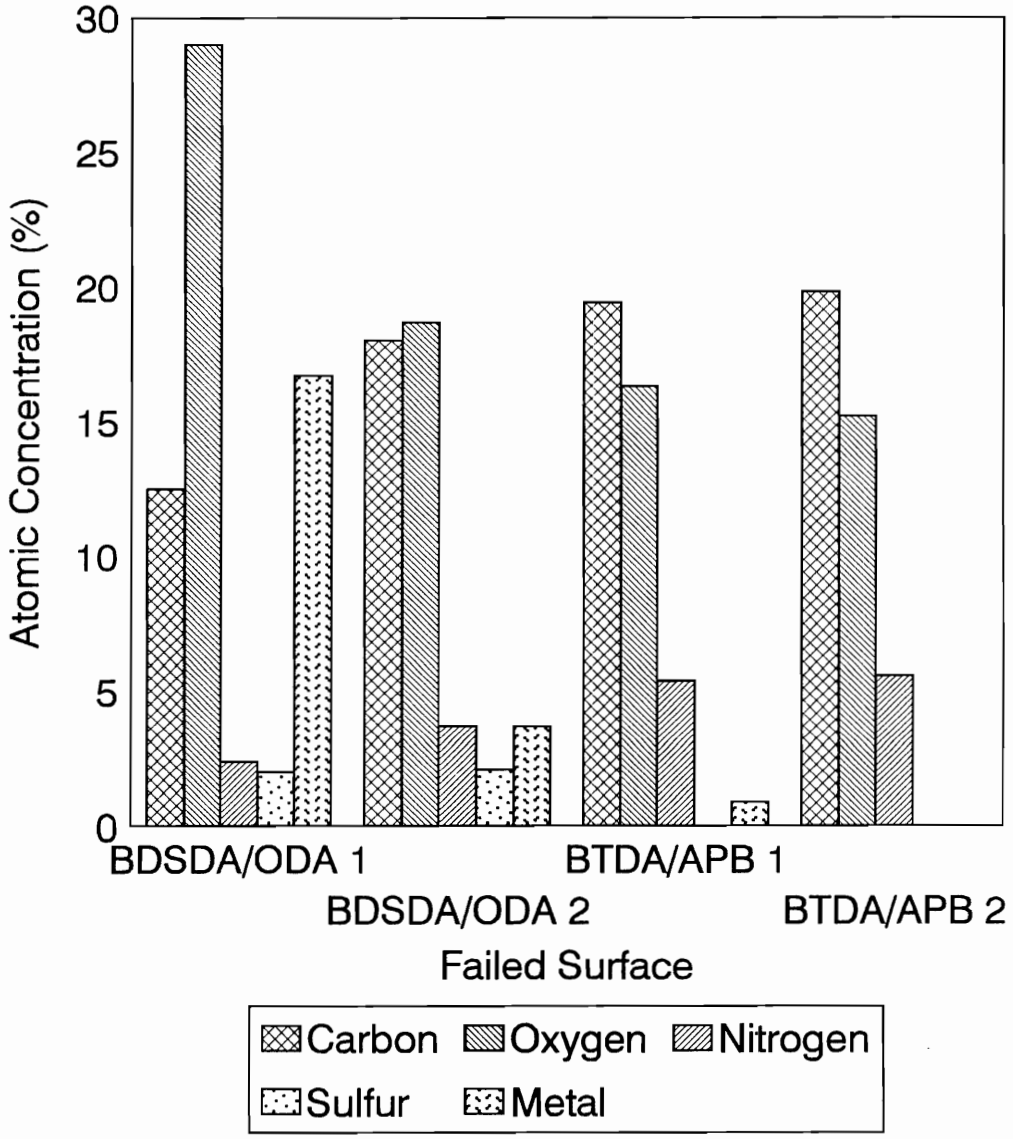

Figure 50. Surface Atomic Concentrations of Failed NaOH Etched Low Tg Polyimide/Aluminum Wedge Bonds Tested in a Dry Environment.

bonds tested in a wet environment had a crack growth of only 24 mm ± 6 mm after twenty-two days. The NaOH etched BDSDA/ODA bonds tested in a wet environment had an average crack growth of 42 mm ± 7 mm after eleven days which was similar to the crack growth of 41 mm ± 16 mm after twenty-two days for the wet wiped BDSDA/ODA bonds. The wet BDSDA/ODA bonds were determined to have failed within the substrate via XPS (Figure 51) because very little polyimide (*i.e.* nitrogen and sulfur concentrations) was observed on either surface. The surface preteatment did not seem to have an effect. Also, some sulfur had been oxidized along these surfaces (Figure 52). The dry wiped BDSDA/ODA bonds failed interfacially since one side had some aluminum (~ 7.6 atomic%); while, the other side had very little (~ 1 atomic%). Meanwhile, the dry etched BDSDA/ODA bonds failed in mixed mode since aluminum and polyimide both were found on each surface in significant amounts.

The etching pretreatment, overall, was detrimental to the durability of the bonded aluminum. It did, however, seem to increase the interfacial strength of the dry bonds.

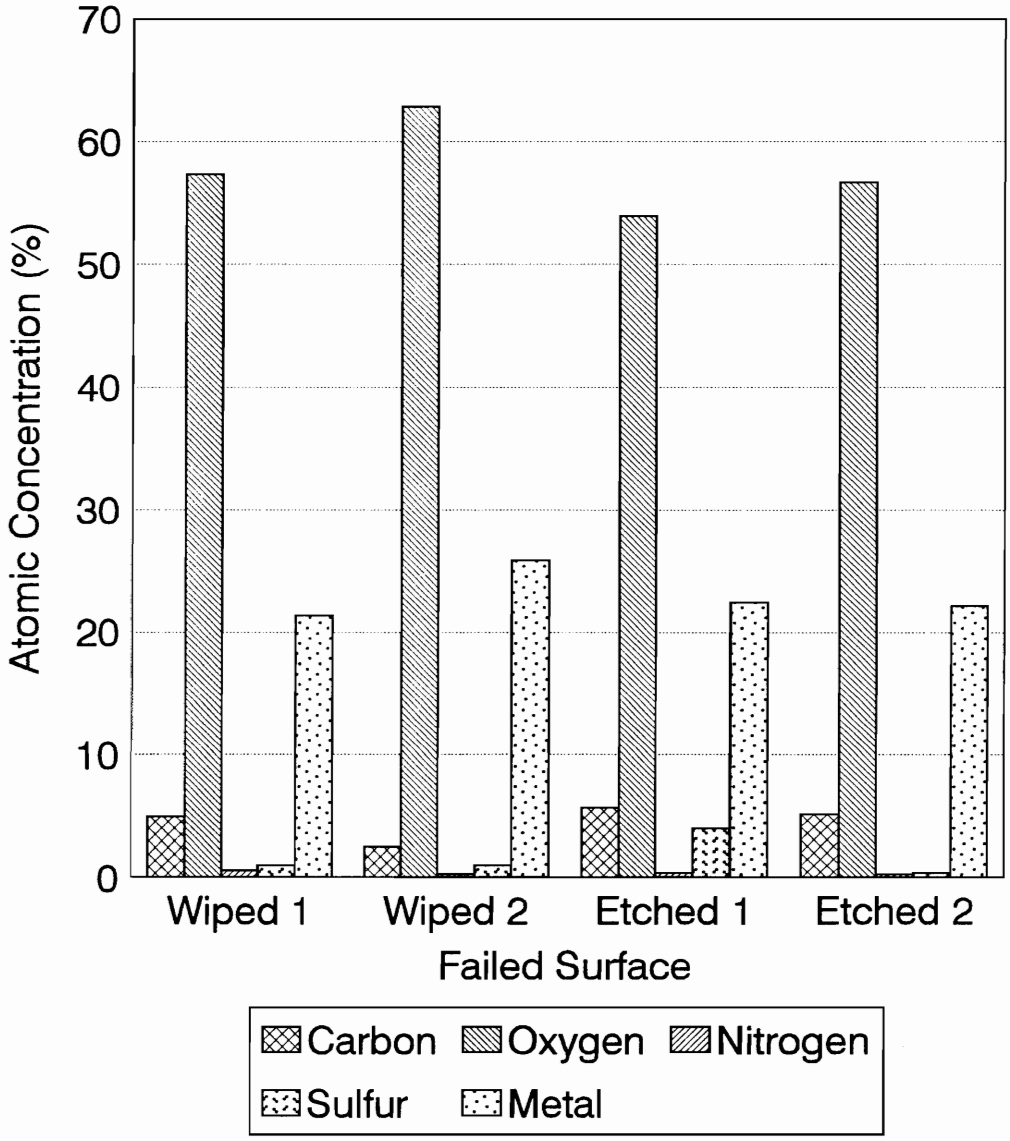

Figure 51. Surface Atomic Concentrations of Failed Acetone Wiped and NaOH Etched BDSDA/ODA/Aluminum Wedge Bonds Tested in a Wet Environment.

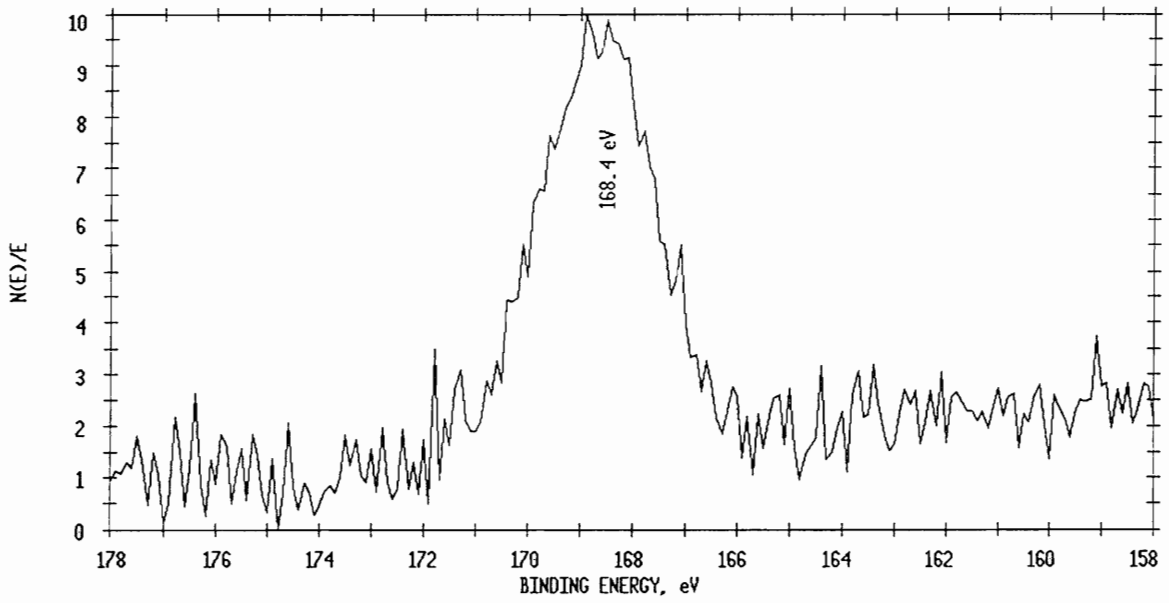

Figure 52. Sulfur 2p XPS Photopeak of Failed BDSDA/ODA Wedge Bond Surface Tested in a Wet Environment(Binding Energy Calibrated to C 1s = 284.6 eV).

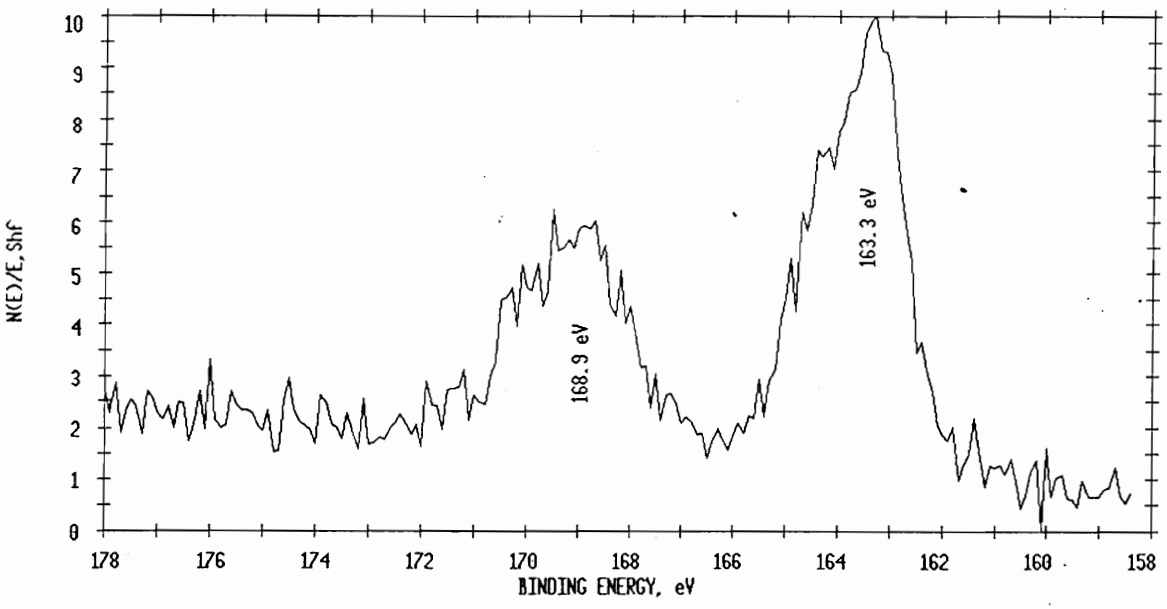

Figure 53. Sulfur 2p XPS Photopeak of Failed BDSDA/ODA Wedge Bond Surface Tested in a Dry Environment (Binding Energy Calibrated to C 1s = 284.6 eV).

If interfacial strength was determined by the locus of failure (adhesive < mixed mode < cohesive), then the etched bonds were generally one step better than the wiped bonds. In other words, if the wiped bond failed adhesively, then the etched bond generally failed in mixed mode.

The wet BDSDA/ODA bonds, both etched and wiped, failed in such a way as to reveal oxidized sulfur. In the case of the wet wiped bonds, all of the sulfur (~ 2.0 atomic%) was converted to the oxidized species on both surfaces. The same was true of the etched wet bonds, but the atomic concentration of sulfur was very small (~ 0.5 atomic%). In the dry bonds, both etched and wiped, one side contained a mixture of oxidized and thioether sulfur while the other side contained only thioether sulfur (Figure 53). The BTDA/ASD bonds did not exhibit oxidized sulfur, but this was most likely due to the fact that these bonds failed predominantly cohesively. The exposed surfaces were not close enough to the interface to observe whether the sulfur was oxidized or not (Figure 54). Oxidized sulfur was not observed on the failed surfaces of the peeled samples. The

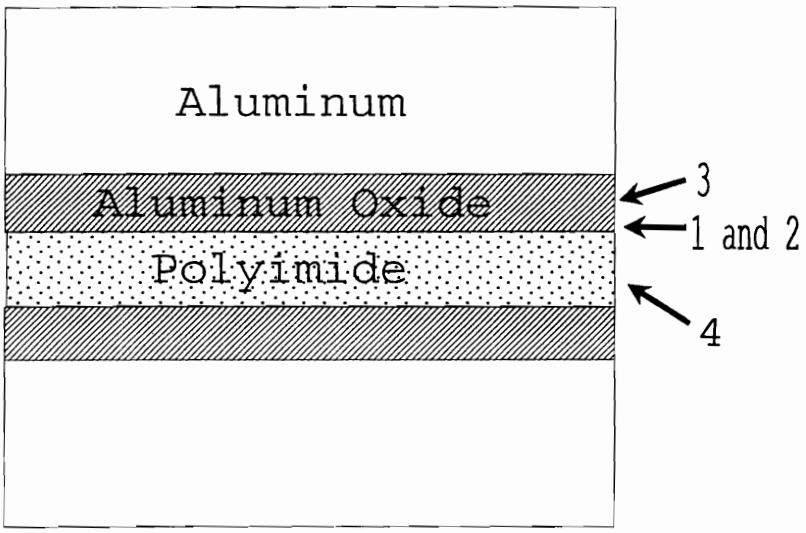

1 - Oxidized sulfur would be found here.

2 - Locus of failure for BDSDA/ODA bonds tested in a dry environment.

3 - Locus of failure for BDSDA/ODA bonds tested in a wet environment.

4 - Locus of failure for BTDA/ASD bonds.

Figure 54. Locus of Failure and Most Probable Location of Oxidized Sulfur.

substrates used in the wedge specimens were alloys, however. Differences in surface topography could account forthe difference in catalytic activity. Also, the peel specimens were prepared from two pieces of 5" x 6" foil, while the wedge specimens were prepared using six sets of two 1" x 6" coupons. Thus, the smaller wedge specimens had more surface area around the edges for oxygen to diffuse into the polyimide to cause the oxidation.

SUMMARY

Surface pretreatment and Tg had more of an effect on peel strength than the presence of sulfur in the polyimide backbone. NaOH etching and comparatively low Tg combined to produce the highest peel strengths. These factors combined the removal of surface oxide from the adherend with a flexible polyimide which could better relieve stress during testing. Little difference was observed between the peel strengths of sulfur and non-sulfur containing polyimides. No oxidation of sulfur was observed in the peel samples either. NaOH etching also caused both wedge and peel

specimens to fail more within the polyimide than in the oxide layer of the adherend. Thus, the NaOH etch appeared to increase interfacial adhesion between the aluminum and the polyimide.

The low Tg polyimides also performed better than the high Tg polyimides in the wedge test with BDSDA/ODA performing the best. This observation could be due to the metal-sulfur interaction (BDSDA/ODA) since oxidized sulfur was observed on the failed surfaces of these bonds regardless of the environment or surface pretreatment. Thus, metal substrates can cause oxidation of thioether sulfur in the interfacial region. These results indicated that oxidation may at least help bond durability. Oxidation was not evident in the peel samples with pure aluminum substrates, and the peel strengths for sulfur and non-sulfur containing polyimides with similar Tg were quite close.

V. SULFUR VERSUS NON-SULFUR CONTAINING POLYIMIDE ADHESIVES FOR BONDING STEEL

INTRODUCTION

Due to their excellent thermal, insulative, and mechanical properties, aromatic polyimides have found considerable use as high-temperature adhesives in aerospace and electronic industries [73]. One of the problems with aromatic polyimides, however, is their general difficulty in processing. Thus, many attempts have been made over the years to synthesize new aromatic polyimides which are more easily processed. In this regard, work at NASA-Langley Research Center has focused on attempts to synthesize thermoplastic polyimide adhesives [33-37, 74]. Two of these polyimides which have proven to be processable and possess acceptable adhesive properties employed 4,4'-bis(3,4-dicarboxyphenoxy)diphenyl sulfide dianhydride (BDSDA) [33-37].

Taylor and co-workers have also employed BDSDA in the synthesis of metal-modified polyimide composite films that exhibit relatively low glass transition temperatures.

Cobalt [24-26], silver [27, 28, 50], copper [23], and iron additives have been shown to catalyze the oxidation of thioether sulfur in the polyimide backbone during thermal curing. The oxidized sulfur species in these free standing films, as discussed earlier, appeared to be "sulfonate/sulfate".

While most reports have examined the adhesion of polyimides to titanium alloys or composites [34-36, 75-77], only a few studies, which were quite old, have examined the bonding of polyimides to steel. One study [78] used the polyimide NR-150, developed by E.I. DuPont de Nemours & Co., Inc., either to bond Type 17-7 PH stainless steel (used in airframe parts [79]) with itself or to bond Type 430 stainless steel (used in automobile trim [79]) with SP-22 composite. The surface pretreatment used in this study was not identified. Lap shear strengths, which had been corrected for the per cent of area bonded, of 29.6 MPa for Type 17-7 and 8.97 MPa for Type 430 were reported for bonds tested at room temperature. The lower value for the steel/composite samples was believed to be due to failure

within the composite. In the steel/steel samples, failure was reported to occur between the metal and the NR-150.

Another adhesive study used stainless steel adherends in an effort to determine the effects of high temperature aging on bonded joints. The polyimides studied were (a) P4A/A5FA, a copolymeric blend of TRW A-type polyimide and Amoco AI 1137 amide-imide resins, and (b) BR34/FM34, an American Cyanimid condensation polyimide [80]. The P4A/A5FA polyimide contained arsenic pentoxide as an oxidation scavenger which was believed to be necessary for bonding stainless steel. One of the key components of the A-type polyimide was thiodianiline (TDA), a sulfur containing diamine. No mention of the possibility of oxidized sulfur could be found in this report. Both polyimides exhibited similar lap shear strengths for bonding stainless steel when tested at room temperature, 19.3 MPa (P4A/A5FA) and 22.1 MPa (BR34/FM34). Lap shear joints were also exposed to +600°F to -423°F to +600°F thermal cycles which did not appear to affect lap shear strength; however, no time was reported for the thermal cycle.

A study by Burgman and co-workers [81] examined the bonding of stainless steel AM350SCT with one of three polyimides. The polyimides examined were I-8 (synthesized from *m*-phenylenediamine and BTDA), I-40 (I-8 endcapped with *p*-aminoacetanilide and phthalic anhydride), and I-66 (I-8 endcapped with only *p*-aminoacetanilide). Polyimides I-40 and I-66 when used with 181-A1100 E-glass cloth produced the best bonds with lap shear strengths in excess of 20.7 MPa when tested at room temperature. Both polyimides also performed well at elevated temperatures having lap shear strengths in excess of 13.8 MPa at 550°C. Over 50% of this strength was retained at temperature after 1000 hours in air at 550°C.

More recently, Tamai and co-workers reported in a patent the development and use of polyimides containing an indane structure (Structure 9) in the diamine portion of the polymer to bond cold rolled steel panels [82]. This polyimide was developed in an attempt to produce an adhesive with both excellent bonding strength and good thermal durability. These bonds possessed lap shear strengths of

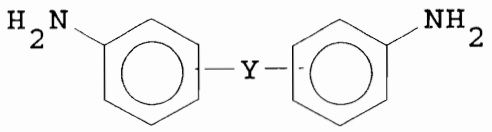

Where Y is

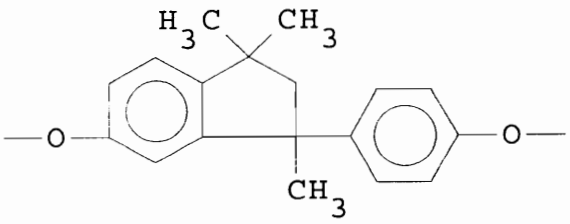

or

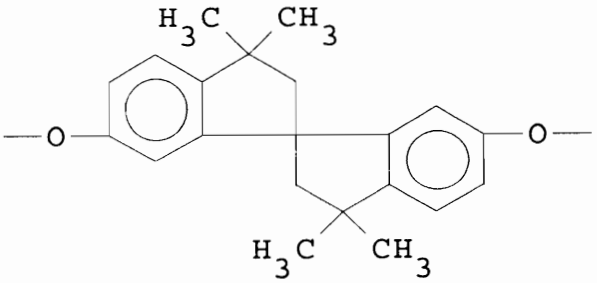

Structure 9. Ether Diamine with Indane Structure

26.0 MPa when tested at room temperature and 19.2 MPa when tested at 200°-240°C. No other reports of polyimides with steel adherends could be found.

Metal-catalyzed oxidation of thioether sulfur may have ramifications for thioether containing polymeric adhesives. Oxidation of the polymeric component of the interface can increase peel strength as in the adhesion of polyethylene to steel and other metals [83-86]. The peel strength of polyethylene bonded to cold rolled mild steel containing an antioxidant and bonded to steel was 0 kg/cm, while the peel strength of the polyethylene/steel specimen without the antioxidant was 6.5 kg/cm [83]. The nature of the reactive groups at the polymer/steel interface was not investigated. In studies with polyethylene bonded to copper and aluminum [85], however, IR analysis detected the formation of carbonyl groups which were believed to be interacting (e.g. chemisorption) with the metal surface. Adhesion, on the other hand, can suffer if the polymer undergoes extensive catalytic oxidative degradation [87] wherein the integrity of the polymer is damaged and a weak boundary layer between

polymer and adherend forms, thus weakening the bond.

Beneficial metal-sulfur adhesive interactions have also been suggested to take place in bonds composed of polyphenylene sulfide and steel where the thioether sulfur was stated to be oxidized to SO_2 and SO_3 when the bonds were prepared in an O_2 atmosphere [88]. These products reacted with the Fe_2O_3 on the steel surface to produce $Fe_2(SO_4)_3$ and $FeSO_4$ as determined by XPS of the failed surfaces. The 1010 cold-rolled steel and the AISI 304 stainless steel substrates were subjected to an acetone wipe prior to coating with the polyphenylene sulfide. The bonds made using the 99.5% O_2 cure atmosphere showed a 50% increase in lap shear strength compared to those made using a 99.9% N_2 cure atmosphere. The failed surfaces of the nitrogen cured bonds showed evidence of FeS formation via XPS, but no $Fe_2(SO_4)_3$ or $FeSO_4$ was observed. Thus it was concluded by Sugama and Carciello that the formation of $Fe_2(SO_4)_3$ and $FeSO_4$ was responsible for the increased lap shear strength, but no speculation as to the manner in which these reaction products enhanced bond strength was provided.

This study examines the possibility of metal-sulfur interactions in sulfur containing polyimide adhesives where the percentage of sulfur is much less than in polyphenylene sulfide. The potential beneficial or detrimental effects of metal-catalyzed sulfur oxidation have been examined using steel adherends. Surface analysis of failed bond specimens was used to determine the chemical state and composition of the interfacial regions. These data were then correlated with bond strength and the mechanism of bond failure.

EXPERIMENTAL

Materials

The monomers used in this study were the same as in Chapter IV. 1010 Cold rolled steel foil (0.0015" thick) and 1010 cold rolled steel coupons (6" x 1" x 0.13") were used as adherends. The steel substrates used were approximately one half as thick as the aluminum substrates used in Chapter IV in order to minimize the effects of different moduli.

Synthesis

Poly(amide acid) solutions were prepared as discussed

in Chapter II.

Bonding

The steel substrates were pretreated by either an acetone wipe or a chemical etch. The etching process was similar to one used by Hollenhead and Wightman [89] and was intended to remove the surface oxide layer. It consisted of immersing the steel in an aqueous 6M HCl bath for five minutes at room temperature followed by a rinse with deionized water and then acetone. The etched substrates were then air dried. Peel samples and wedge samples were prepared as discussed in Chapter IV.

Measurements

The T-peel and wedge tests were performed as described in the previous chapter. Surface analysis of the failed surfaces was performed via XPS as described in Chapter II.

RESULTS AND DISCUSSION

The same four polyimides used in the aluminum bonding study were used in this study to bond steel to steel. Two were low Tg polyimides; one containing sulfur (BDSDA/ODA,

217°C) and one not containing sulfur (BTDA/APB, 198°C). The other two were high Tg polyimides; sulfur containing (BTDA/ASD, 285°C) and non-sulfur containing (BTDA/ODA, 285°C). From previous work with iron-modified free standing films, it was hypothesized that the iron from the steel substrates would significantly interact with and catalyze the oxidization of thioether sulfur in the sulfur containing polyimides. Such a mechanism of interaction obviously would not exist for the non-sulfur containing polyimides. The surface pretreatments were chosen to examine the interaction of thioether sulfur with both a hydrated "as is" steel surface and one in which the oxide layer has been partially removed revealing bare iron. The T-peel test was chosen to compare these polyimides due to the simplicity of the test and its emphasis on interfacial strength; while the wedge test was chosen because of its emphasis on bond durability. While the stress situation in the peel test is difficult to assess, the peel test has often been used to compare the relative strengths of adhesives and the effects of surface pretreatment [71, 72].

Steel Foil and Coupon Substrates

Surface analysis was performed on both the HCl acid etched and acetone wiped steel surfaces to characterize the chemistry at the surface prior to casting the poly(amide acid) solution. Unfortunately, several factors combined to make the analysis of the iron 2p region difficult. First, the baseline climbs steeply in this region. This factor, by itself, would not present much difficulty if the peaks were clear and well defined. This, however, was not the case. Multiplet splitting of the iron 3d electrons, excess surface oxygen, and non-stoichiometry combined to cause shake-up satellite peaks to occur quite readily. These satellite peaks can have the same relative intensity as the parent Fe 2p photopeak, thereby resulting in broad signals with a half-width of 3.8 to 4.4 eV [43, 90, 91]. Thus, it can often be difficult to detect slight changes in the binding energies of the iron ions. Another problem was the fact that iron oxides dissociatively chemisorb water and oxygen [43]. This chemisorption process produces a surface rich in hydroxyl groups; which, in turn, broadens the high binding

energy side of the oxygen 1s photopeak.

Analysis of the surface of the acetone wiped steel foil revealed Fe $2p_{3/2}$ and Fe $2p_{1/2}$ photopeaks with binding energies of 710.7 ± 0.2 eV and 724.2 ± 0.2 eV, respectively (Figure 55). The Fe 3p photopeak had a binding energy of 55.2 ± 0.2 eV. These photopeaks indicated that the iron on the surface was in the form of Fe^{3+} [43-44, 92-94]. The binding energy of iron metal was Fe $2p_{3/2}$ 706.6 ± 0.3 eV for the Fe $2p_{3/2}$ photopeak, while FeO exhibits a Fe $2p_{3/2}$ binding energy of 709.5 ± 0.4 eV [43-44, 92-94]. Unfortunately, the binding energies for the Fe2p photopeaks in the various iron(III) oxides (e.g. Fe_2O_3, FeOOH, and Fe_3O_4) are all within a range of 1 eV, thus making it difficult to identify the exact forms of iron oxide or oxyhydroxide that were present. The O 1s photopeak at a binding energy of 529.9 ± 0.1 eV (Figure 56). The position of this photopeak was indicative of the oxide oxygen found in Fe_2O_3 [43-44, 93]. It was evident, however, that the surface also contained chemisorbed water due to the high binding energy shoulder that appeared on the O 1s photopeak at 531.6 ± 0.1 eV. This

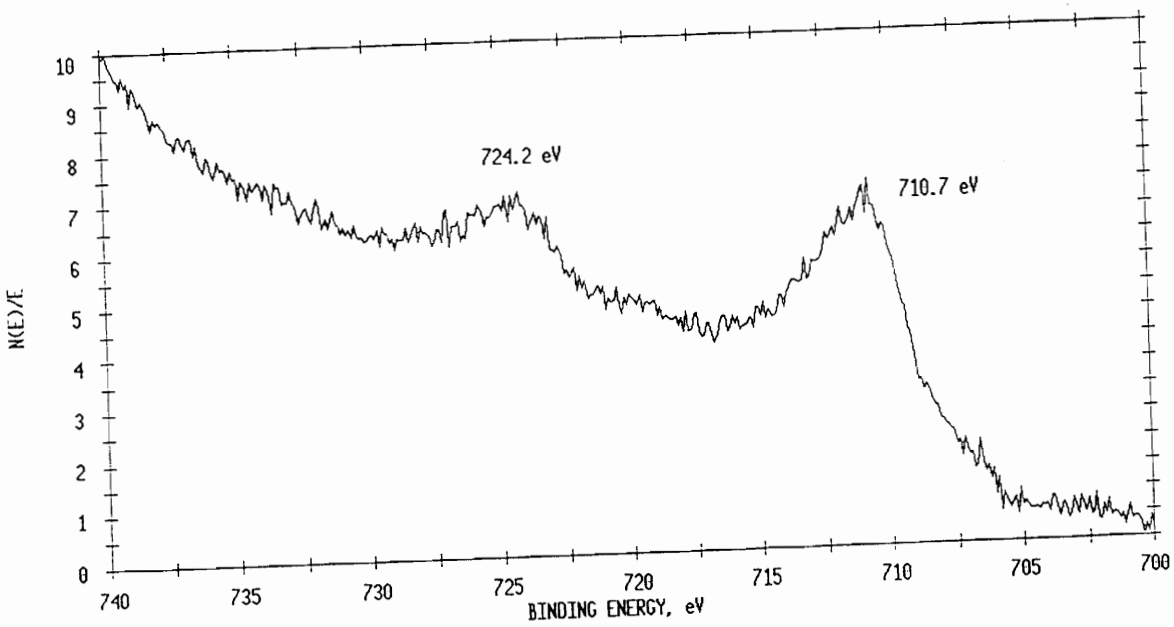

Figure 55. Iron 2p XPS Photopeak of Acetone Wiped 1010 Low Carbon Steel Foil (Binding Energy Calibrated to C 1s = 284.6 eV).

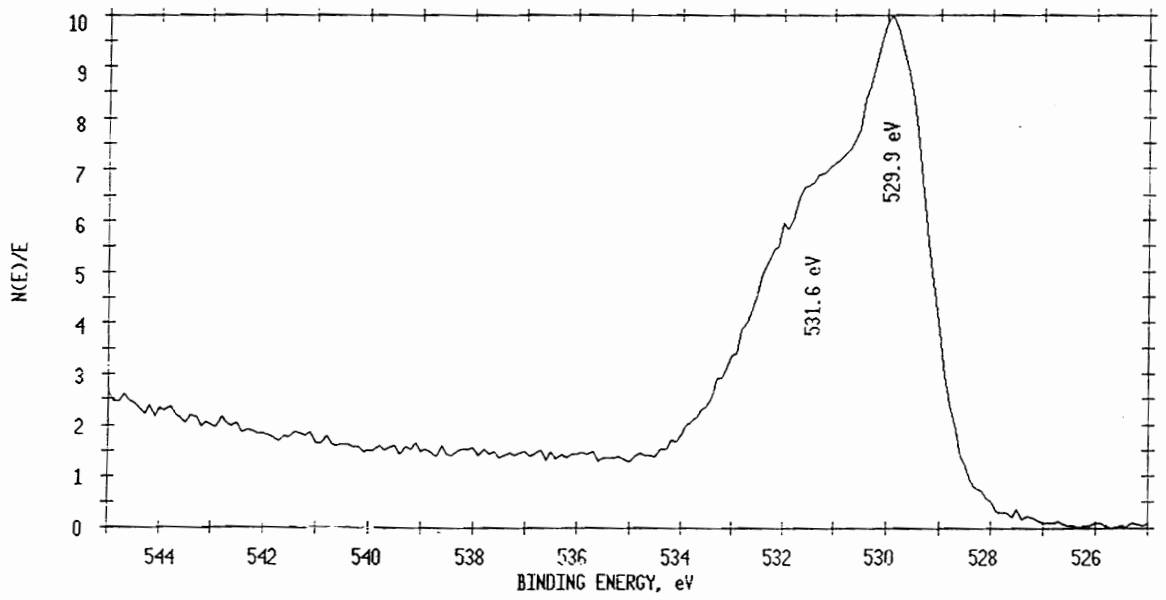

Figure 56. Oxygen 1s XPS Photopeak of Acetone Wiped 1010 Low Carbon Steel Foil (Binding Energy Calibrated to C 1s = 284.6 eV).

photopeak position is typical of the oxygen signal found in species that contain Fe-O-H bonds [43, 95-97]. Thus, the surface seemed to be composed of a mixture of Fe_2O_3 and FeOOH.

Analysis of the 6M HCl etched steel foil surface was similar to that of the acetone wiped surface. The Fe $2p_{3/2}$ and Fe $2p_{1/2}$ binding energies were 711.1 ± 0.2 and 724.5 ± 0.2 eV (Figure 57), respectively, and the primary O 1s binding energy was 530.2 ± 0.1 eV (Figure 58). Some surface contamination due to adsorbed water or FeOOH formation as indicated by the O 1s shoulder at 531.6 ± 0.1 eV was also observed. These assignments indicated that the predominant iron species on the surface was Fe_2O_3 and FeOOH. The acid etch, however, did expose some iron metal as indicated by the low binding energy shoulders in the Fe $2p_{3/2}$ and Fe $2p_{1/2}$ photopeaks at 707.4 ± 0.2 and 720.1 ± 0.2 eV [43-44, 92-94].

The acetone wiped coupon surface appeared to be primarily FeOOH rather than a mixture of Fe_2O_3 and FeOOH with Fe $2p_{3/2}$ and Fe $2p_{1/2}$ binding energies at 711.0 ± 0.2 eV and 724.7 ± 0.2 eV, respectively (Figure 59). The signals

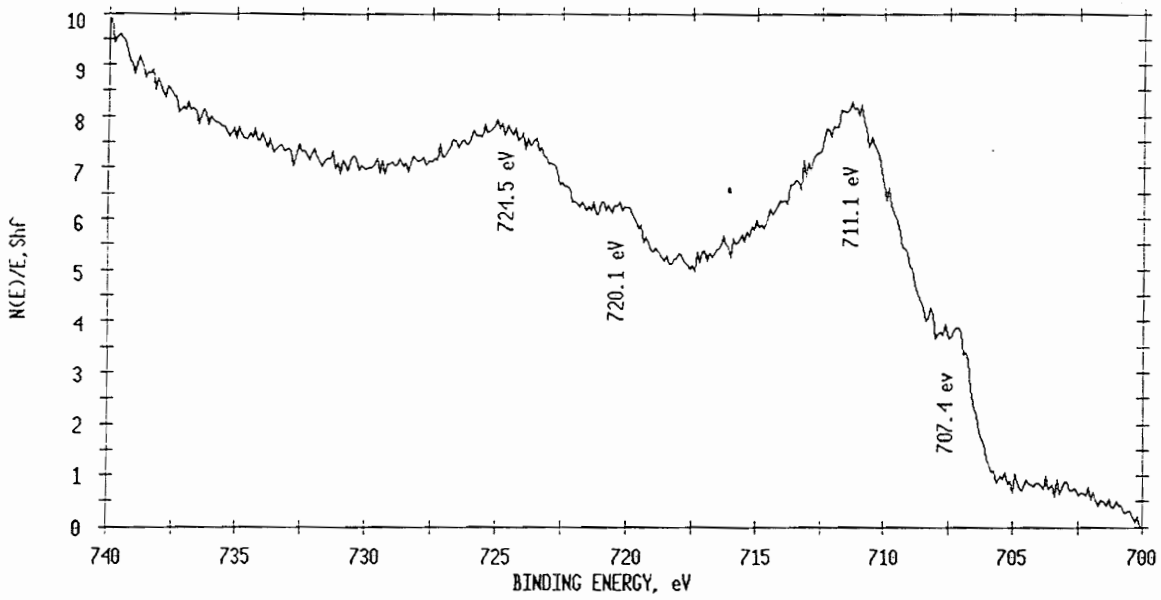

Figure 57. Iron 2p XPS Photopeak of HCl Etched 1010 Low Carbon Steel Foil (Binding Energy Calibrated to C 1s = 284.6 eV).

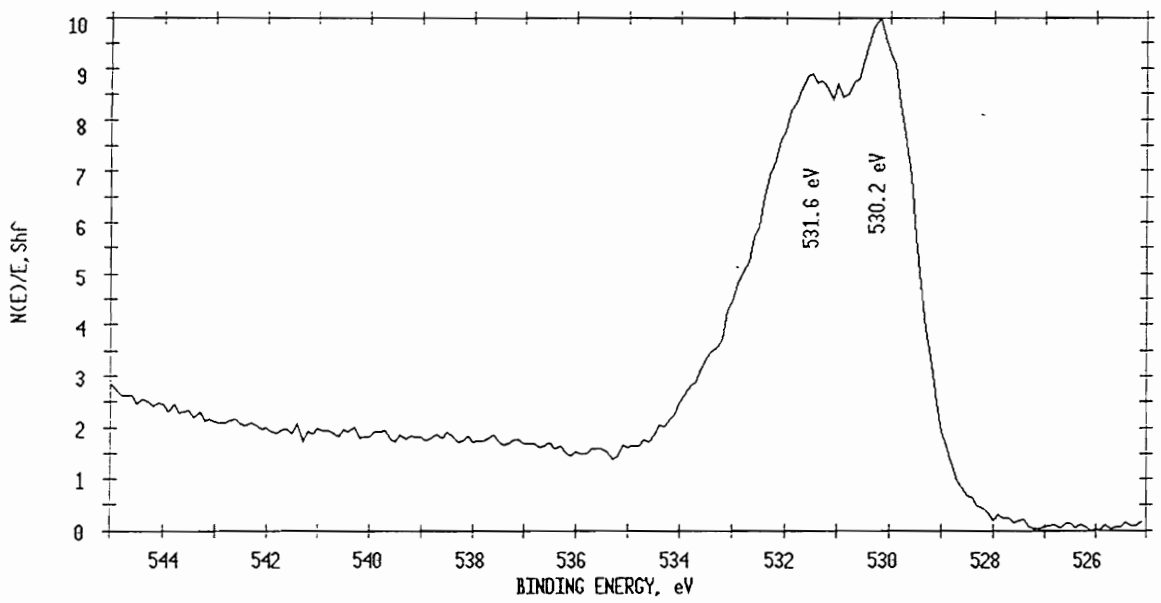

Figure 58. Oxygen 1s XPS Photopeak of HCl Etched 1010 Low Carbon Steel Foil (Binding Energy Calibrated to C 1s = 284.6 eV).

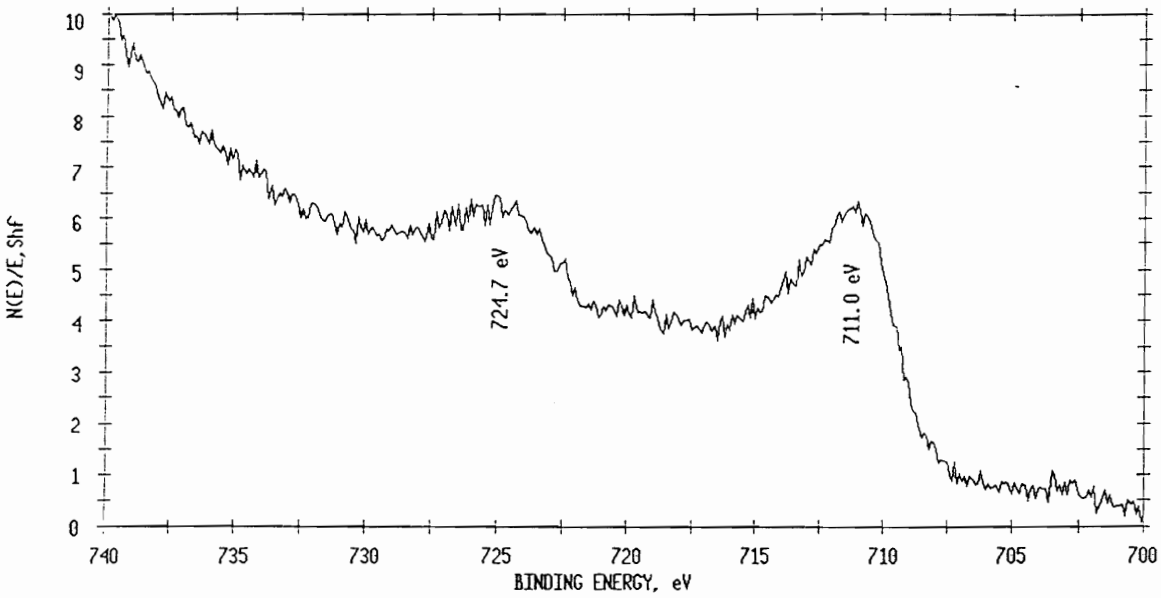

Figure 59. Iron 2p XPS Photopeak of Acetone Wiped 1010 Low Carbon Steel Coupon (Binding Energy Calibrated to C 1s = 284.6 eV).

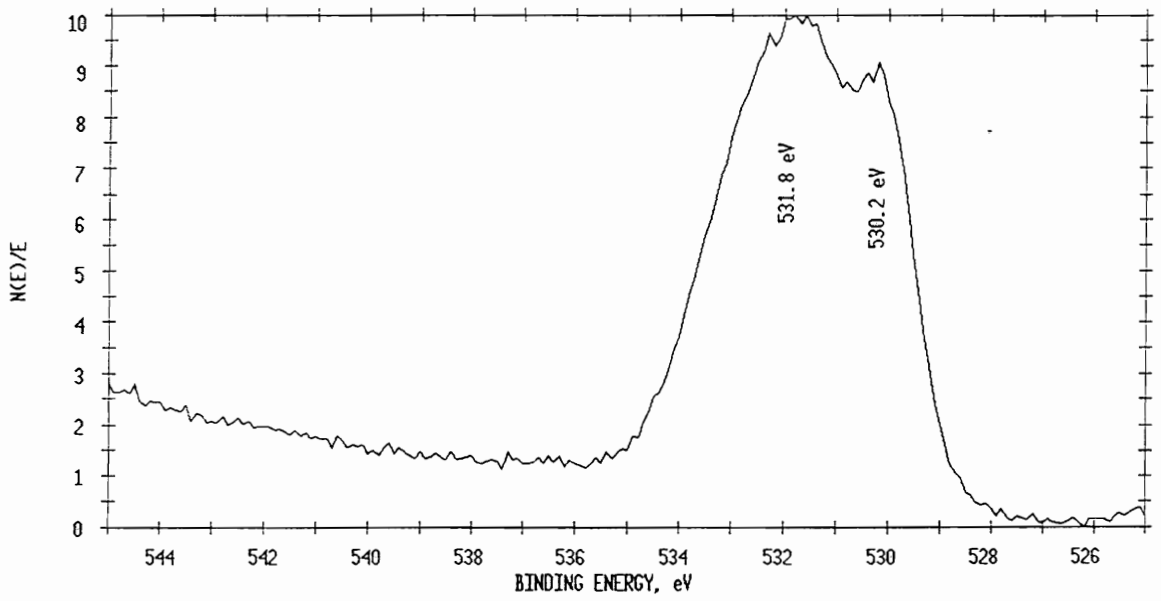

Figure 60. Oxygen 1s XPS Photopeak of Acetone Wiped 1010 Low Carbon Steel Coupon (Binding Energy Calibrated to C 1s = 284.6 eV).

observed here for the hydroxide oxygen with a binding energy of 531.8 ± 0.1 eV and the oxide oxygen at 530.2 ± 0.1 eV were nearly equal as would have been predicted from the compound formula (Figure 60).

The acid etched coupon surface was quite different from the acetone wiped coupon surface. Over twice as much iron was observed on the etched surface (13.9 atomic% compared to 6.1 atomic%) as compared with the wiped surface, but no iron was visible in the metallic state in contrast to the etched steel foil case. The binding energies for Fe $2p_{3/2}$ and Fe $2p_{1/2}$ were 711.6 ± 0.2 and 725.2 ± 0.2 eV, respectively (Figure 61). Also, a strong oxide oxygen photopeak was observed at 530.2 eV (Figure 62). These assignments indicated that the iron was present as Fe_2O_3 [43-44, 92-94]. The presence of the high binding energy shoulder on the oxygen photopeak, however, indicated that chemisorbed oxygen/water was also present.

Peel Tests - Wiped Substrates

The T-peel results of several repetitions have been tabulated in Table IX. No peel data for steel/polyimide

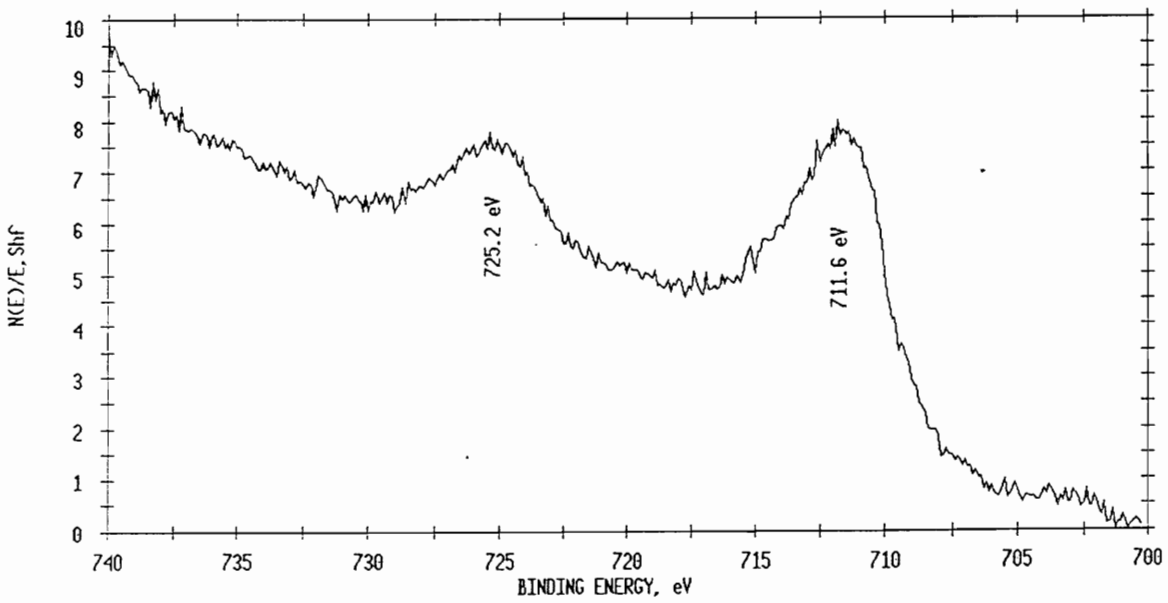

Figure 61. Iron 2p XPS Photopeak of HCl Etched 1010 Low Carbon Steel Coupon (Binding Energy Calibrated to C 1s = 284.6 eV).

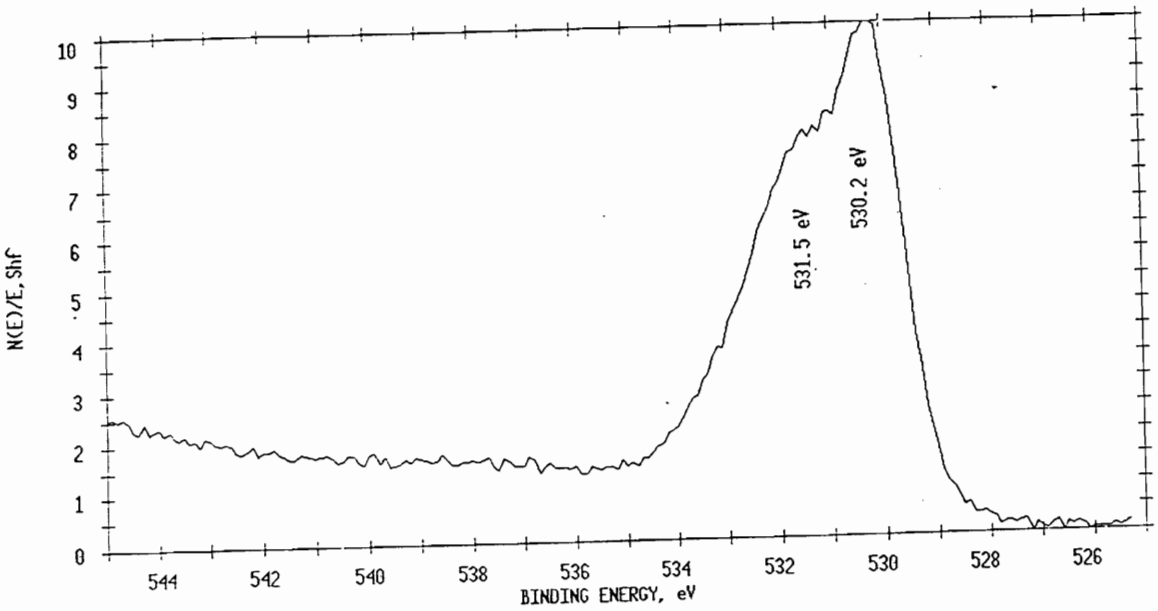

Figure 62. Oxygen 1s XPS Photopeak of HCl Etched 1010 Low Carbon Steel Coupon (Binding Energy Calibrated to C 1s = 284.6 eV).

Table IX. T-Peel Strength and Mode of Failure in the Polyimide/1010 Steel Foil Bonds

Polyimide	Tg	Sulfur	Wiped Bonds		Etched Bonds	
			T-Peel Strength (N/cm)	Failure Mode	T-Peel Strength (N/cm)	Failure Mode
BTDA/APB	Low	No	2.84 ± 0.60	Mixed Mode	2.75 ± 0.44	Mixed Mode
BDSDA/ODA	Low	Yes	2.83 ± 0.84	Cohesive	0.78 ± 0.33	Cohesive
BTDA/ODA	High	No	0.53 ± 0.09	Mixed Mode	0.36 ± 0.11	Mixed Mode
BTDA/ASD	High	Yes	0.78 ± 0.27	Mixed Mode	0.39 ± 0.04	Mixed Mode

previous study with aluminum. Standard deviations for peel samples wherein the steel foil was acid etched were much better than for bonds containing NaOH etched aluminum. On the other hand, standard deviations for bonds containing the acetone wiped steel substrates were similar to those of the bonds containing acetone wiped aluminum substrates.

The low Tg BTDA/APB/wiped steel bonds had a peel strength of 2.84 ± 0.60 N/cm. These bonds appeared to fail in mixed mode as judged by the fact that both failed surfaces contained primarily polyimide as indicated by the atomic concentration of surface nitrogen (e.g. one failed surface had 4.5 atomic% nitrogen and the other had 3.5 atomic% (Figure 63), close to the expected value of 4.5 atomic% nitrogen calculated for BTDA/APB. Some iron was, nevertheless, observed on both surfaces (e.g. 1.4 atomic% iron on one side and 2.5 atomic% on the other), and the Fe 2p binding energy indicated that it was primarily in the form of Fe_2O_3. The carbon concentrations in Figure 63 have been divided by four in order to make the smaller sulfur, nitrogen, and metal concentrations more noticeable.

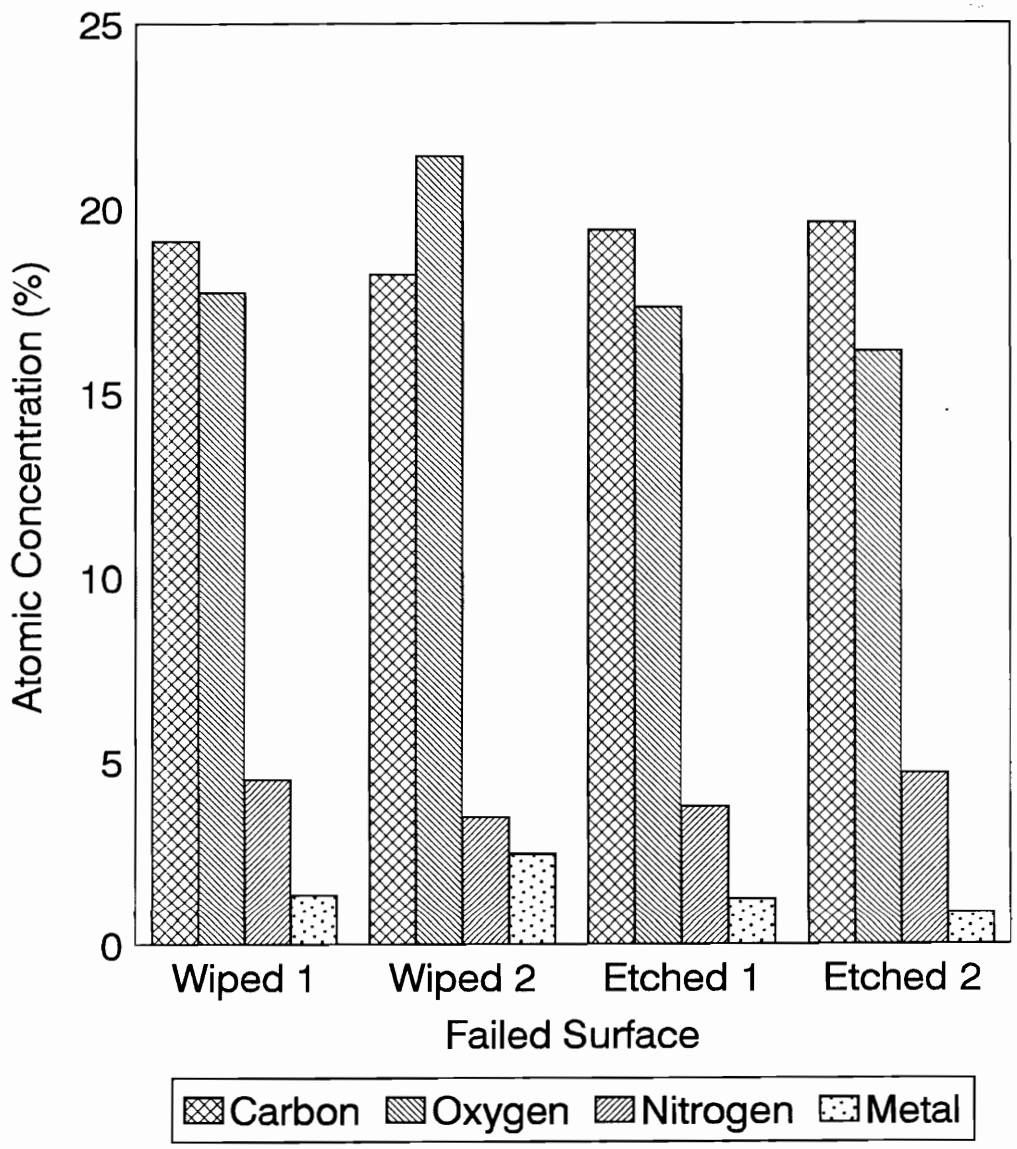

Figure 63. Atomic Concentrations of Failed BTDA/APB/1010 Steel Peel Bond Surfaces (Carbon concentration/4).

Wiped steel bonds with the low Tg, sulfur-containing polyimide (BDSDA/ODA) exhibited a peel strength of 2.83 ± 0.84 N/cm, similar to BTDA/APB. By just examining peel strengths, therefore, it would appear that the presence of thioether sulfur in the backbone had no beneficial effect on bonding. Analysis of the failed BDSDA/ODA surfaces, however, provided an interesting difference. Less than 0.2 atomic% iron was observed on either surface (Figure 64) in contrast to the 1-3 atomic% iron on the failed BTDA/APB surfaces. The sulfur 2p photopeaks from the two failed surfaces had binding energies of 163.2 ± 0.1 eV (Figure 65) which was characteristic of the thioether sulfur found in this polyimide [9, 28]. Had the sulfur been oxidized, the S2p photopeak would have had a binding energy of 168.3 ± 0.1 eV [28]. Since only trace amounts of iron were observed, it was assumed that these bonds failed cohesively (i.e. within the adhesive itself). Thus, it was not surprising that the observed sulfur was not oxidized because it was obviously not close enough to the interphase to have interacted with the iron. Oxidized sulfur, if any, would have only been

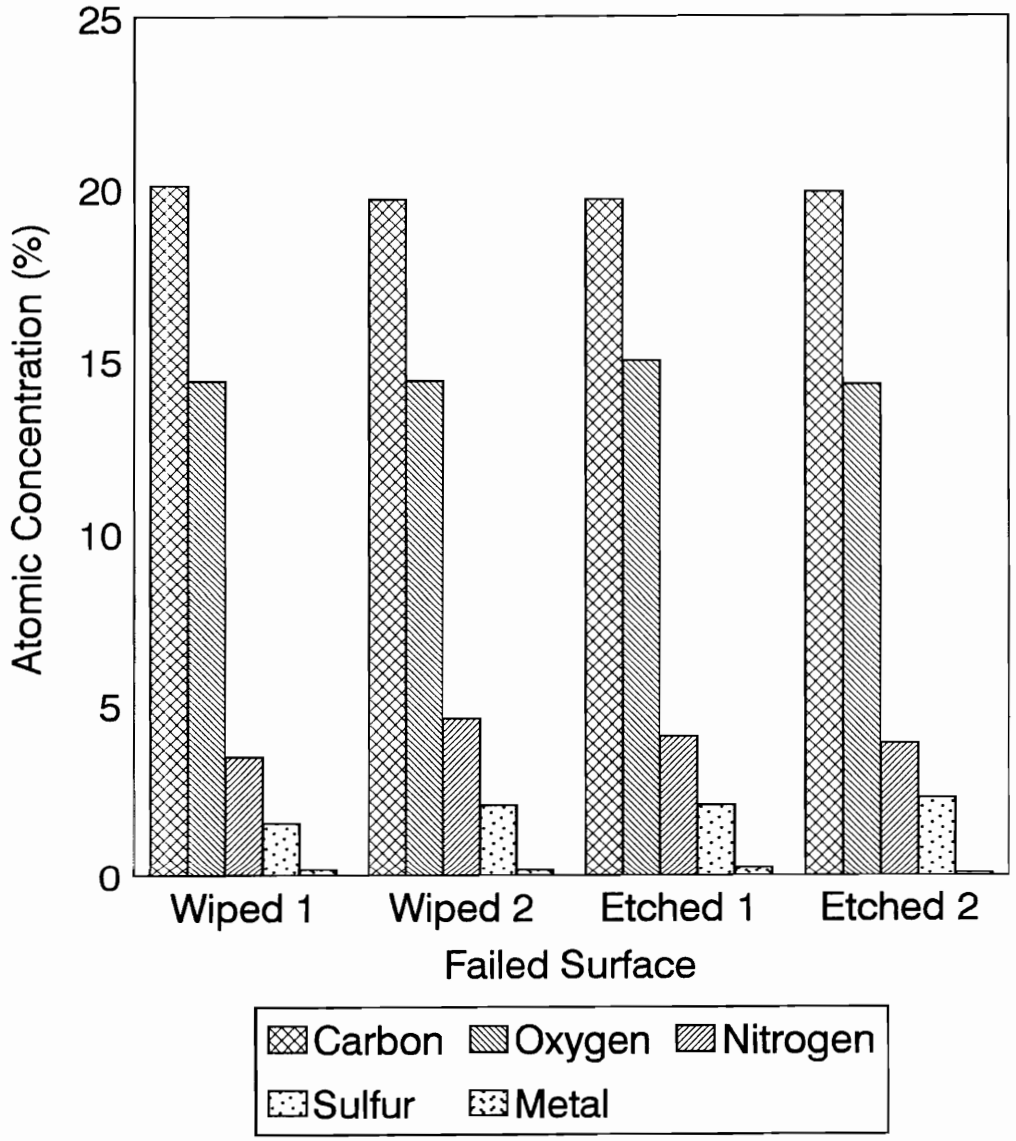

Figure 64. Atomic Concentrations of Failed BDSDA/ODA/1010 Steel Peel Bond Surfaces (Carbon concentration/4).

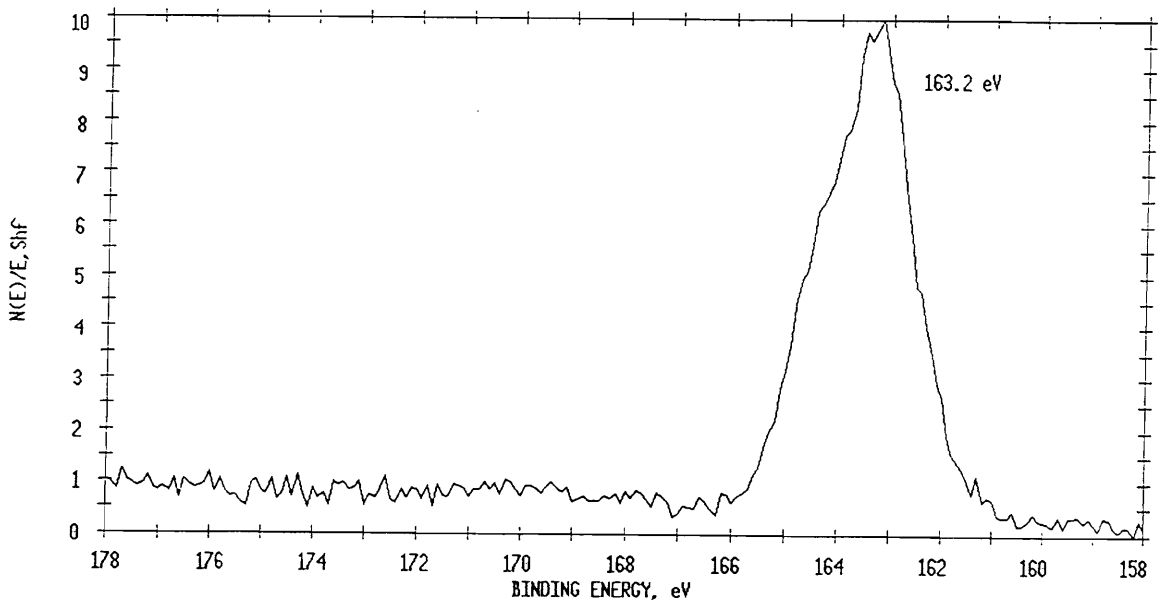

Figure 65. Sulfur 2p XPS Photopeak of Failed Acetone Wiped BDSDA/ODA/Steel Peel Bond Surface (Binding Energy Calibrated to C 1s = 284.6 eV).

observed on the failed surfaces if the bonds had failed in the interphase region, which they did not. One could argue that the absence of oxidized sulfur within the polyimide could be indirect evidence that polyimide sulfur had oxidized in the interphase region, thereby creating functional groups that could bond directly to the metal substrate resulting in increased interfacial strength.

Wiped steel bonds using the high Tg, non-sulfur containing polyimide (BTDA/ODA) had peel strengths much worse than either of the two low Tg polyimides (0.53 ± 0.9 N/cm). These bonds failed in mixed mode as evidenced by the high atomic concentration of iron (4.3 atomic% on side 1 and 3.1 atomic% on side 2)and the presence of polyimide nitrogen (3.4 atomic% on side 1 and 4.4 atomic% on side 2) for each of the two sides (Figure 66). The amount of nitrogen present on either side was lower than the expected 5.6 atomic% of the neat polyimide. The nitrogen concentration was used as an indication of polyimide concentration on the failed surface since both carbon and oxygen were observed on the steel surfaces prior to bonding. The Fe $2p_{3/2}$ photopeak

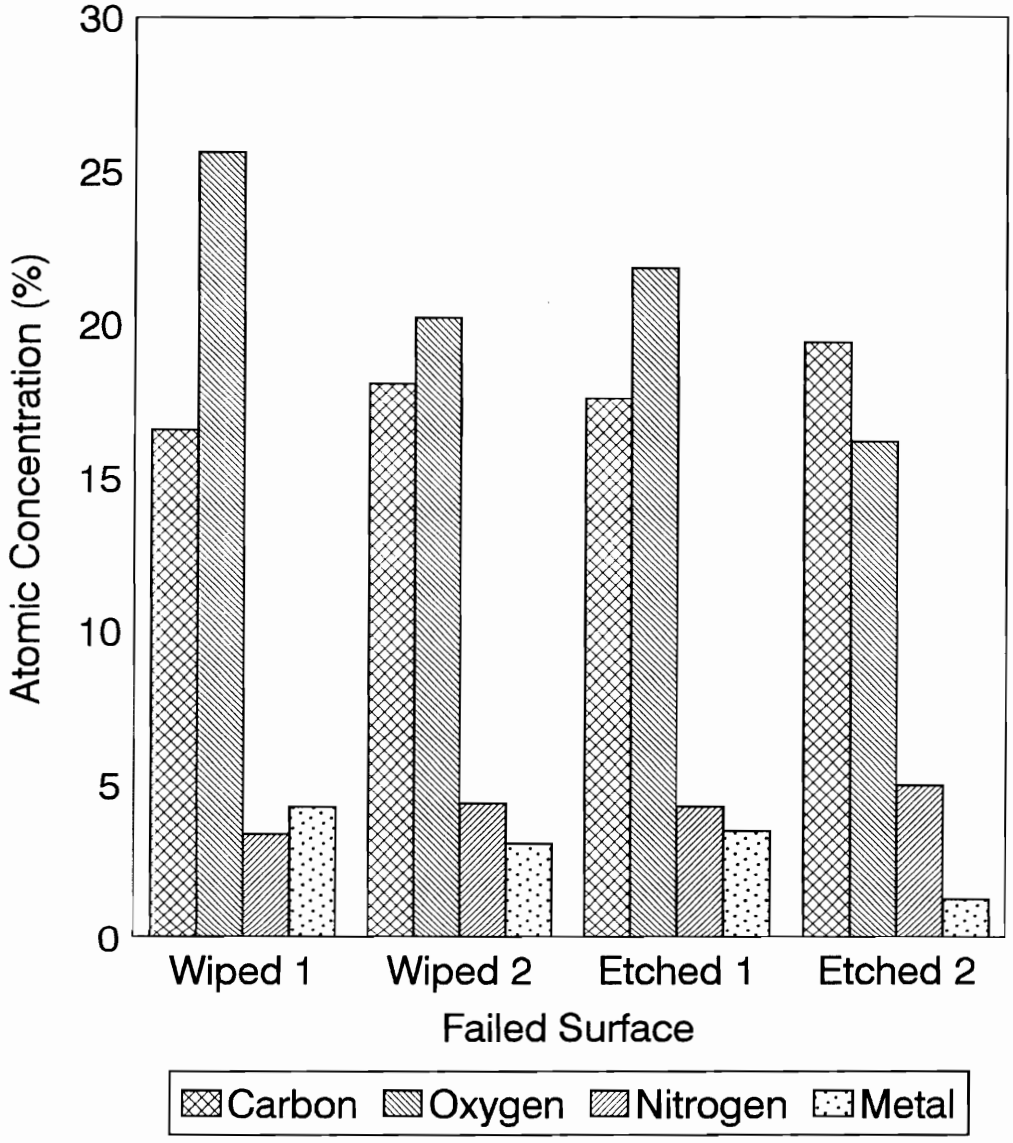

Figure 66. Atomic Concentrations of Failed BTDA/ODA/1010 Steel Peel Bond Surfaces (Carbon concentration/4).

on either failed surface had a binding energy of 711.4 ± 0.2 eV, again indicative of Fe_2O_3.

The peel strength, 0.78 ± 0.27 N/cm, of the wiped steel bonds made using the high Tg sulfur containing polyimide (BTDA/ASD) was quite similar to that of the high Tg BTDA/ODA/wiped steel bonds. Even though the peel strengths for both high Tg polyimides were similar, the BTDA/ASD/wiped steel bonds failed more cohesively. Little iron, for example, was observed on either failed surface (1.2 atomic% and 0.8 atomic%) (Figure 67). While this concentration of iron was more than had been seen on the failed BDSDA/ODA/wiped steel bonds, it was, nevertheless, much less than what was observed in the case of the high Tg BTDA/ODA/wiped steel bonds.

Peel Tests - Etched Substrates

The T-peel strength (2.75 ± 0.44) of the BTDA/APB bonds synthesized using the etched steel substrates was nearly the same as that of the bonds which used acetone wiped steel. The mode of failure (i.e. mixed mode) seems to be similar also. Through surface analysis, it was shown, however, that

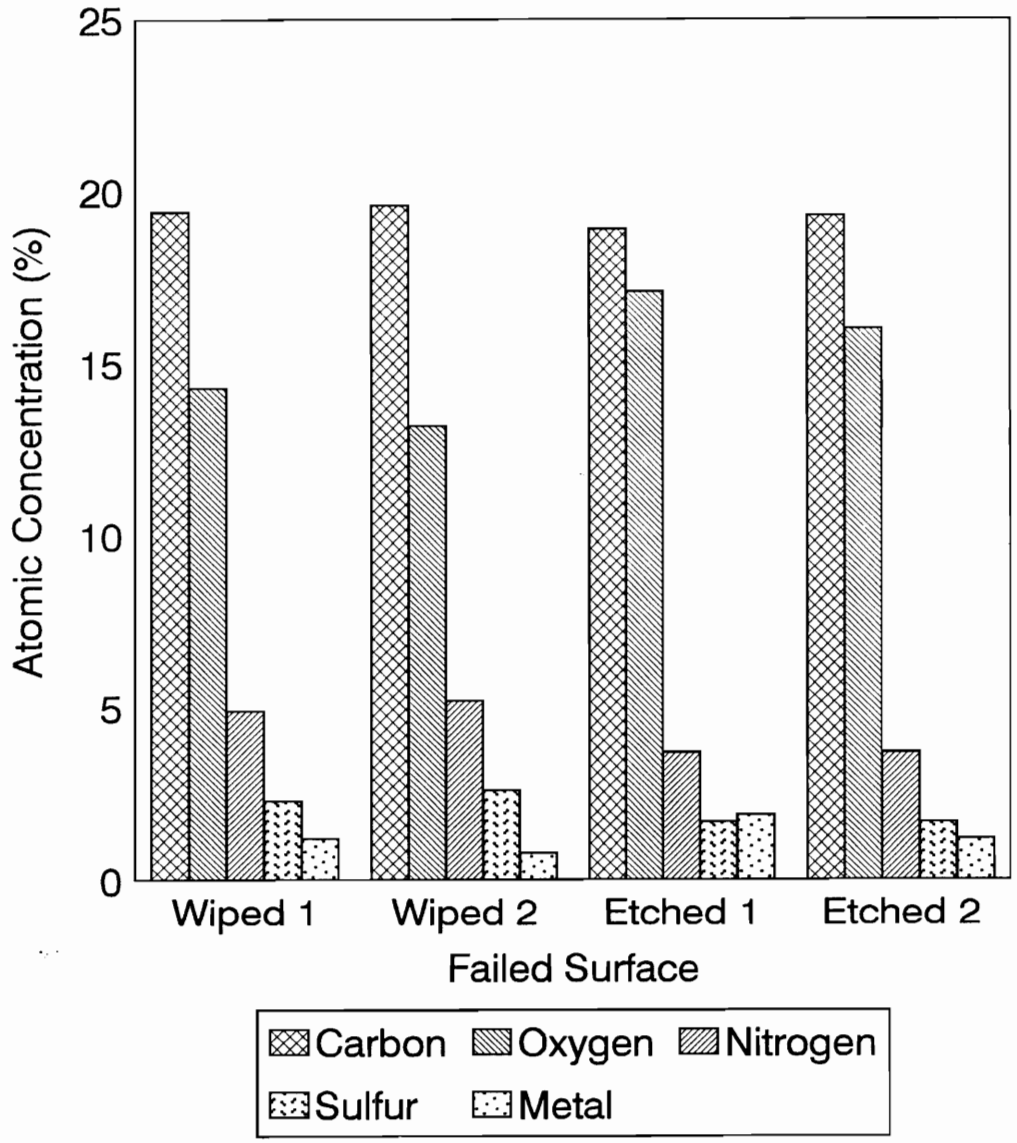

Figure 67. Atomic Concentrations of Failed BTDA/ASD/1010 Steel Peel Bond Surfaces (Carbon concentration/4).

polyimide was the major component on both failed surfaces. The nitrogen concentrations were (Figure 63) 4.7 atomic% and 3.8 atomic% on the two failed surfaces which corresponded closely to the expected value for neat BTDA/APB, 4.5 atomic%; however, less iron was observed on each surface (e.g. 0.9 atomic% on one side and 1.3 atomic% on the other). The iron composition as determined via XPS was still the same, i.e. primarily Fe_2O_3.

While the T-peel strengths of the BTDA/APB bonds with wiped and etched steel were similar, the results were much different in the case of the BDSDA/ODA bonds. The etched steel bonds of BDSDA/ODA had a T-peel strength of only 0.78 ± 0.33 N/cm, less than 30% of the strength of the wiped steel bonds. While this drop in peel strength could be due to the oxidation of thioether sulfur, the XPS results did not corroborate that theory. The nitrogen and sulfur concentrations on both failed surfaces (Figure 64) were similar to that of the polyimide itself, 4.0 atomic% and 2.0 atomic%, respectively. Again, hardly any iron was observed, ~ 0.2 atomic%. Not surprisingly, no oxidized sulfur was

observed, only thioether sulfur. The mode of failure, therefore, was the same as discovered with the wiped steel substrates (e.g. cohesive failure). If thioether oxidation was the cause of the decreased peel strength, then the bonds should have failed at the interface where the oxidation would have occurred. Most likely, the poor performance was due to a problem with the surface pretreatment.

Etched steel bonds using BTDA/ODA had a very poor T-peel strength (0.36 ± 0.11 N/cm), but it was close to the strength of the BTDA/ODA/wiped steel bonds. Also, like the wiped steel bonds, the etched bonds failed in mixed mode. The iron concentrations (Figure 66) on the failed surfaces were not as high with the etched steel bonds (3.5 atomic% and 1.3 atomic%) as with the acetone wiped specimens. The iron appeared to be Fe_2O_3.

As was the case with BDSDA/ODA, the etched steel bonds of BTDA/ASD had a much lower T-peel strength than the wiped steel bonds using the same polyimide. The T-peel strength, 0.39 ± 0.4 N/cm, dropped 50% compared to the wiped steel bonds. Slightly more iron was observed on the failed

surfaces (Figure 67) (1.9 atomic% and 1.2 atomic%) compared to the wiped steel bonds, but it was still in the form of iron oxide. Again, no oxidized sulfur was observed.

Of all the steel bonds, both wiped and etched, only the BDSDA/ODA bonds failed cohesively; all of the others failed in a mixed mode. It is interesting to note, however, that for a given set of parameters (i.e. similar Tg and surface pretreatment) the sulfur containing polyimides consistently showed less iron on the failed surfaces than the non-sulfur containing polyimides. Also, the bonds synthesized using etched steel and sulfur containing polyimides were considerably weaker than the wiped steel bonds. The surface pretreatment, on the other hand, did not have a noticeable effect on the peel strength of the non-sulfur containing polyimides.

Comparison of the T-peel strengths (Table X) of these polyimide/steel bonds with the polyimide/aluminum bonds studied previously revealed several interesting observations. One is the close agreement in T-peel strengths between the acetone wiped steel and acetone wiped

Table X. T-Peel Strength of the Acetone Wiped Polyimide/Aluminum and Polyimide/1010 Steel Foil Bonds.

Polyimide	Adherend	Peel Strength (N/cm)
BDSDA/ODA	Aluminum	2.88 ± 0.15
BDSDA/ODA	1010 Steel	2.83 ± 0.84
BTDA/APB	Aluminum	3.85 ± 0.42
BTDA/APB	1010 Steel	2.84 ± 0.60
BTDA/ASD	Aluminum	1.04 ± 0.09
BTDA/ASD	1010 Steel	0.78 ± 0.27
BTDA/ODA	Aluminum	0.38 ± 0.10
BTDA/ODA	1010 Steel	0.53 ± 0.09

aluminum bonds for a given polyimide. Since the modulus of steel is approximately twice that of aluminum, the thickness of the steel was chosen to be half that of aluminum to compensate for this factor. Even though T-peel strengths were very similar, bond failure occurred in different locations. The study with aluminum substrates reported that bonds, both wiped and etched substrates, failed in the aluminum oxide layer since large amounts of aluminum (5-15 atomic%)were found on both failed surfaces. This mode of failure was not observed with the steel bonds as was seen earlier from our analysis of the failed steel surfaces.

The similarities between wiped steel and wiped aluminum were not observed in the etched substrate cases. When etched aluminum substrates were used, the T-peel strength of all of the polyimides increased relative to the wiped aluminum bonds. With etched steel, however, the non-sulfur containing polyimides had T-peel strengths that were almost the same as the acetone wiped steel bonds. For the sulfur containing polyimides, however, the etched steel bonds were actually worse than the acetone wiped steel bonds. This was

most notable in the BDSDA/ODA/etched steel bond case which lost >70% of their strength compared to the acetone wiped bonds.

Wedge Tests

Wedge tests on steel substrates were performed under dry (Table XI) and wet (Table XII) environments using these four polyimides with both surface pretreatments (e.g. wiped and etched). Again, the steel coupons were half as thick as the aluminum coupons used in the previous study. Also, no complete set of steel bonded specimens failed for a given polyimide, surface pretreatment, or test environment compared to the aluminum case.

The initial crack lengths of the BTDA/APB/steel bonds were similar to each other regardless of surface pretreatment: 49 ± 4 mm for the acetone wipe and 47 ± 7 mm for the HCl etch (Figures 68 and 69). The total crack growth for these bonds was also the same, 7 ± 4 mm for the acetone wipe after twelve days and 5 ± 1 mm for the HCl etch after twelve days, regardless of the pretreatment. In both cases, the bonds failed cohesively since practically no

Table XI. Crack Growth and Mode of Failure in the Polyimide/1010 Steel Wedge Bonds Tested in a Dry Environment.

Polyimide	Tg	Sulfur	Wiped Bonds			Etched Bonds		
			Initial Crack Length (mm)	Crack Growth (mm)	Failure Mode	Initial Crack Length (mm)	Crack Growth (mm)	Failure Mode
BTDA/APB	Low	No	49 ± 4	7 ± 4	Cohesive	47 ± 7	5 ± 1	Cohesive
BDSDA/ODA	Low	Yes	34 ± 7	13 ± 5	Mixed Mode	32 ± 3	14 ± 5	Mixed Mode
BTDA/ODA	High	No	65 ± 17	11 ± 1	Cohesive	62 ± 13	7 ± 3	Mixed Mode
BTDA/ASD	High	Yes	52 ± 4	13 ± 5	Mixed Mode	71 ± 11	15 ± 8	Mixed Mode

Table XII. Crack Growth and Mode of Failure in the Polyimide/1010 Steel Wedge Bonds Tested in a Wet Environment.

Polyimide	Tg	Sulfur	Wiped Bonds			Etched Bonds		
			Initial Crack Length (mm)	Crack Growth (mm)	Failure Mode	Initial Crack Length (mm)	Crack Growth (mm)	Failure Mode
BTDA/APB	Low	No	49 ± 4	36	Oxide	47 ± 7	28 ± 1	Oxide
BDSDA/ODA	Low	Yes	34 ± 7	26 ± 12	Oxide	32 ± 3	31 ± 6	Oxide
BTDA/ODA	High	No	65 ± 17	17 ± 10	Oxide	62 ± 13	23 ± 19	Oxide
BTDA/ASD	High	Yes	52 ± 4	10	Mixed Mode	71 ± 11	18 ± 15	Oxide

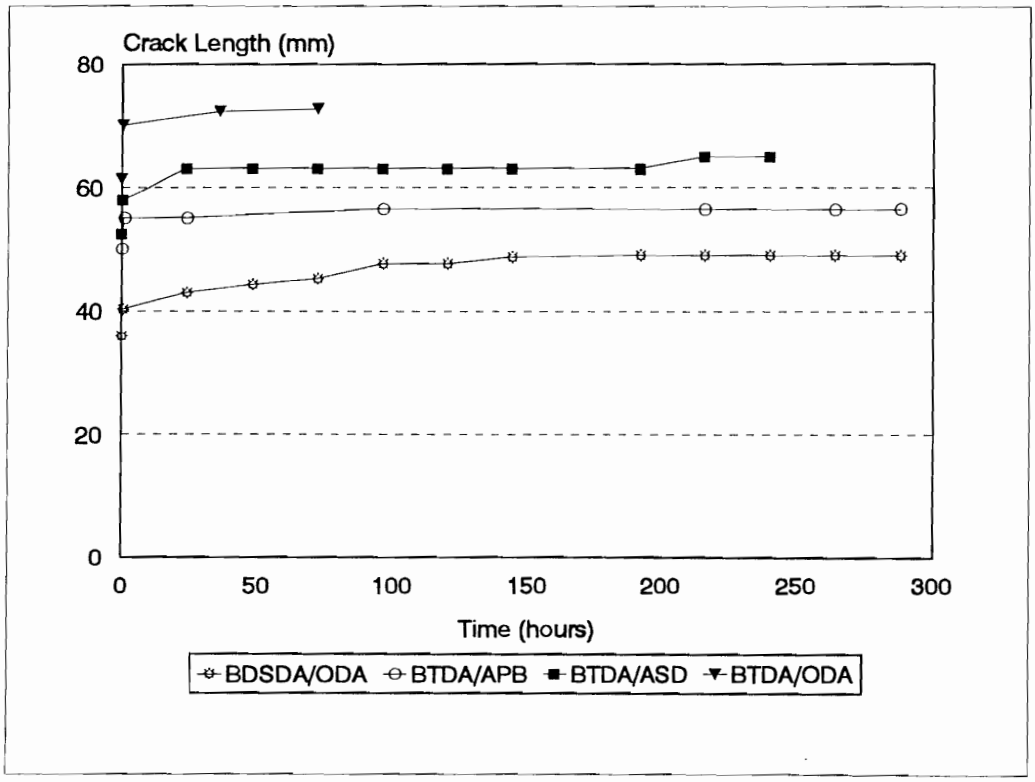

Figure 68. Crack Growth in Acetone Wiped Polyimide/1010 Steel Wedge Bonds Tested in a Dry Environment.

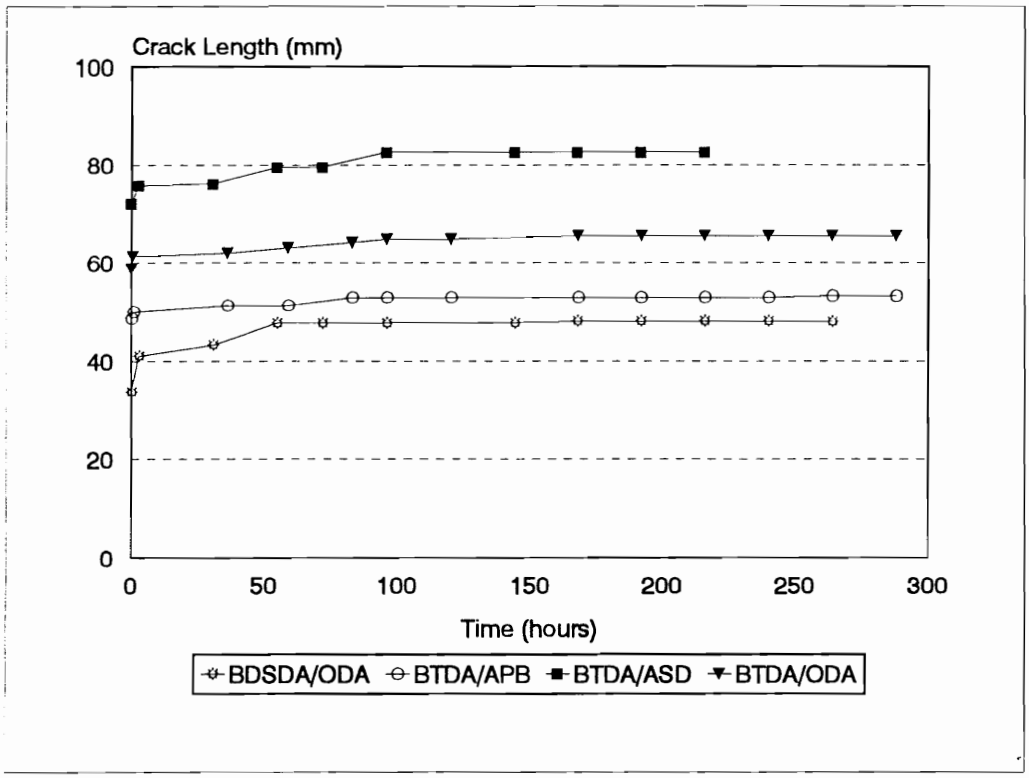

Figure 69. Crack Growth in HCl Etched Polyimide/1010 Steel Wedge Bonds Tested in a Dry Environment.

iron (< 0.5 atomic%) was observed on either failed surface (Figure 70 and 71).

The initial crack length for the wet BTDA/APB steel bonds was the same as that for the dry bonds, since it was measured before being exposed to either environment. The crack growth in the wet/wiped bond case was quite large, 36 mm, after twelve days (Figure 72). Analysis of the failed surfaces of this bond indicated that it failed predominantly within the iron oxide layer. Sizable amounts of iron (9-12 atomic%) and reduced amounts of nitrogen (2-3.5 atomic%) were observed on both surfaces (Figure 73). Neat BTDA/APB would be expected to have an atomic concentration of 4.5 atomic% nitrogen. The wet/etched BTDA/APB bonds had a slightly smaller total crack growth of 28 ± 1 mm after twelve days (Figure 74). These bonds failed almost completely within the oxide layer. Only about 1 atomic% nitrogen and more than 10 atomic% iron was observed on each surface (Figure 75).

BDSDA/ODA bonds with steel proved to have the best resistance to crack growth of the four polyimides regardless

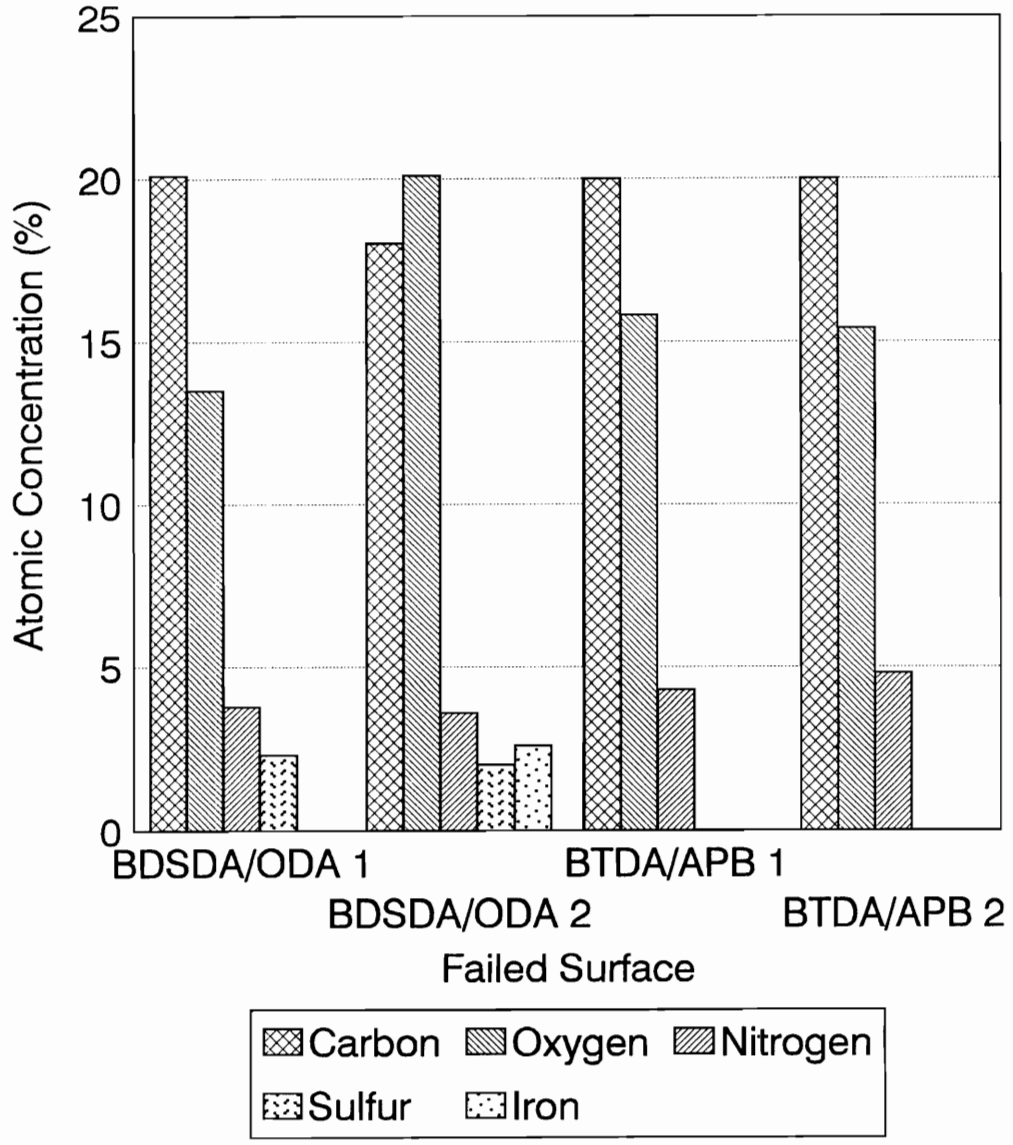

Figure 70. Surface Atomic Concentrations of Failed Acetone Wiped Low Tg Polyimide/1010 Steel Wedge Bonds Tested in a Dry Environment.

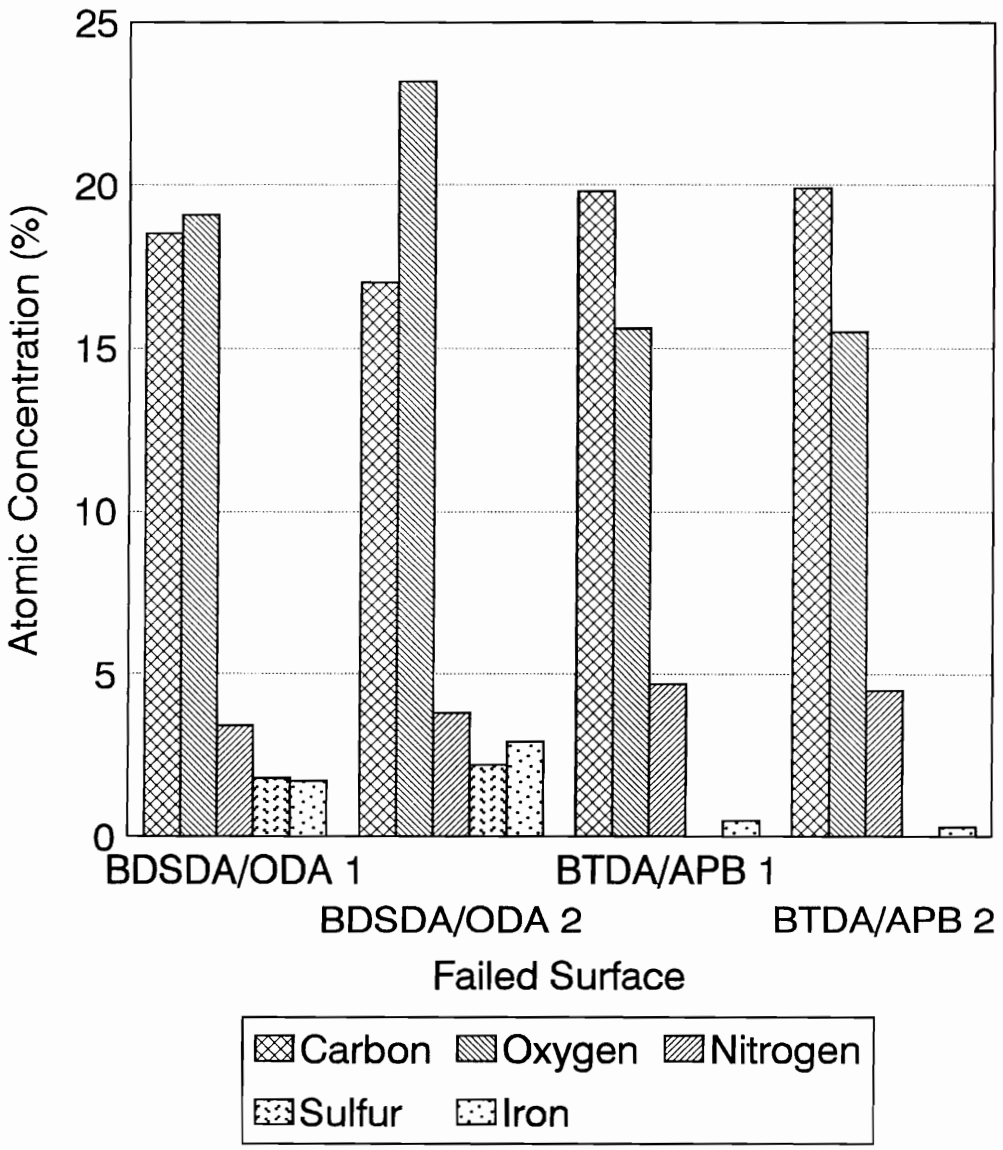

Figure 71. Surface Atomic Concentrations of Failed HCl Etched Low Tg Polyimide/Aluminum Wedge Bonds Tested in a Dry Environment.

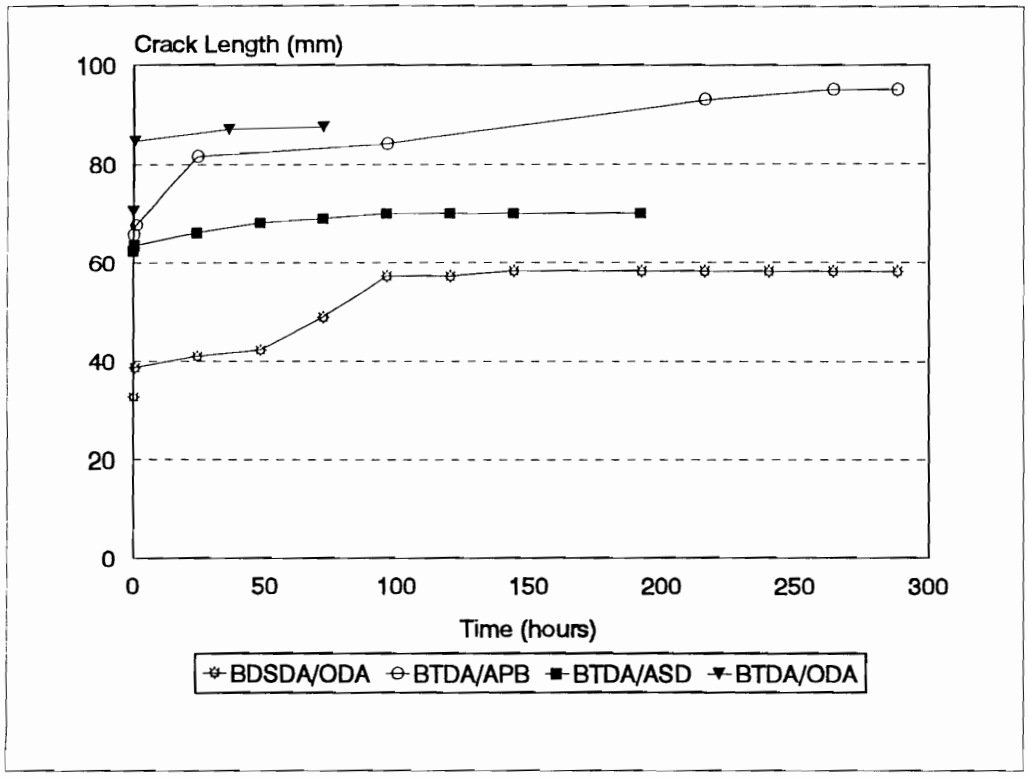

Figure 72. Crack Growth in Acetone Wiped Polyimide/1010 Steel Wedge Bonds Tested in a Wet Environment.

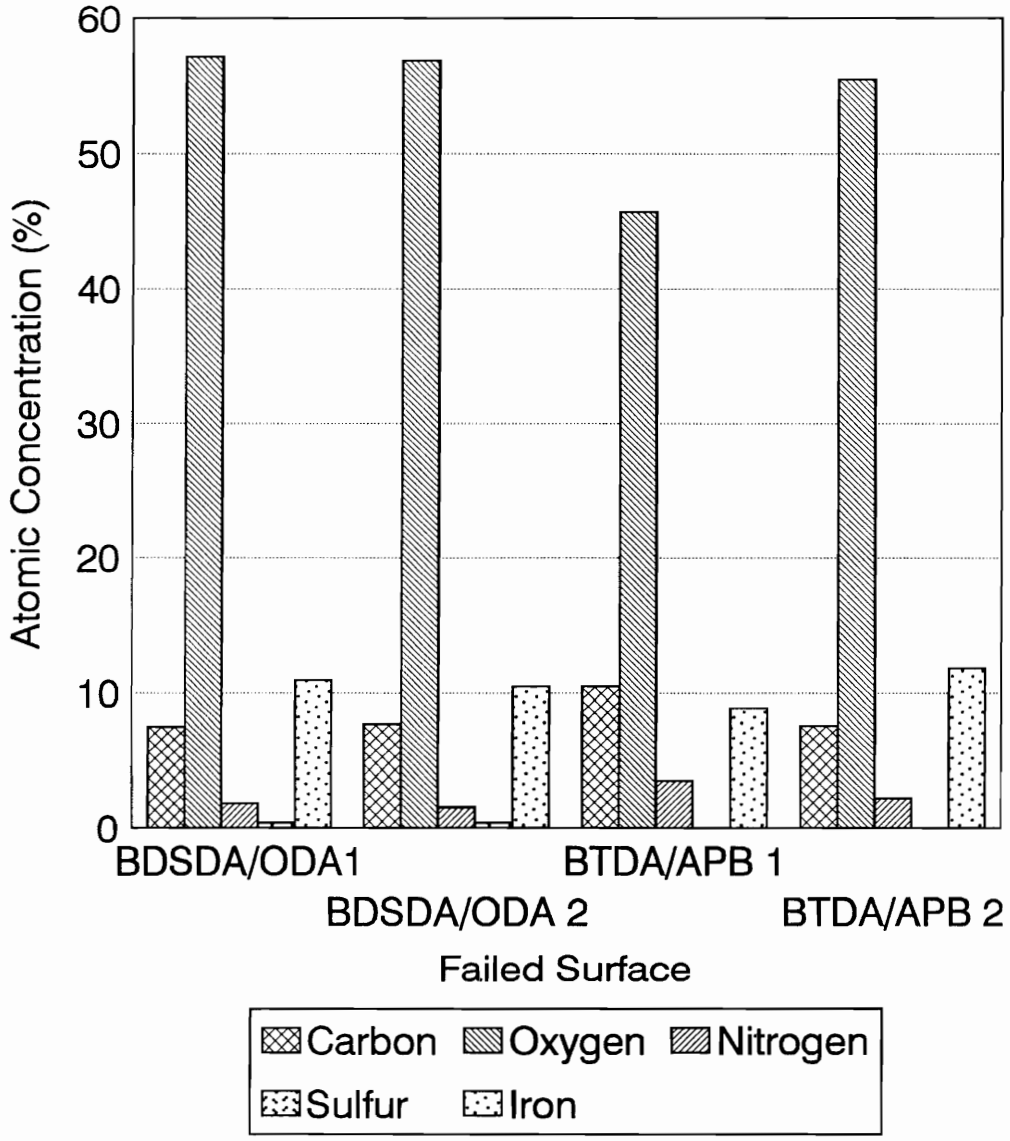

Figure 73. Surface Atomic Concentrations of Failed Acetone Wiped Low Tg Polyimide/1010 Steel Wedge Bonds Tested in a Wet Environment.

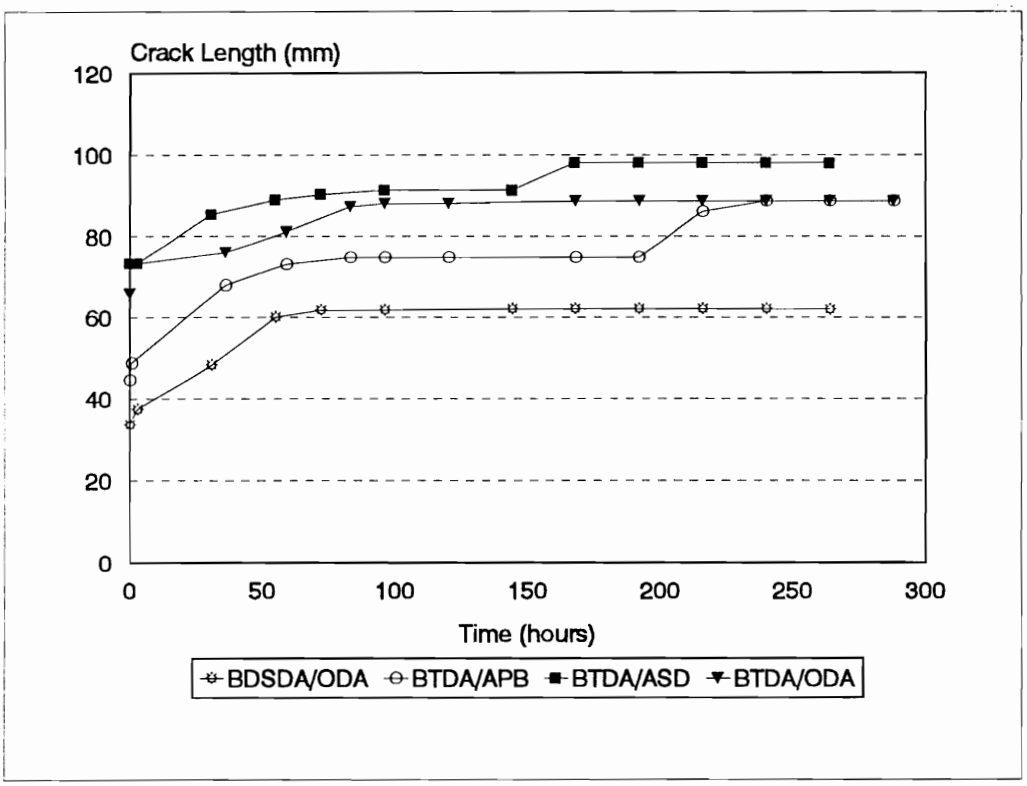

Figure 74. Crack Growth in HCl Etched Polyimide/1010 Steel Wedge Bonds Tested in a Wet Environment.

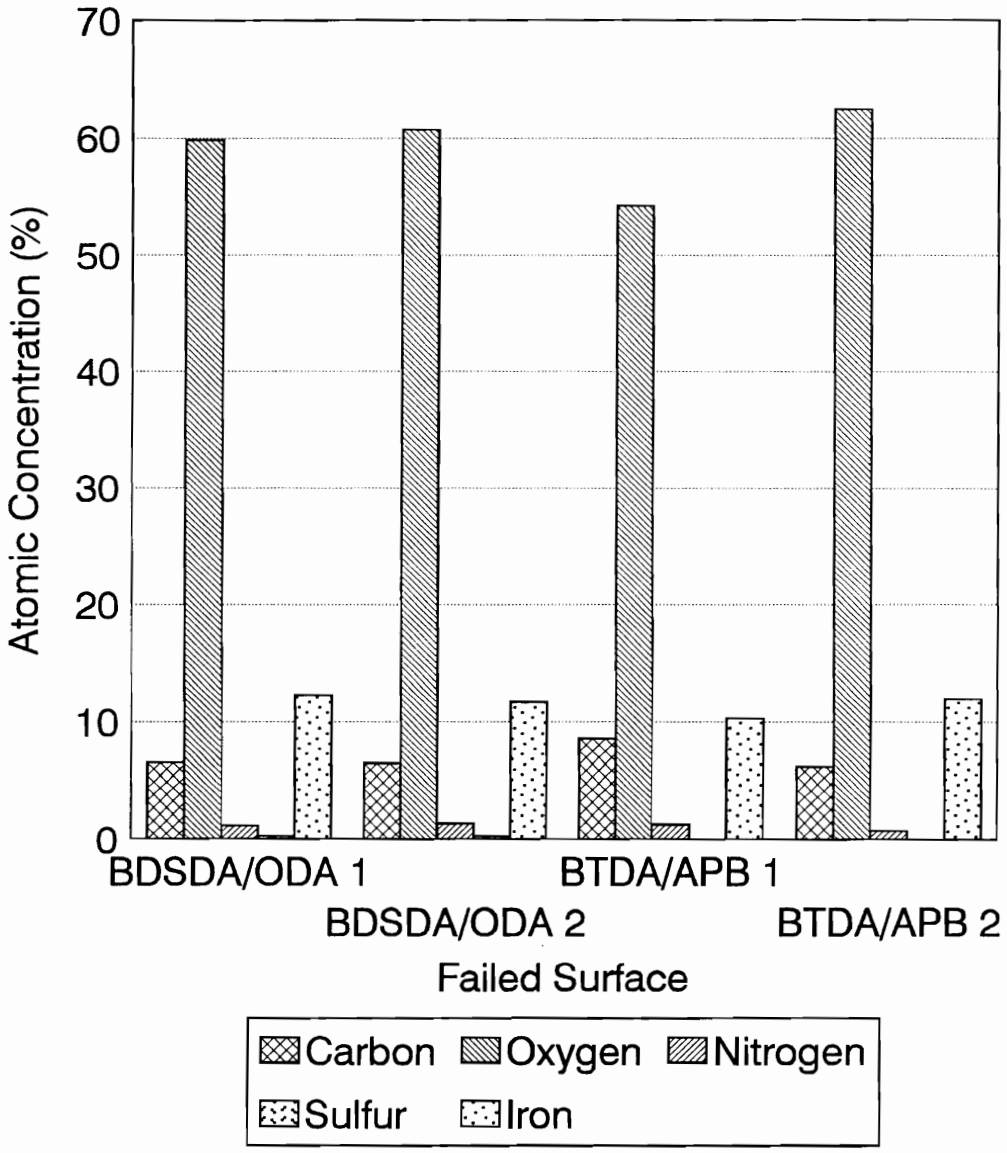

Figure 75. Surface Atomic Concentrations of Failed HCl Etched Low Tg Polyimide/1010 Steel Wedge Bonds Tested in a Wet Environment.

of surface pretreatment or testing environment. While the initial crack lengths (Figures 68 and 69), 34 ± 7 mm for the acetone wipe and 32 ± 3 mm for the HCl etch, were virtually the same, they were significantly lower than the other three polyimides. The extent of crack growth for the dry bonds was similar to the other polyimides, 13 ± 5 mm for the acetone wipe after twelve days and 14 ± 5 mm for the HCl etch after eleven days. Thus, the overall crack length was still less for the dry BDSDA/ODA/steel bonds compared to the other polyimides. The dry BDSDA/ODA steel bonds seemed to fail similarly regardless of surface pretreatment according to XPS (Figures 70 and 71). Both bonds showed some iron (~ 2 atomic%) and some polyimide (~ 2 atomic% sulfur and 3.5-4 atomic% nitrogen) indicating mixed mode failure. Unfortunately, no oxidized sulfur was observed on these surfaces. Again, these bonds probably did not fail close enough to the interface for oxidized sulfur to be observed.

The wet BDSDA/ODA/steel bonds also had somewhat similar crack growths, 26 ± 12 mm for the acetone wipe after twelve days and 31 ± 6 mm for the HCl etch after eleven days

(Figures 72 and 74). These bonds both failed within the oxide layer of the steel (Figures 73 and 75). Practically no sulfur was observed on either the acetone wiped or HCl failed etched surfaces (< 0.5 atomic%), so it could not be determined if the sulfur had been oxidized at the interface.

The BTDA/ODA/steel bonds had practically the same initial crack length regardless of surface pretreatment, 65 ± 17 mm for the acetone wipe and 62 ± 13 mm for the HCl etch (Figures 68 and 69). The extent of crack growth in the dry BTDA/ODA/steel bond case was also similar regardless of pretreatment, 11 ± 15 mm for the acetone wipe after three days and 7 ± 3 mm after twelve days for the HCl etch. The dry and wet BTDA/ODA/steel bonds did have different failure modes, however (Figures 76 and 77). The dry/wiped bonds failed entirely cohesively; no iron was detected on either surface. The dry/etched BTDA/ODA bond failed in mixed mode since some iron (1.4 atomic% and 4.1 atomic%) was found on both surface.

The crack growth in the wet BTDA/ODA/steel bond case (Figures 72 and 74) was also similar regardless of surface

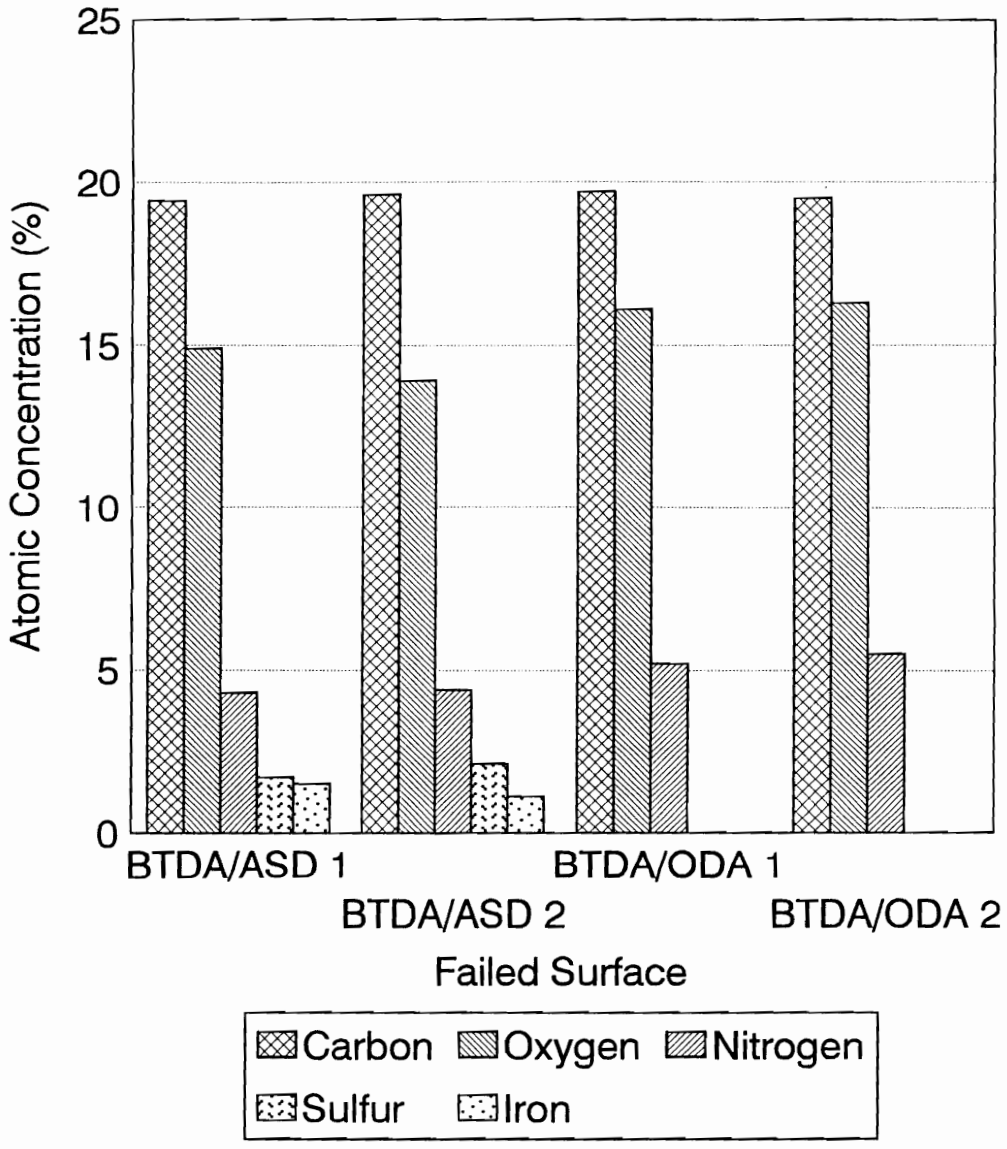

Figure 76. Surface Atomic Concentrations of Failed Acetone Wiped High Tg Polyimide/1010 Steel Wedge Bonds Tested in a Dry Environment.

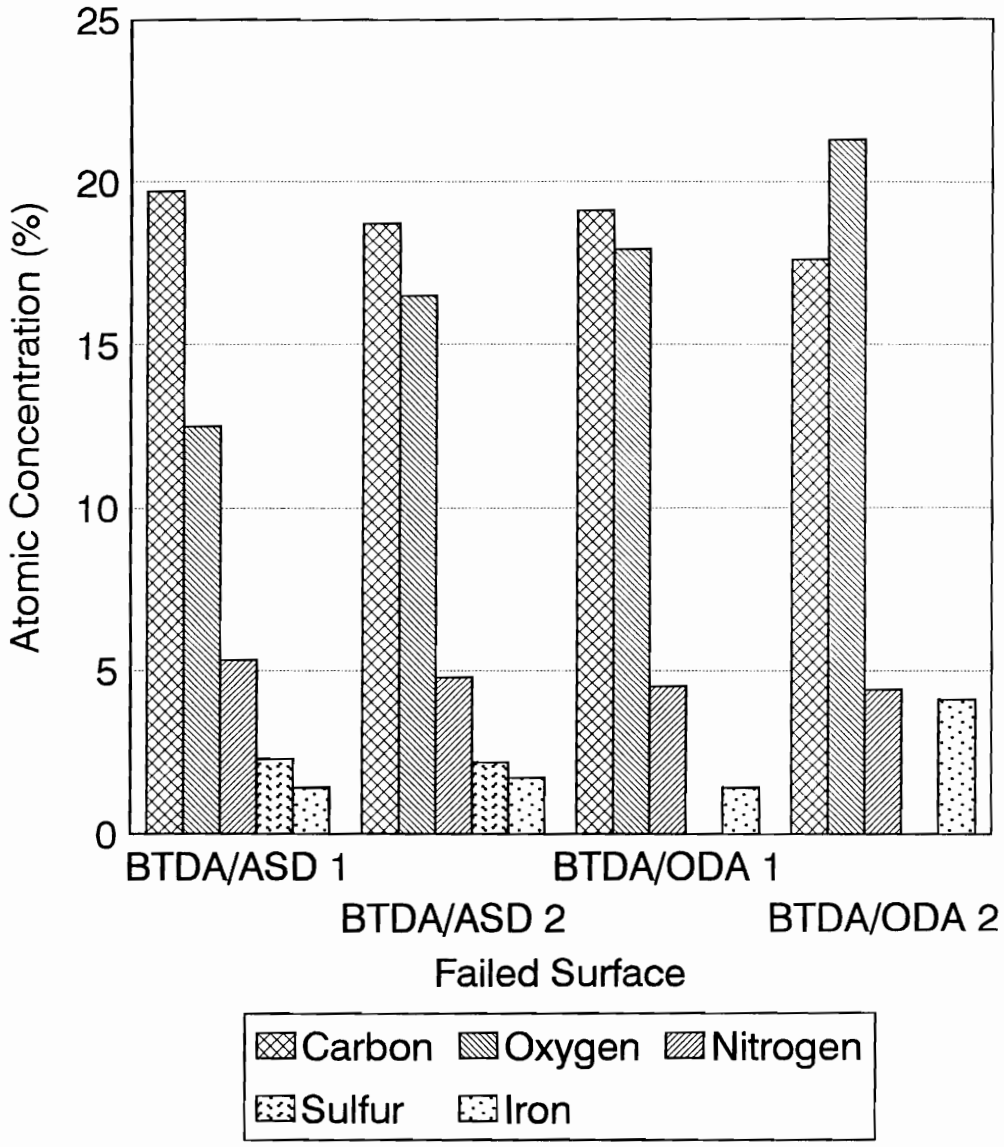

Figure 77. Surface Atomic Concentrations of Failed HCl Etched High Tg Polyimide/1010 Steel Wedge Bonds Tested in a Dry Environment.

pretreatment, 17 ± 10 mm for the acetone wipe after three days and 23 ± 19 mm for the HCl etch after twelve days. The wet/wiped BTDA/ODA/steel bond failed deep into the oxide layer since large amounts of iron (8-10 atomic%) were found on either failed surface (Figures 78 and 79). Also very little nitrogen (2-3 atomic%) was observed on these surfaces. The expected nitrogen concentration in the neat BTDA/ODA was 5.4 atomic%. The wet/etched BTDA/ODA/steel bonds, on the other hand, failed completely within the oxide layer of the steel as was the case with the wet/etched BTDA/ASD. Large amounts of iron (11-13 atomic%) and practically no nitrogen (~ 0.5 atomic%) were observed on either surface.

The initial crack length for BTDA/ASD was 52 ± 4 mm for the acetone wiped bonds (Figure 68). The HCl etch pretreatment produced a significantly larger crack length of 71 ± 11 mm (Figure 69). The extent of crack growth, however, was essentially the same for both types of pretreated BTDA/ASD bonds tested in a dry atmosphere, 13 ± 5 mm for the acetone wipe after nine days and 15 ± 8 mm for

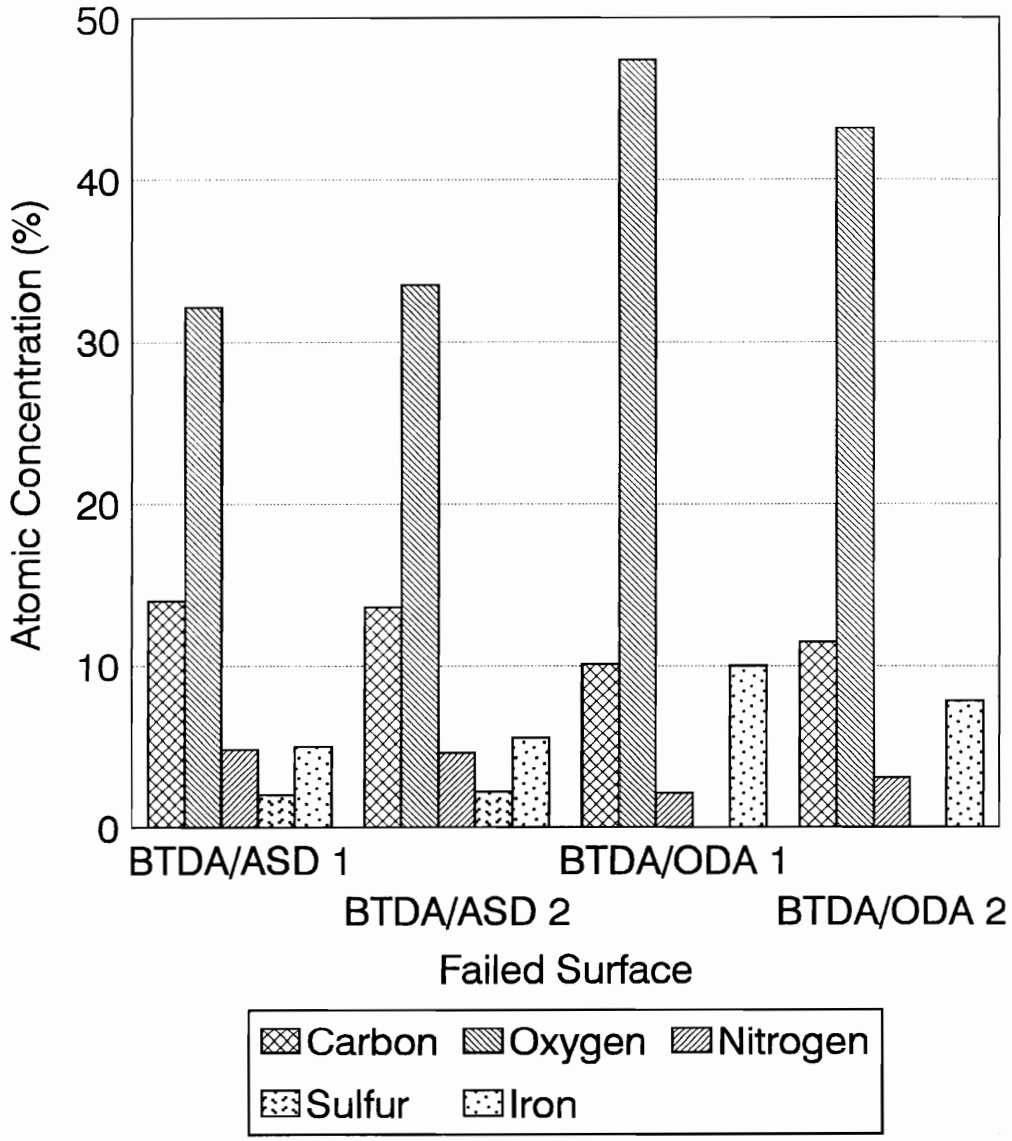

Figure 78. Surface Atomic Concentrations of Failed Acetone Wiped High Tg Polyimide/1010 Steel Wedge Bonds Tested in a Wet Environment.

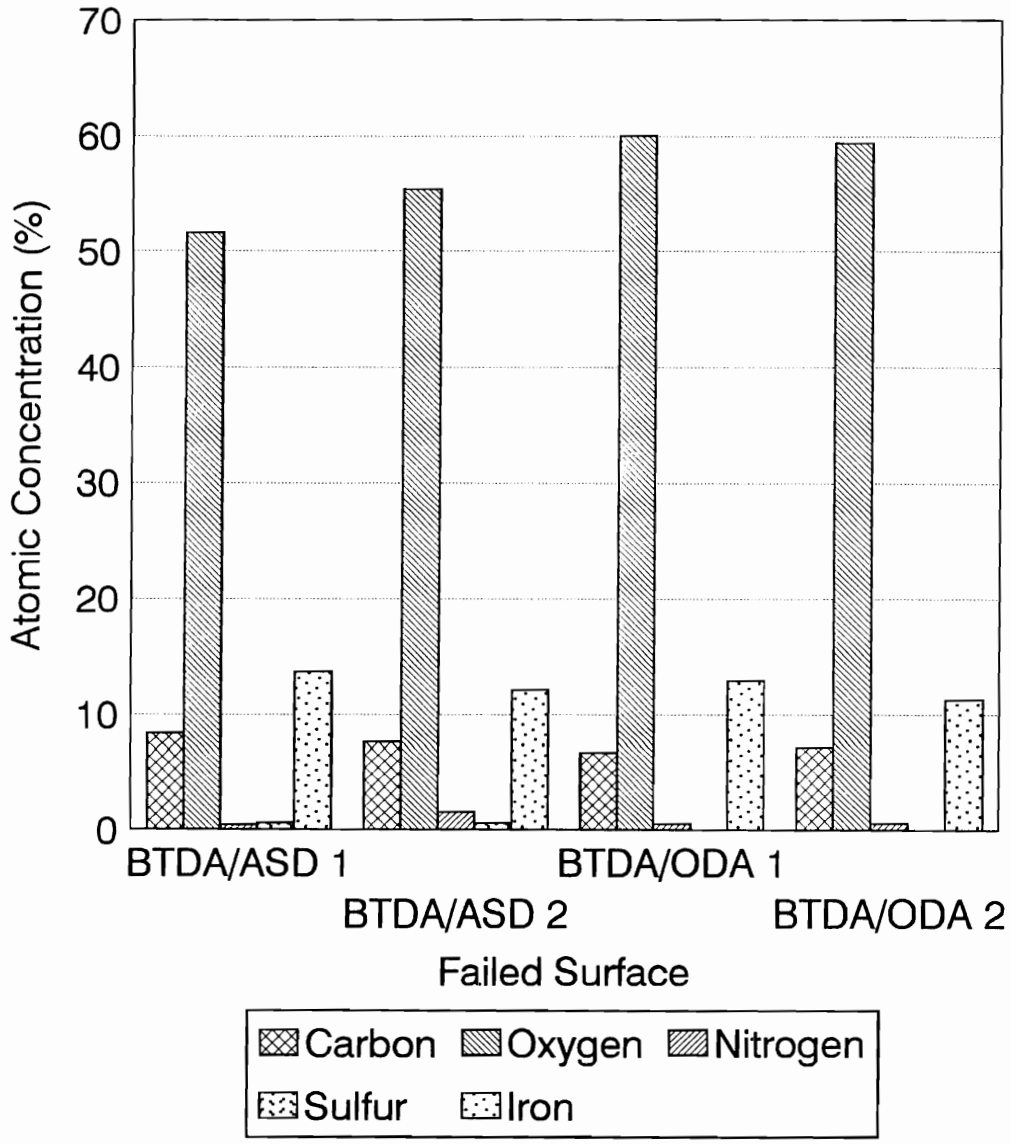

Figure 79. Surface Atomic Concentrations of Failed HCl Etched High Tg Polyimide/1010 Steel Wedge Bonds Tested in a Wet Environment.

the HCl etch after ten days. Surface analysis of the failed BTDA/ASD bonds tested in a dry environment revealed similar atomic concentrations regardless of the surface pretreatment (Figures 76 and 77). These results also indicated that the bonds failed in mixed mode, since a small amount of iron (~ 1.5 atomic%) was found on both surfaces. Since this amount of iron was very similar to that found on the failed peel surfaces of BTDA/ASD bonds, it was not suprising that no oxidized sulfur was observed.

The acetone wiped BTDA/ASD/steel bond tested in a wet environment had a crack growth of 10 mm after eight days; while, the HCl etched BTDA/ASD/steel bonds had a crack growth of 18 ± 15 mm after ten days (Figures 72 and 74). Surface analysis of the failed surfaces of these bonds indicated different modes of failure from the dry bonds and each other. The wet/wiped bonds failed in mixed mode with approximately 5 atomic% iron on either surface (Figure 78). The sulfur peak from these surfaces was significantly broadened compared to the photopeak found in the XPS analysis of the dry surfaces (Figures 80 and 81). This

broadening indicated that some oxidation of sulfur had occurred at the interface. The wet/etched bonds failed within the oxide layer of the steel since little nitrogen (0.4-1.6 atomic%) or sulfur (0.6 atomic%) was observed in contrast to large amounts of iron (12-14 atomic%) (Figure 79). Too little sulfur was observed, however, to determine if any oxidized species were present.

While the etching pretreatment seemed to have a detrimental effect on the bond strength of the aluminum bonds, it did not seem to have much of an effect at all on the steel bonds. In fact, the wet BTDA/APB/wiped steel bonds were the worst of all the steel wedge samples. The initial crack lengths and subsequent crack growth were usually very similar regardless of whether the steel was etched or just wiped with acetone prior to casting. Most of the failed surfaces for a given polyimide were also similar within the same test environment. If the failed surfaces were different between the etched and the wiped bonds (as in the case of the dry BTDA/ODA bonds), then more iron was observable on the failed etched surfaces which was also

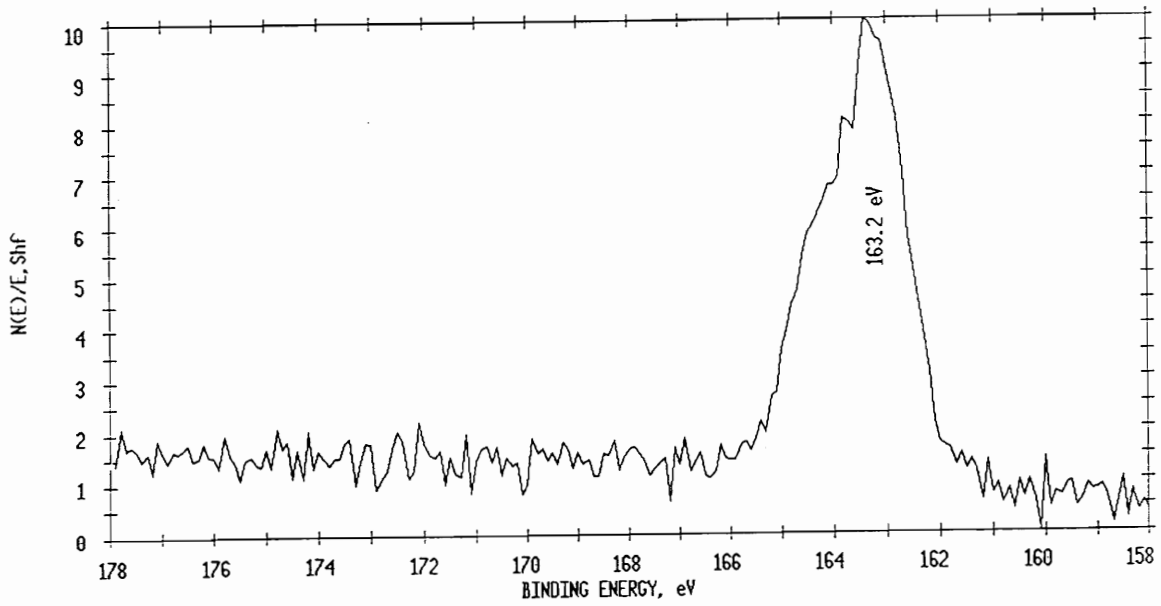

Figure 80. Sulfur 2p XPS Photopeak of Failed Acetone Wiped BTDA/ASD Wedge Bond Surface Tested in a Dry Environment (Binding Energy Calibrated to C 1s = 284.6 eV).

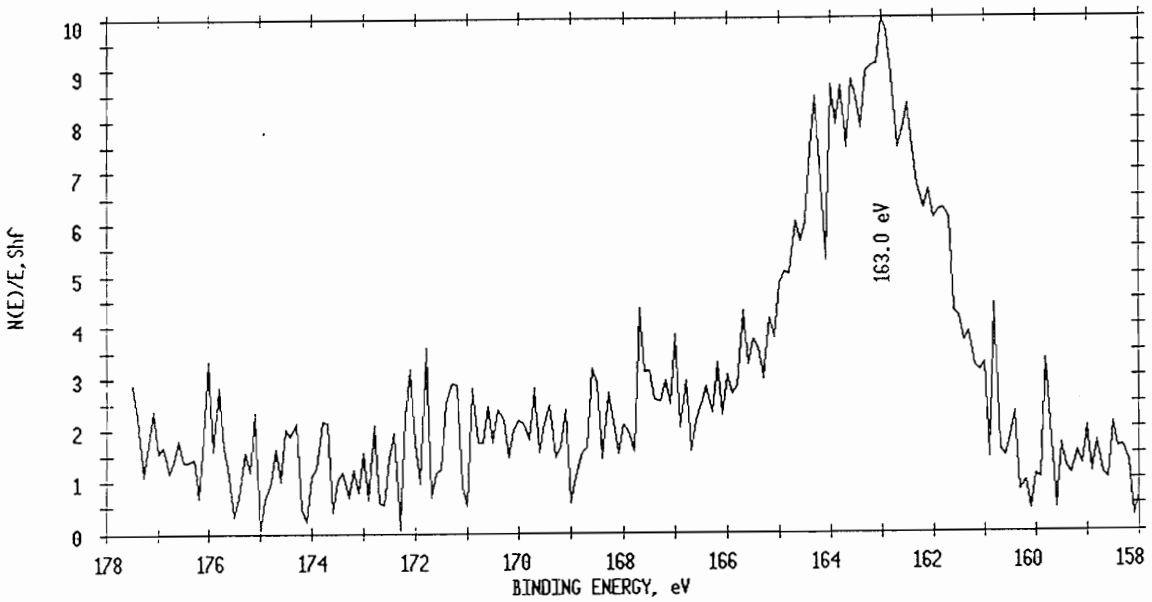

Figure 81. Sulfur 2p XPS Photopeak of Failed Acetone Wiped BTDA/ASD Wedge Bond Surface Tested in a Wet Environment (Binding Energy Calibrated to C 1s = 284.6 eV).

counter to the findings with aluminum.

Also, oxidized sulfur had been observed on the failed surfaces of the wet BDSDA/ODA/aluminum bonds in the previous study. No oxidized sulfur was observed on the failed surfaces of the wet BDSDA/ODA/steel bonds, but very little sulfur (< 0.5 atomic%) was present. Thus, it was quite possible that the sulfur had been oxidized, but was not at the locus of failure (Figure 82). This hypothesis is supported by the noticeable broadening of the sulfur peak on the failed surfaces of the wet/wiped BTDA/ASD/steel bonds which indicated that some oxidation had taken place (Figures 80 and 81). In an attempt to further clarify this situation, a BDSDA/ODA solution was cast on a steel coupon and fully cured to 300°C in the oven. The film was then peeled off of the coupon, and the surface that had been cured against the steel was analyzed via XPS. The sulfur in this film did show oxidized sulfur in addition to thioether sulfur (Figure 83) indicating that sulfur oxidation can take place along the interface between the polyimide and the metal substrate.

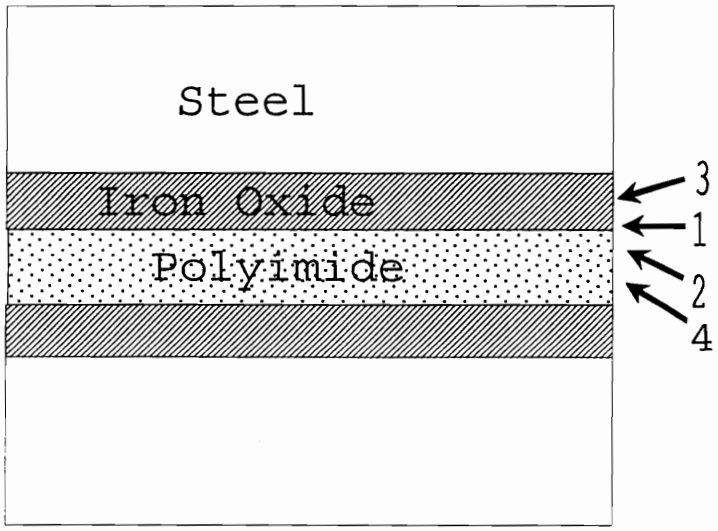

1 - Oxidized sulfur would be found here.

2 - Locus of failure for BDSDA/ODA and BTDA/ASD wedge bonds tested in a dry environment.

3 - Locus of failure for BDSDA/ODA and BTDA/ASD wedge bonds tested in a wet environment.

4 - Locus of failure for BDSDA/ODA peel bonds.

Figure 82. Locus of Failure and Probable Location of Oxidized Sulfur in Steel Bonds.

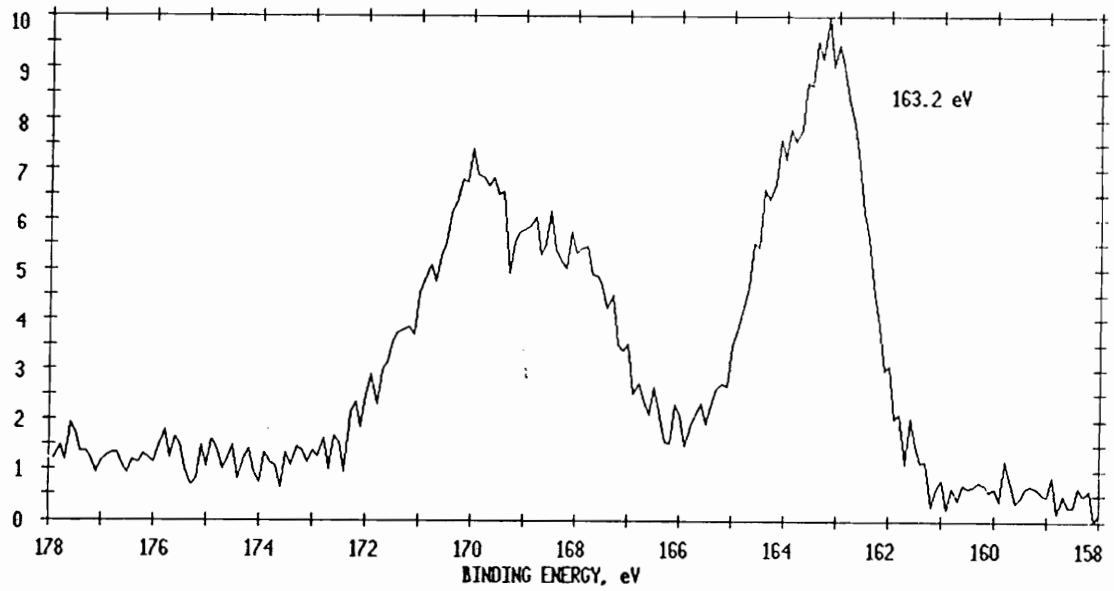

Figure 83. Sulfur 2p XPS Photopeak of BDSDA/ODA Film Cured on Steel Coupon (Binding Energy Calibrated to C 1s = 284.6 eV).

SUMMARY

With the wiped steel bonds, low Tg polyimides had significantly higher T-peel strengths than the high Tg polyimides as was the case with aluminum. The lowered T-peel strengths of the sulfur containing etched bonds cannot be attributed to the oxidation of the thioether sulfur, however, since no oxidized sulfur was observed at the point of failure. It is also possible that the surface area around the edges of the peel specimens was not enough to permit significant amounts of oxygen to diffuse into the polyimide and aid in the oxidation of thioether sulfur, as discussed in Chapter IV. In contrast with the aluminum substrates, the chemical etch steel surface pretreatment only affected the T-peel strength of sulfur containing polyimides, and that effect was a detrimental one. The locus of failure was not as significantly affected by the type of pretreatment of steel.

In the wedge test, all of the polyimides performed about equally except for BDSDA/ODA which proved superior.

Even though no oxidized sulfur was observed on the failed surfaces, it can be assumed that thioether sulfur along the interface was oxidized due to the XPS photopeak broadening that was noticed in the wiped steel BTDA/ASD bond tested in a wet environment (Figure 81) and the oxidized sulfur observed in the BDSDA/ODA film cast on the steel coupon (Figure 83). These results would seem to indicate that the oxidation of sulfur may aid bond durability since BDSDA/ODA performed the best. At worst, the oxidation of sulfur did not appear to reduce bond performance. If this had been the case, then oxidized sulfur should have been observed on the failed surfaces of the bond since that would have been the cause of bond failure.

VI. SUMMARY

CONCLUSIONS

This study has examined the interaction between various metals, either as a matrix modifier or bonding substrate, and thioether sulfur in the polyimide backbone and how these interactions affect the adhesive properties of the polyimide. First, observations of metal-thioether sulfur interactions in BDSDA/ODA were carefully studied in an attempt to fully understand the metal-catalyzed oxidation. Several metal complexes were used as modifiers, and it was observed that both vanadium and iron catalyzed the oxidation of the thioether sulfur in the polyimide backbone. Aluminum, however, was shown only minimally to catalyze the oxidation of the thioether sulfur. Both XPS and internal reflectance FT-IR indicated that this oxidized sulfur was either a sulfonic acid ($RSO_3^-M^+$) or sulfate ($RSO_4^-M^+$) salt. Further evidence was added when it was observed that iron also catalyzed the oxidation to sulfonate sulfur in the sulfone containing DSDA/ODA polyimide.

The possibility of metal-catalyzed oxidation of

thioether sulfur in adhesive applications was explored by utilizing aluminum and steel substrates. As expected, the T-Peel strengths of the sulfur and non-sulfur containing polyimides (with similar Tg's) were similar when aluminum was used as the substrate. Had the aluminum significantly catalyzed the oxidation of the sulfur, the T-peel strength of the sulfur containing polyimide should have been different. Also, as expected, no oxidized sulfur was observed via XPS. Oxidized sulfur did seem to have an effect in the wedge tests with aluminum substrates where the sulfur-containing BDSDA/ODA polyimide performed best. The difference in substrates, pure aluminum for peel and aluminum alloy for wedge tests, was probably responsible for the difference in the amount of oxidized sulfur observed on the two surfaces.

Steel was also used as a substrate that had been predicted to catalyze the oxidation of thioether sulfur significantly. In the T-Peel test, sulfur and non-sulfur containing polyimides performed similarly with the acetone wiped substrates, but the sulfur containing polyimides

performed worse than the non-sulfur containing polyimides when the acid etched substrates were used. No oxidized sulfur, however, was observed on the failed surfaces which could have indicated increased interfacial strength causing the bonds to fail cohesively. Again, BDSDA/ODA performed better in the wedge test, but no oxidized sulfur was observed on the failed surfaces via XPS. Oxidized sulfur was observed, however, in a BDSDA/ODA film that was cured on a steel coupon and subsequently removed. Thus, metal-catalyzed oxidation of thioether sulfur was observed to take place at the interface between the sulfur-containing polyimide and the metal adherend. The lack of observable oxidized sulfur on the failed surfaces was most likely due to the fact that the bonds did not fail close enough to the interface where the oxidized sulfur would be located. Unfortunately, it did not seem to affect the T-Peel strength of the polyimide, but it did seem to affect bond durability as evidenced by the wedge test results. The lack of effect in the T-Peel test was most likely due to the limited presence of sulfur in the polyimide. Sulfur composes less

than 5%, by weight, of BDSDA/ODA as opposed to almost 30%, by weight, of polyphenylene sulfide. Thus, even though the oxidation occurred, there were too few sulfur atoms for the oxidation to have much effect.

FUTURE WORK

Based on the results of this study, many paths are available for further examination. First, varying the sulfur content in the polymer backbone by adding more thioether groups would allow for the determination of what level of sulfur was needed to produce noticeable effects on peel strength. If those effects were beneficial, it would warrant examining other metal substrates which might also catalyze the oxidation of sulfur (i.e. titanium, copper). Another area of examination would include incorporating thioether sulfur groups into other monomers to determine if the same beneficial effects are observed in different polymers. A more extensive examination of surface pretreatment of metal substrates could also be performed to identify which ones cause the most oxidation of sulfur.

VII. REFERENCES

1. Patrick, R.L. In *Treatise on Adhesion and Adhesives*, Vol. 1, Patrick, R.L., Ed.; Marcel Dekker, Inc.: New York, 1967, pp. 1-2.

2. Skeist, I. and Miron, J. In *Handbook of Adhesives*, 2nd Ed., Skeist, I., Ed; Van Nostrand Reinhold Company: Atlanta, 1977, p. 3.

3. Shields, J. *Adhesives Handbook*, 3rd Ed., Butterworth & Co.: Toronto, 1984, pp. 3-6.

4. Kinloch, A.J. In Durability of Structural Adhesives, Kinloch, A.J., Ed.; Applied Science Publishers: New York, 1983, pp. 2, 13-17.

5. Sharpe, L.H. In *Engineered Materials Handbook*, Vol. 3, Brinson, H.F., Ed. ASM International. 1990, pp. 33, 37.

6. Hagquist, J.; Meyer, F.K.; and Swanson, S.K.M. In *Engineered Materials Handbook*, Vol. 3, Brinson, H.F., Ed. ASM International. 1990, pp. 44-47.

7. Adams, R.D. and Wake, W.C. Structural Adhesive Joints in Engineering, Elsevier Applied Science Publishers: New York, 1984, pp. 134-142, 272.

8. Drain, K. and Chandrasekharan, S. In *Engineered Materials Handbook*, Vol. 3, Brinson, H.F., Ed. ASM International. 1990, pp. 551-557.

9. Zalucha, D.J. In *Engineered Materials Handbook*, Vol. 3, Brinson, H.F., Ed. ASM International. 1990, pp. 40-43.

10. Good, M.S.; Nestleroth, J.B.; and Rose, J.L. In *Adhesion Aspects of Polymeric Coatings*, Mittal, K.L., Ed.; Plenum Press: New York, 1983, pp. 623-634.

11. Clark, W.G. Jr.; Sadhir, R.K.; and Junker, W.R. *Materials Evaluation*, **48**, 60, (1990).

12. Clark, W.G. Jr. and Shannon, R.E. *Advanced Materials and Processes*, **4**, 59, (1990).

13. Clark, W.G. Jr. *Proceedings of the 23rd International SAMPE Technical Conference on Advanced Materials*, 233, (1991).

14. Clark, W.G. Jr. *Adhesives Age*, 22, (June 1992).

15. Bolger, J.C. In *Adhesion Aspects of Polymeric Coatings*, Mittal, K.L., Ed.; Plenum Press: New York, 1983, pp. 3-18.

16. Buchwalter, L.P. *J. Adhesion Sci. Tech.*, **1**, 341, (1987).

17. Taylor, L.T. and Rancourt, J.D. In *Inorganic and Metal Containing Polymeric Materials*, Sheats, J., Ed.; Plenum Press: New York, 1990, pp. 109-126.

18. Ezzell, S.A.; Furtsch, T.A.; Khor, E.; Taylor, L.T. *J. Polym. Sci., Polym. Chem. Ed.*, **21**, 865, (1983).

19. Rancourt, J.D.; Porta, G.M.; and Taylor, L.T. *Thin Solid Films*, **158**, 189, (1988).

20. Bergmeister, J.J. and Taylor, L.T. *Chem. Mater.*, **4**, 729, (1992).

21. Bott, R.H.; Taylor, L.T.; and Ward, T.C. *J. Appl. Polym. Sci.*, **36**, 1295, (1988).

22. Taylor, L.T.; Carver, V.C.; Furtsch, T.A.; and St. Clair, A.K.; *ACS Symp. Ser.*, **121**, 71, (1980).

23. Porta, G.M.; Rancourt, J.D.; and Taylor, L.T. *Chem. Mater.*, **1**, 269, (1989).

24. Boggess, R.K. and Taylor, L.T. *J. Polym. Sci., Polym. Chem. Ed.*, **25**, 685, (1987).

25. Rancourt, J.D.; Boggess, R.K.; Horning, L.S.; and Taylor, L.T. *J. Electrochem. Soc.*, **134**, 85, (1987).

26. Rancourt, J.D. and Taylor, L.T. *ACS Symp. Ser.*, **367**, 395, (1988).

27. Rancourt, J.D.; Porta, G.M.; and Taylor, L.T. *Int. SAMPE Tech. Conf.*, **19**, 564, (1987).

28. Boggess, R.K. and Taylor, L.T. *Recent Advances in Polyimide Science and Technology, Proceedings of the Second International Conference on Polyimides: Chemistry, Characterization, and Applications*. Weber, W.D. and Gupta, M.R., Eds. (Poughkeepsie, Mid-Hudson Chapter, Society of Plastics Engineers). 1987. pp. 463-70.

29. St. Clair, T.L. and St. Clair, A.K. *J. Polym. Sci., Polym. Chem. Ed.*, **15**, 1529, (1977).

30. St. Clair, A.K.; St. Clair, T.L.; and Shevket, K.I. *Polym. Mater. Sci. Eng.*, **51**, 62, (1984).

31. Crivello, J.V.; Lee, J.L.; and Conlon, D.A., *J. Polym. Sci., Polym. Chem. Ed.*, **25**, 3293, (1987).

32. Takekoshi, T.; Kochanowski, J.E.; Manello, J.S.; and Webber, M.J. *J. Polym. Sci., Polym. Symp.*, **74**, 93, (1986).

33. Burks, H.D. and St. Clair, T.L., *J. Appl. Poly. Sci.*, **29**, 1027, (1984).

34. Burks, H.D. and St. Clair, T.L., *J. Appl. Poly. Sci.*, **29**, 4037, (1984).

35. Progar, D.J. and St. Clair, T.L., *Int. J. Adhesion and Adhesives*, **6**, 25, (1986).

36. Progar, D.J., *J. Adhesion Sci. Technol.*, **2**, 449, (1988).

37. Burks, H.D. and St. Clair, T.L., *J. Appl. Poly. Sci.*, **30**, 2401, (1985).

38. Mashkina, A.V. *Catal. Rev.-Sci. Eng.*, **32**, 105, (1990).

39. Briggs, D. and Beamson, G. *Anal. Chem.*, **65**, 1517, (1993).

40. Lindberg, B.J.; Hamrin, K.; Johansson, G.; Gelius, U.; Fahlman, A.; Nordling, C.; and Siegbahn, K. *Physica Scripta*, **1**, 286, (1974).

41. Navarre, M. In *Polyimides: Synthesis, Characterization, and Applications*. Mittal, K.L., Ed.; Plenum Press: New York, 1984, pp. 438-9.

42. Silverstein, R.M.; Bassler, G.C.; and Morrill, T.C. *Spectrometric Identification of Organic Compounds*, 4th Ed., John Wiley & Sons: New York, 1981, pp. 116, 133.

43. Allen, G.C.; Curtis, M.T.; Hooper, A.J.; and Tucker, P.M.; *J. C. S. Dalton*, 1525, (1974).

44. McIntyre, N.S. and Zetaruk, D.G. *Anal. Chem.*, **49**, 1521, (1977).

45. Beamson, G. and Briggs, D. *High Resolution XPS of Organic Polymers: The Scienta ESCA 300 database*, John Wiley & Sons: New York, 1992, p. 264.

46. Clark, D.T. and Thomas, H.R. *J. Polym. Sci., Polym. Chem. Ed.*, **16**, 791, (1978).

47. Socrates, G. *Infrared Characteristic Group Frequencies*, John Wiley & Sons: New York, 1980, pp. 111-6.

48. Schwertmann, U. and Cornell, R.M. *Iron Oxides in the Laboratory: Preparation and Characterization*, VCH Publishers, Inc.: New York, 1991, p. 28.

49. Mukhlenov, I.P., Buzanova, G.N., Parkhomova, E.A., Selivanov, N.T., Zayats, Y.N., and Saukhin, Z.A. *Chem. Abstr.*, **100**, 70336w (1984).

50. Personal Communication, Dr. Adley F. Rubira.

51. Handbook of X-Ray Photoelectron Spectroscopy, Muilenberg, G.E., Ed.; Perkin-Elmer Corporation: Eden Prairie, MN, 1979, pp. 50-1, 70-71.

52. Horning, L.S. *Development of Polyimide/Metal Gradient Microcomposite Films*, M.S. Thesis, Virginia Polytechnic Institute & State University, 1990.

53. Smith, L.L.; Dillard, J.G.; Horning, L.S.; Rancourt, J.D.; Taylor, L.T.; and Wightman, J.P. *Int. J. Adhesion and Adhesives*, **11**, 80, (1991).

54. Wohlford, T.L.; Schaff, J.; Taylor, L.T.; St. Clair, A.K.; Furtsch, T.A.; and Khor, E. in *Conductive Polymers*, R.B. Seymour, Ed. (Plenum Publishing Corporation: New York), 7, 1981.

55. Madeleine, D.G.; Ward, T.C.; and Taylor, L.T. *J. Polym. Sci., Polym. Physics*, **26**, 1641, (1988).

56. Porta, G.M. and Taylor, L.T. *J. Mater. Res.*, **3**, 211, (1988).

57. Porta, G.M.; Rancourt, J.D.; and Taylor, L.T. in *Polyimides: Materials, Chemistry, and Characterization*, C. Feger, M.M. Khojasteh, and J.E. McGrath. Eds. (Elsevier Science Publishers B.V.: Amsterdam), 251, 1989.

58. Silvain, J.F.; Ehrhardt, J.J.; and Lutgen, P. *J. Adhesion Sci. Technol.*, **5**, 501, (1991).

59. Bartha, J.W.; Hahn, P.O.; LeGoues, F.; and Ho, P.S. *J. Vac. Sci. Technol. A*, **3**, 1390, (1985).

60. Ho, P.S.; Hahn, P.O.; Bartha, J.W.; Rubloff, G.W.; LeGoues, F.; and Silverman, B.D. *J. Vac. Sci. Technol. A*, **3**, 739, (1985).

61. Tromp, R.M.; LeGoues, F.; and Ho, P.S. *J. Vac. Sci. Technol. A*, **3**, 782, (1985).

62. LeGoues, F.; Silverman, B.D.; and Ho, P.S. *J. Vac. Sci. Technol. A*, **6**, 2200, (1988).

63. Ho, P.S. *Appl. Surf. Sci.*, **41/42**, 559, (1989).

64. Kim, Y.-H.; Walker, G.F.; Kim, J.; and Park, J. *J. Adhesion Sci Technol.*, **1**, 331, (1987).

65. Kowalczyk, S.P.; Kim, Y.-H.; Walker, G.F.; and Kim, J.; *Appl Phys. Lett.*, **52**, 375, (1988).

66. Kim, Y.-H.; Kim, J.; Walker, G.F.; Feger, C.; and Kowalczyk, S.P. *J. Adhesion Sci Technol.*, **2**, 95, (1988).

67. Shih, D.-Y.; Kim, J.; Walker, G.F.; Chang, C.-A.; Paraszczak, J.; Nunes, S.; and Yang, C. *Appl. Phys. Lett.*, **59**, 1424, (1991).

68. Crompton, J.S. *J. Mater. Sci.*, **24**, 1575, (1989).

69. Adema, G.M.; Turlik, I.; Hwang, L.-T.; Rinne, G.A.; and Berry, M.J. *IEEE Trans. on Components, Hybrids, and Manufacturing Technology*, **13**, 766, (1990).

70. Driscoll, S.B.and Walton, T.C. *SAMPE J.*, **23**, 9 (1987).

71. Adams, R.D. In *Engineered Materials Handbook*, Vol. 3, Brinson, H.F., Ed. ASM International. 1990, p. 331.

72. Anderson, G.P.; Bennett, S.J.; and DeVries, K.L. *Analysis and Testing of Adhesive Bonds*, Academic Press: New York, 1977, pp. 14, 82.

73. Rossi, R.D. In *Engineered Materials Handbook*, Vol. 3, Brinson, H.F., Ed. ASM International. 1990, p. 151.

74. Progar, D.J., *J. Adhesion Sci. Technol.*, **1**, 53, (1987).

75. Progar, D.J. and St. Clair, T.L., *J. Adhesion*, **30**, 185, (1989).

76. Progar, D.J. and St. Clair, T.L., *J. Adhesion Sci. Technol.*, **4**, 527, (1990).

77. Darmory, F.P. *Adhesives Age*, 22, (March 1974).

78. Gibbs, H.H. *Proc., Annu. Conf., Reinf. Plast. Comp. Inst., Soc. Plast. Ind.*, **29**, 11D (1974).

79. Flinn, R.A. and Trojan, P.K. *Engineering Materials and their Applications*, Fourth Ed. (Princeton: Houghton Mifflin Company). 1990. p. 424.

80. Vaughn, R.W. *SAMPE Q.*, **7**, 1980 (1976).

81. Burgman, H.A.; Freeman, J.H.; Frost, L.W.; Bower, G.M.; Traynor, E.J.; and Ruffing, C.R. *J. Appl. Polym. Sci.*, **12**, 805, (1968).

82. Tamai, S., *et al.*, U.S. Patent No. 4,734,482 1988.

83. Bright, K. and Malpass, B.W. *Eur. Polymer J.*, **4**, 431, (1968).

84. Sykes, J.M. and Hoar, T.P. *J. Polymer Sci., A-1*, **7**, 1385, (1969).

85. Evans, J.R.G. and Packham, D.E. *J. Adhesion*, **10**, 39, (1979).

86. van Ooij, W.J. In *Physicochemical Aspects of Polymer Surfaces*, Vol. 2. Mittal, K.L., Ed., Plenum Press: New York, 1983, p. 1035.

87. van Ooij, W.J. In *Industrial Adhesion Problems*, Brewis, D.M. and Briggs, D., Ed., John Wiley & Sons: New York, 1985, p. 92.

88. Sugama, T. and Carciello, N.R. *Int. J. Adhesion and Adhesives*, **11**, 97 (1991).

89. Hollenhead, Jr.; J.B. and Wightman, J.P. *J. Adhesion.*, **37**, 121 (1992).

90. Novakov, T. and Prins, R. In *Electron Spectroscopy*, Shirley, D.A., Ed., North Holland: Amsterdam, (1972), 821.

91. Fadley, C.S. and Shirley, D.A. *Phys. Rev.*, **A2**, 1109, (1970).

92. Konno, H. and Nagayama, M. *J. Electr. Spectr. Rel. Phenom.*, **18**, 341, (1980).

93. Asami, K. and Hashimoto, K. *Corros. Sci.*, **17**, 559 (1977).

94. Carver, J.C.; Schweitzer, G.K.; and Carlson, T.A. *J. Chem. Phys.*, **57**, 973, (1972).

95. Asami, K.; Hashimoto, K.; and Shimodaira, S. *Corros. Sci.*, **16**, 35 (1976).

96. Robert, T; Bartel, M.; and Offergeld, G. *Surf. Sci.*, **33**, 123, (1972).

97. Allen, G.C.; Curtis, M.T.; Hooper, A.J.; and Tucker, P.M.; *J. C. S. Dalton*, 1675, (1973).

98. Sharrock, M.P. and Bodnar, R.E. *J. Appl. Phys.*, **57**, 3919, (1985).

99. Corradi, A.R., *IEEE Transactions on Magnetics*, **MAG-14**, 655, (1978).

100. Magnetic Recording, Lowman, E.E., Ed., McGraw-Hill: New York, 1972, pp. 45-61.

101. Calvert, P. and Mana, S. *J. Mater. Sci.*, **23**, 3801, (1988).

102. Bergmeister, J.J.; Rancourt, J.D.; and Taylor, L.T. *Chem. Mater.*, **2**, 640, (1990).

VIII. APPENDIX: MAGNETIC PROPERTIES OF MIXED METAL MODIFIED POLYIMIDE FILMS.

INTRODUCTION

For successful use, magnetic recording materials must have a sufficiently large remnant induction, an adequate coercivity, and a size small enough for satisfactory recording resolution but large enough to be thermally stable [98]. The particles need to be small (< 50nm) in order to have good print-through performance, while large particles (800-1000 nm) reduce the signal-to-noise ratio. High coercivities are needed to withstand demagnetizing effects [99]. The most common method of preparation is to coat a polymer substrate with a slurry of magnetic oxide, usually γ-Fe_2O_3 or Fe_3O_4, dispersed in a non-magnetic (organic) binder [100]. An alternative method of preparation is to synthesize the magnetic oxide *in situ* during the preparation of the polymer matrix [20, 101, 102]. The metal oxide precursor could either be thermally decomposed as the polymer is cured or dried or additional reactants can be disolved into the polymer. Previous work by Bergmeister and Taylor [20, 102] used the first method to synthesize

polyimide films modified with iron oxide. This study examines the effects of adding a second metal complex in addition to the iron complex. It is known that doping iron oxide with cobalt will increase the coercivity [98, 99]. Therefore, this study will examine cobalt and other metals as a means of distorting the lattice in the metal precipitate to improve the magnetic properties of the composite.

EXPERIMENTAL

Materials

3,3',4,4'-Benzophenonetetracarboxylic acid dianhydride (BTDA, Structure 6), was obtained from Allco Chemical Corp. (Galena, KS) and vacuum dried at 120°C. Zone refined 4,4'-diaminodiphenyl ether (ODA) was obtained from Aldrich Chemical Co. (Milwaukee, WI) and was vacuum dried overnight at 70°C before use. N,N-Dimethylacetamide (DMAc) was also obtained from Aldrich Chemical Co. and was stored under nitrogen and over molecular sieves. The iron additive used in this study were tris(2,4-pentanedionato)iron(III)

($Fe(acac)_3$), obtained from Amspec, Inc. (Gloucester, NJ). Other metal additives included cobalt(II) chloride ($CoCl_2$), zinc(II) iodide (ZnI_2), nickel(II) chloride ($NiCl_2$), manganese(II) chloride ($MnCl_2$), and 2,4-pentanedionatolithium (Li(acac)). All of the metal complexes were vacuum dried at 80°C overnight prior to use.

Synthesis

Poly(amide acid) solutions were made by reacting equal molar amounts of diamine and dianhydride in DMAc (15% solids) under a nitrogen atmosphere. The monomers were allowed to react for three hours in the stirred solution. After this period, modified poly(amide acid) solutions were made by adding the metal complexes (20 mole% or 33 mole% total concentration) and stirred for six more hours. The metal complexes were added in a 2:1 ratio between $Fe(acac)_3$ and the metal(II) halide used, except in the case of Li where the ratio was 2.5:0.5.

The free standing films were made by casting the modified and unmodified poly(amide acid) solutions onto a dust free glass plate at a thickness of 0.51 mm with a

doctor blade. The film was then cured under either a dynamic air or nitrogen atmosphere at 80°C for twenty minutes and at 100°C, 200°C, and 300°C for one hour each. Upon cooling, the films were removed from the glass plate using a razor blade to lift off the film. The side exposed to the cure atmosphere will be referred to as the atmosphere side in the subsequent discussion. The glass side will be the side of the film which was in contact with the glass plate during the cure.

Measurements

The coercivity (Hc), saturation induction (Bm), and the remnant induction (Br) were measured using an LDJ 7500A BH meter. A field strength of 3000 Oe was used during the tests, except for the Co/Fe composites which required a field strength of 4500 Oe in order to reach saturation.

Transmission electron micrographs were taken with a Philips Model 420 scanning transmission electron microscope. The samples for TEM analysis were embedded in Polyscience ultralow viscosity resin and cured for eight hours at 70°C. A Reichert-Jung ultramicrotome and a microstar diamond knife

were then used to obtain cross sections of the samples having thicknesses of between 500 and 800 Å. These sections were then placed on 200-mesh copper grids for analysis.

RESULTS AND DISCUSSION

The results of the magnetic testing of these films are tabulated in Table XIII. The saturation induction (Bm) is the size of the induced magentic field when the film has been fully saturated (Figure 84). When the applied magnetic field has been reduced to 0 Oe, the remaining induced magnetic field is the remnant induction (Br) (Figure 84). The size of the applied field necessary to reduce the induced magnetic field to zero is the coercivity (Hc). All of the films were saturated when using an applied field strength of 3000 Oe except for the films containing cobalt which required a field strength of 4500 Oe (Figure 85). These films also possessed the highest coercivity (1970 Oe for 20 mole% (Figure 86) and 1860 Oe for 33 mole%. For most of the other films, the coercivities were almost negligible. One exception were the films containing manganese which

produced coercivities of 74 Oe for the 20 mole% film (Figure 87) and 93 Oe for the 33 mole% film.

One factor that is important in magnetic media is the ratio between Bm and Br, often called squareness, which indicates the ability to retain induced field strength. As can be seen from the results of the computer disk that was tested (Table XIII), a high Br/Bm value is very desirable. The only films that come close are the ones that contain cobalt or manganese in addition to the iron. These films also possessed high Bm's. Other films also possessed high Bm values; e.g. 33 mole% nickel/iron, 20 mole% iron, and 20 mole% lithium /iron; but their Br values were very low (approximately 0.10). Thus the cobalt/iron and manganese/iron films proved to be the best of the ones tested. The high coercivity for the cobalt/iron films indicated that it had a hard magnetic character. In other words, once it was magnetized, it was hard to get it unmagnetized. The manganese/iron films, on the other hand, possessed characteristics of soft magnets being fairly easy to remove the induced field. As can be seen by the

coercivity on the computer disk, soft magnets are more useful for magnetic media.

Individual films containing only the amounts of iron or cobalt contained in the 20 mole% cobalt/iron composite were synthesized in order to determine what component contributed to which property. It was evident that the coercivity was mainly dependent on the cobalt involved. Both the 20 mole% cobalt/iron film and the cobalt-modified composite had extremely high coercivities. The iron-modified composite, on the other hand had a ver low coercivity. The saturation induction values for the cobalt-modified composite and the iron-modified composite, when combined, were very similar to that for the cobalt/iron-modified composite. The combined remnant induction value for the two films, however, was only about 15% of the value obtained when the two metals were added in the same film. This increase for the combined film would seem to suggest some interaction between the two metals in order to create such a large increase.

These data indicated that magnetic composite films were synthesized. The induction values obtained, however, were

much less than those seen in commercial products, i.e. the computer disk, and that appears mainly due to the shape of the metal particles. The particles in both the cobalt/iron modified films (Figure 88) and the manganese/iron modified films (Figure 89) were similar in size, 20-30 nm in diameter. Most magnetic media use long, needle-like, acicular particles. The particles observed via TEM in these films were cubic.

Table XIII. Magnetic Characteristics of Mixed Metal Modified Films.

Film	Metal Concentration	Bm (G)	Br (G)	Br/Bm	Hc (Oe)
Co/Fe	20 mole%	3.16	1.43	0.45	1970
Co/Fe	33 mole%	6.94	3.33	0.48	1860
Mn/Fe	20 mole%	3.31	1.15	0.35	74
Mn/Fe	33 mole%	6.96	2.03	0.29	93
Fe	20 mole%	4.23	0.41	0.10	18
Computer Disk	------	26	15	0.58	285
2/3 Fe	13 mole%	2.05	0.17	0.08	26
1/3 Co	7 mole%	1.25	0.03	0.02	2130
Ni/Fe	20 mole%	0.78	0.01	0.01	2
Ni/Fe	33 mole%	4.33	0.42	0.10	28
Zn/Fe	20 mole%	1.67	0.07	0.04	9
Li/Fe	20 mole%	3.87	0.42	0.11	15

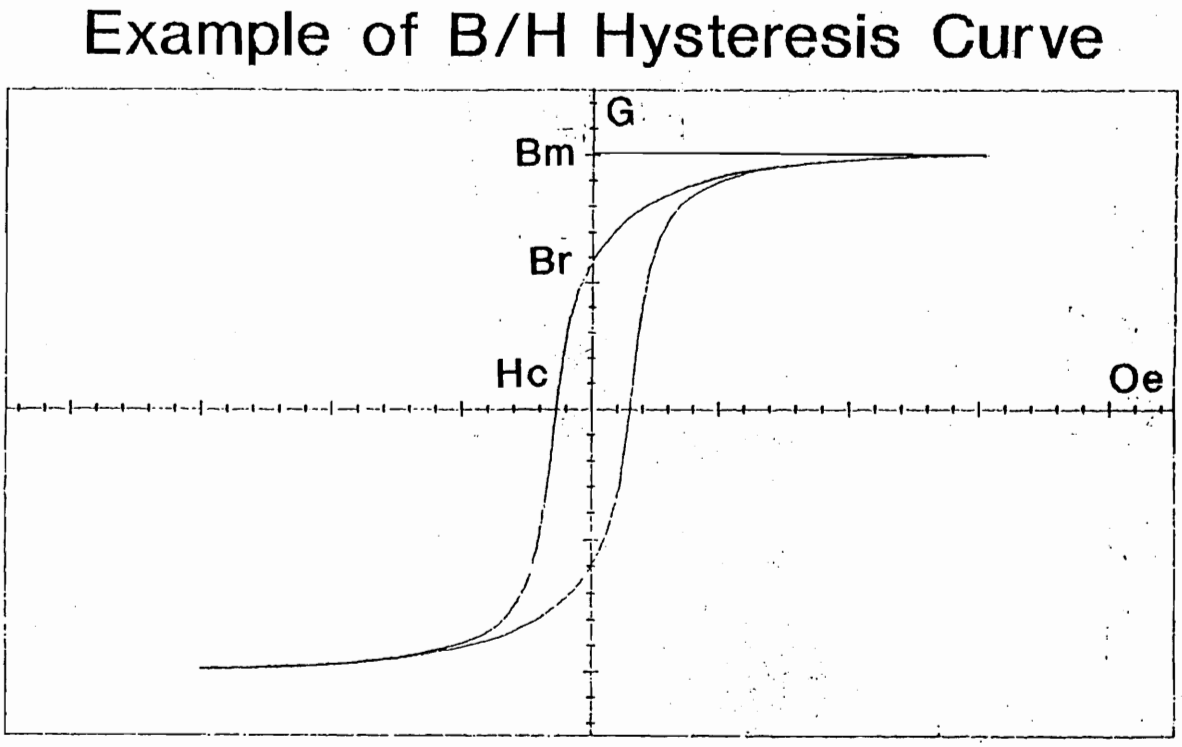

Hc = Coercivity; the size of the magnetic field applied in the opposite direction to reduce the induced magnetic field to zero.

Bm = Saturation induction; the size of the induced magnetic field when the sample has saturated.

Br = Remnant induction; the size of the induced magnetic field when the applied field has been reduced to zero.

Figure 84. Magnetic Parameters Associated with Hysteresis.

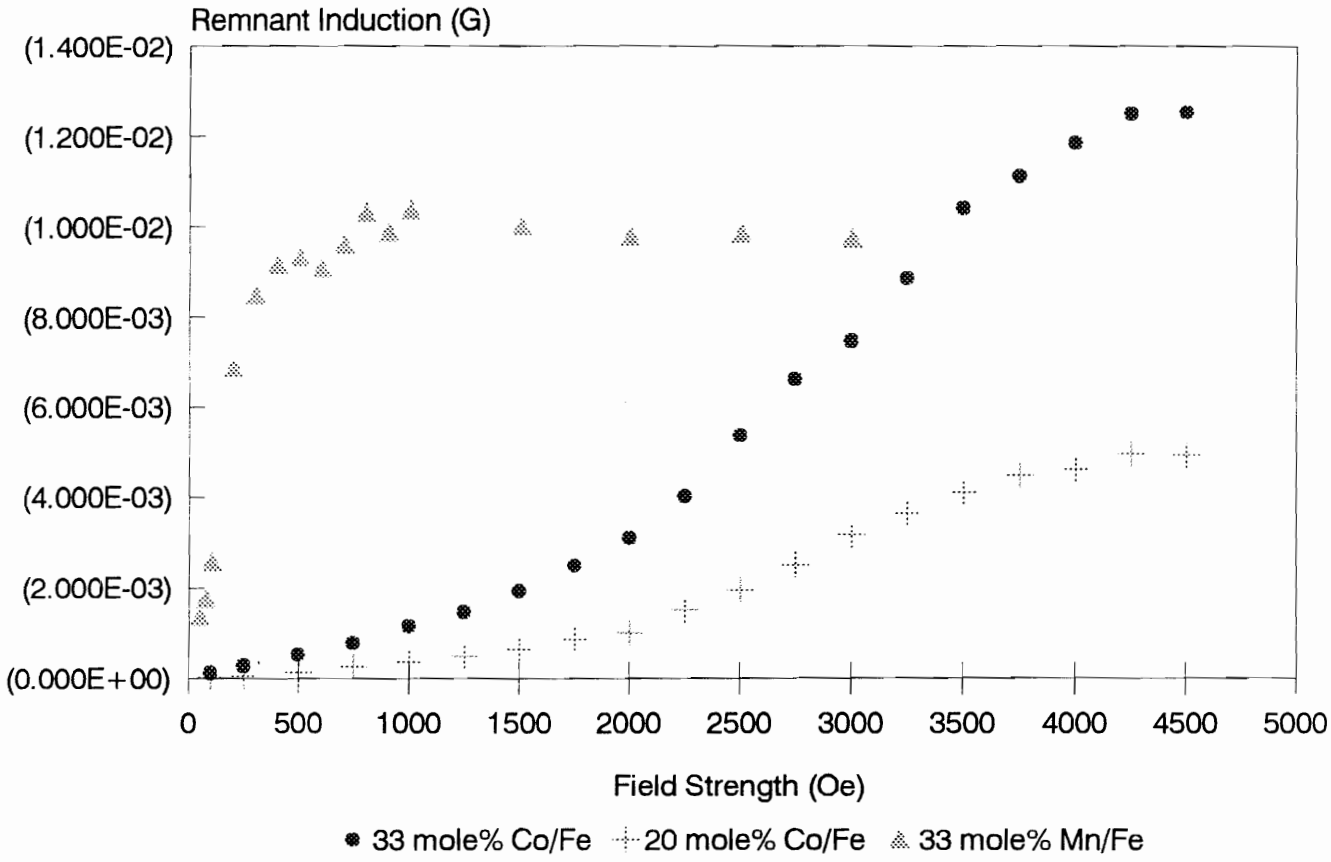

Figure 85. Br Versus Applied Field Strength

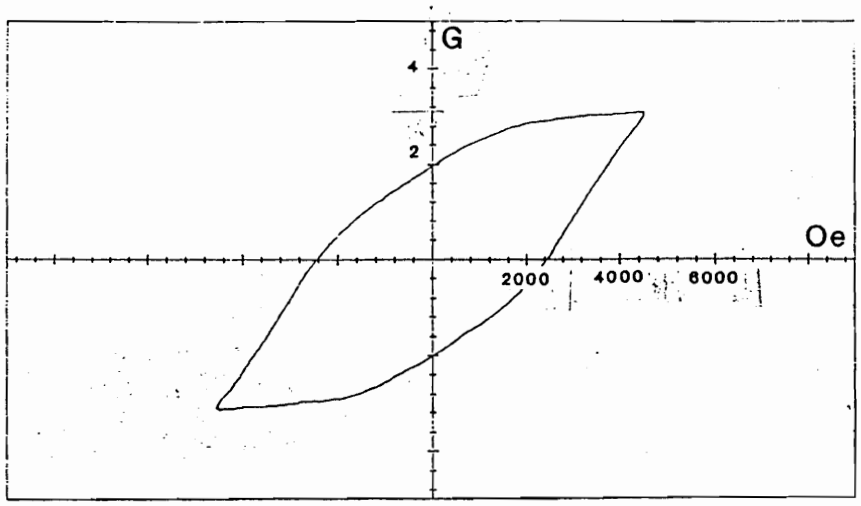

Field Strength = 4500 Oe

Figure 86. B/H Loop for 20 mole% Cobalt/Iron Modified Composite.

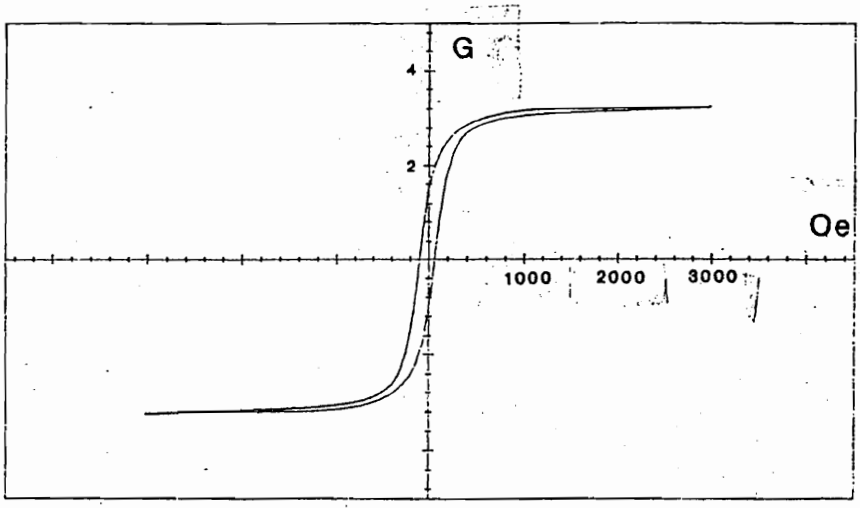

Field Strength = 3000 Oe

Figure 87. B/H Loop for 20 mole% Manganese/Iron Modified Composite.

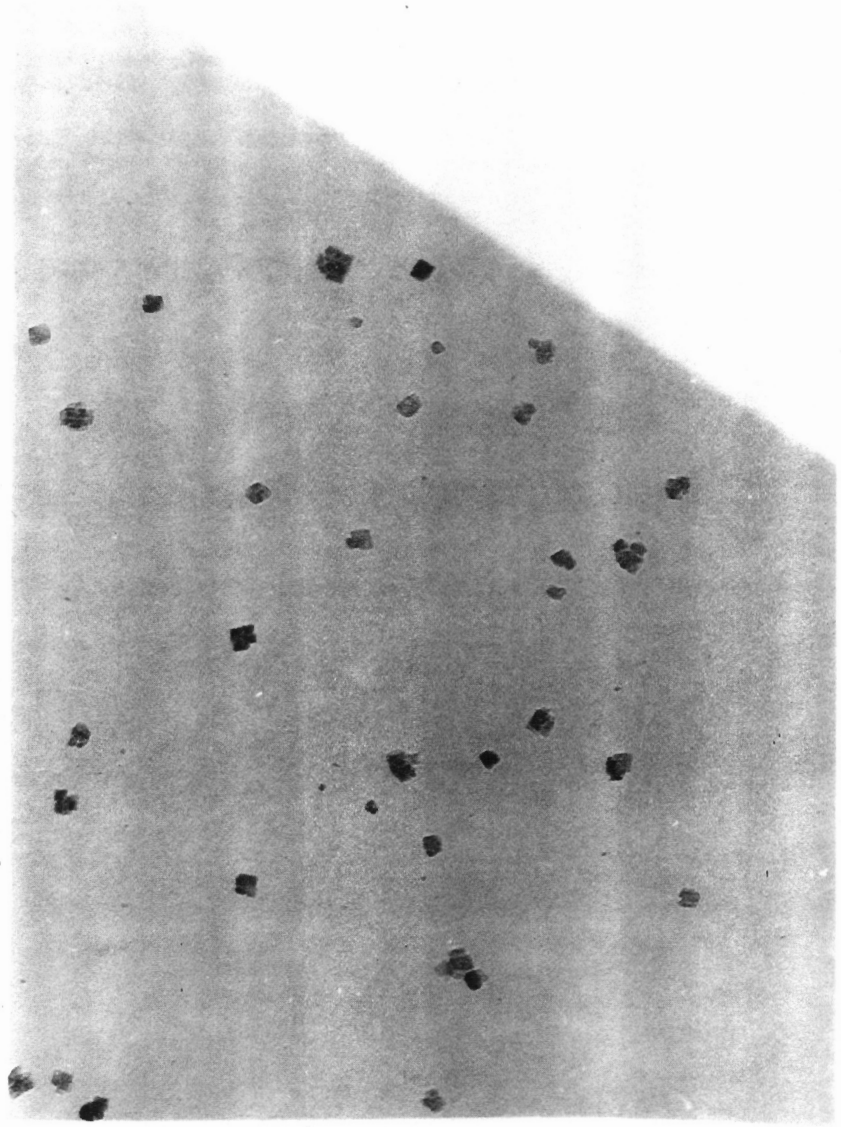

Figure 88. TEM of 20 mole% Cobalt/Iron Modified Composite - Glass Side (106,000x).

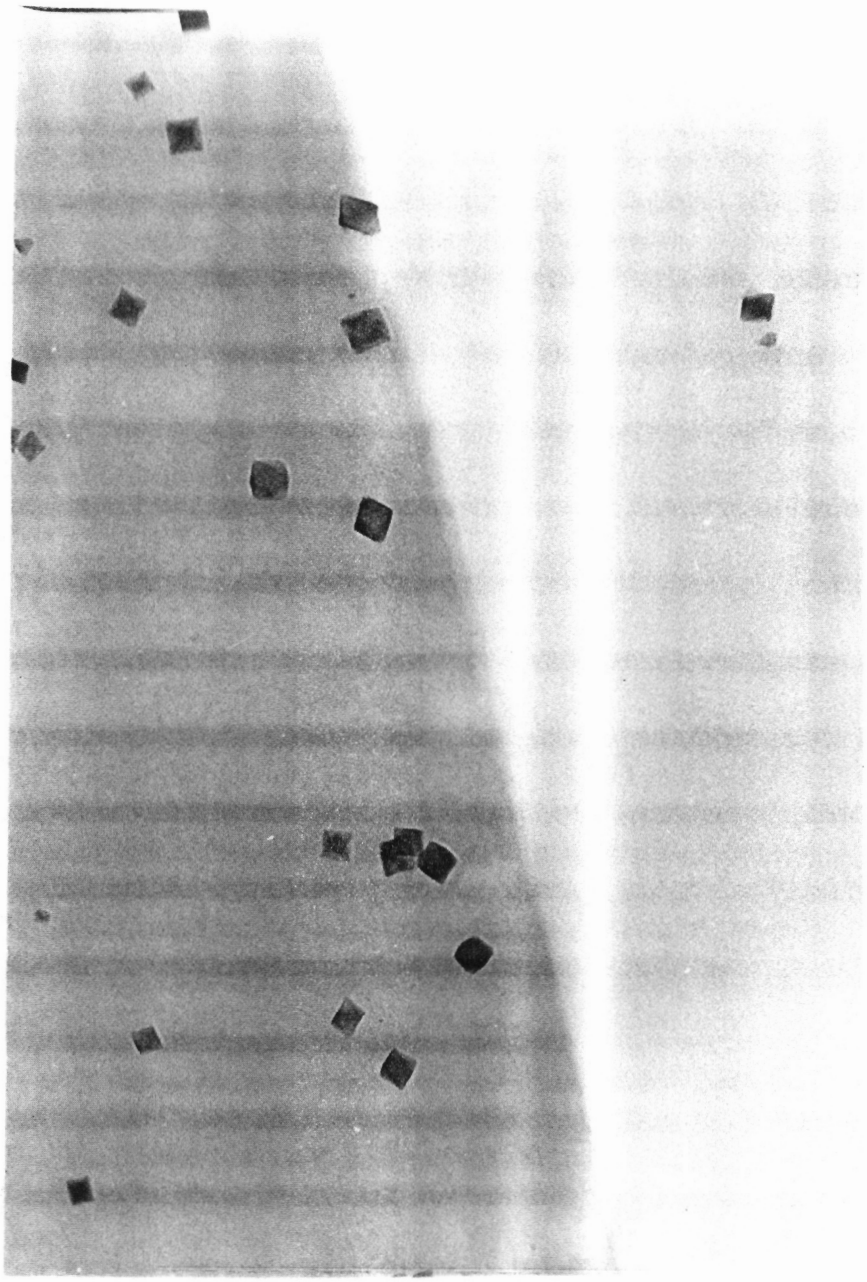

Figure 89. TEM of 20 mole% Manganese/Iron Modified Composite - Glass Side (106,000x).

VITA

The author was born in Charlotte, NC, on 11 December 1967 to Dr. and Mrs. Thomas M. Ellison. He grew up in Charlotte and attended South Mecklenburg High School where he graduated as salutatorian in 1986. In the fall of that year, he entered Wofford College. He graduated *summa cum laude* from Wofford in May of 1990 with a B.S. in Chemistry and a B.A. with Honors in History for his honors project on the development of the atomic theory.

While at Wofford, he met Veronica Hodge whom he married in May of 1990. That summer, they moved to Blacksburg so he could enter the graduate program in Chemistry at Virginia Polytechnic Institute and State University, working under the direction of Dr. Larry T. Taylor. He was awarded an Adhesive and Sealant Council Fellowship from 1992 to 1994 to study the effects of metal-catalyzed oxidation of sulfur in polyimide adhesives. The high point of his life occurred on 16 February 1995 at 5:08 AM when he saw his son, Matthew David Ellison enter this world.